Proceedings of the

17th Conference

of the Nuclear Societies of Israel

Editor : Ż.B. Alfassi

May 4, 1992
Ben Gurion University
Beer Sheva, Israel

Proceedings of the

17th Conference

of the Nuclear Societies of Israel

Editor : Z.B. Alfassi

May 4, 1992

Ben Gurion University

Beer Sheva, Israel

Contents

Invited Talks

Reactor Physics

Reactor Technology, Economics and Safety

Health Physics and Dosimetry

Use of radioisotopes

Nuclear Instrumentation and Radiochemistry

Late additions

MESSAGE TO THE 17TH MEETING OF THE NUCLEAR SOCIETIES IN ISRAEL

Louis Tepper
President, The Israel Nuclear Society

The last Meeting of the Nuclear Societies in Israel took place exactly one month before the first Scud attack on Israel. Many other conventions had to be cancelled because of the crisis, but our own American guests all came as planned. We said then that underneath the conflict there was basically an oil crisis, at least as one of its components. The abrupt end of the war, with Iraq's arsenal largely intact but the Gulf's oil flowing again, confirmed those assumptions. Unfortunately, and contrary to our own prior appraisal, the war did not cause any fundamental reassessment of the world energy landscape, not yet at any rate. Which means that until such a change takes place, there is bound to be another crisis in the offing, sooner or later, quite independently from the Israel-Arab conflict.

A basic change of the world energy balance should have produced a massive shift away from oil and toward large-scale electrification - including electric surface transport - using non-pollutant fuels, which today means nuclear energy. However, this hoped for reassessment did not materialize.

Looking at the world at large, it seems that the continuing development of nuclear energy goes in direct relation to the lack of supply of other forms of energy. Japan and the rest of the bustling Far East, totally devoid of any form of energy, naturally are today at the head of the reactor-building countries. Japan supplies nearly 30% of its electricity from nuclear power and constructs three plants a year. On the other hand the U.S. and most of Western Europe, relatively rich in energy, and after nuclearizing a sizable chunk of their electricity, can afford to postpone the construction of new plants, yielding to the pressure of anti-nuclear movements. An exception is France, with nearly 80% of its electricity nuclear, exporting electricity to neighboring countries and still building a new plant a year on average.

The former USSR and Eastern Europe are badly in need of energy, nuclear energy in particular. This not only because of the terrible pollution which their present-day fossil plants cause, but also in order to unlock an estimated 50% of their railroad network which today is loaded with coal transport. On the other hand, the fear instilled in the population by the Chernobyl disaster of 1986, and the less-than optimal safety record of at least part of their reactors, make it that more difficult for them to build new plants, although undoubtedly they will be built. The close cooperation with the West today, in the area of Nuclear Safety, and the adoption of Western standards, will surely facilitate the process of building new and safer nuclear plants. There is no doubt however about the basically high capability of Russian engineering.

There is a sad irony in the fact that safety mishaps occurring in the former USSR and Eastern Europe are debited to the Nuclear Industry in the world at large, in spite of the absolutely unequaled safety record of Western Power Reactors. In 35 years of commercial nuclear electricity in the West there has not been a single accident in which a member of the public died of radiation. Nearly 20 trillion Kwh were produced during this period, costing about one trillion dollars. No other industry can supply such a record.

The Chernobyl disaster did not only instill fear in the Russian population. It provided ammunition to anti-nuclear movements of long standing, who use, misuse and distort facts, in order to promote their own non-scientifically based views. The bare facts, bad as they are, are not enough for them. They demonize the whole nuclear industry, indeed the entire nuclear scientific community the world over. They have also appeared in our own shores, as was almost inevitable, and are accusing the world nuclear community of no less than an "unholy alliance" with Russian bureaucracy, to set up a huge cover-up of the so-called "hidden consequences" of Chernobyl, as if the real and scientifically documented consequences were not serious enough.

The damage caused by the anti-nuclear activists is not limited to the nuclear industry. Indeed this industry seems to suffer little damage if at all. Westinghouse, General Electric, Siemens and the other giants make good business with any form of power plants, not necessarily nuclear. It is the public at large which is the main sufferer, that same public which is purportedly being warned and protected by those people. This public is deprived of the cleanest and safest form of energy which is practically available today.

Still, without public acceptance nuclear plants cannot be built, even if that means going against the public interest. It is imperative therefore, not only to build safe plants, but to convince the public that their operation is safe. That they provide the cleanest form of energy that can be practically obtained today. Convincing the public is today the biggest challenge of the entire nuclear community, in the world at large as well as here in Israel.

Looked at in a broader context, the energy community at large - not just the nuclear community - has the moral duty to work toward abundant, clean and safe energy, away from oil as far as possible. As long as oil is vital, the reasons for oil crises will stay with us.

As far as Israel is concerned, the political obstacles for acquiring nuclear power reactors are still with us. We have no other choice but to take the long view, with the conviction that at some stage the impasse will be resolved. In the meanwhile, we must be careful to keep and develop our own capabilities in the field of nuclear reactors and nuclear fuel technology for electricity production. For this we must actively encourage real projects of development, the teaching of nuclear engineering and the access of the younger generation to the centers of learning, research, development, design, construction and operation.

CAN WE DISPOSE OF RADIOACTIVE WASTES?

Frank L. Parker
Vanderbilt University/Clemson University

Radioactive waste was first produced in the 1870s when the Czechoslovakian miners in Schneeburg and Joachimsthal suffered lung cancers from radon daughter products. Major concern about radioactive waste problems began in 1943, when the University of Chicago group planned to move to Oak Ridge, Tennessee to develop the processes for producing sufficient enriched uranium and plutonium-239 to make the first atomic bombs. The first significant unclassified scientific meeting on radioactive waste disposal took place in 1955 when the U.S. National Academy of Sciences recommended the use of deep geological formations as the best place to dispose of radioactive wastes. Since that time disposal in more exotic environments, e.g. space and the oceans, and transmutation (conversion to less hazardous materials) have been proposed and rejected though interest still continues in subseabed disposal and transmutation. Every nation which has a high-level waste disposal program plans on deep geologic disposal in the near future or some decades hence.

In the meantime, most high-level waste including spent nuclear fuel designated as waste is stored in the spent fuel pools at the reactors. Some of the excess spent fuel is stored in casks and concrete structures at the reactor site. Centralized storage of spent fuel is practiced in a number of countries including the CLAB in Sweden. Vitrified reprocessed wastes is stored at the reprocessing centers in France and the United Kingdom. Some reprocessed wastes in underground tanks awaits vitrification in the USA and the CIS.

Low and intermediate level waste is disposed of near surface in most countries in increasingly engineered structures. In Sweden these wastes are disposed of in near surface geological structures while in Switzerland, United Kingdom, and Germany they will be disposed of in deep geologic facilities.

No country has yet completely faced up to the problem of the disposal of the wastes from the decontamination and decommissioning of nuclear facilities.

Perhaps the greatest potential for impact upon the public are the wastes disposed to the environment in the earlier days of nuclear weapons production. The most severe problems are at Kyshtym (Cheliabinsk-40) in Russia, and at Hanford and Savannah River in the United States of America. In the USA alone, the cleanup costs are estimated in the hundreds of billions of dollars. No estimates have been made of the costs in the Soviet Union, but the contamination there exceeds that in the USA by orders of magnitude.

With the experience, both good and bad, obtained over the last 50 years, what is the prognosis for safe disposal of radioactive waste?

USE OF NUCLEAR REACTORS FOR DESALINATION PLANT POWER SUPPLY

Yu. A. Sergeev

Institute of Physics and Power Engineering

Obinsk, The Russian Federation

SUMMARY

The presentation elucidates the history, current status and prospects of desalted water production installations using nuclear reactor power.

The main section is dedicated to the design and operation of the world's first and unique nuclear desalination plant, with the BN-350 reactor constructed on the eastern coast of the Caspian Sea. This plant provides for the complete supply of fresh and drinking water for the inhabitants and industries of the town of Shevchenko (now the town of Aktau, Kazakhstan).

It is followed by a review of design studies and proposals for further development of desalination plants supplied by heat and electricity from nuclear power plants, with the reactors of a new generation that can be commissioned before the year 2000.

Invited paper, presented at the 17th National Meeting of the Israel Nuclear Society, Beer-Sheva, Israel, May 4, 1992.

AN OVERVIEW OF THE IAEA PROGRAMME ON THE SAFETY OF WWER-440 MODEL 230 NUCLEAR POWER PLANTS

Luis Lederman
IAEA

1. BACKGROUND

Soviet designed reactors of all types make up 11% of the world's operating reactors and 32% of those under construction. Of the pressurized water reactors (WWER), which are the only type to have been exported, there are a total of 44 in operation and 25 under construction. In eastern Europe there are in addition to Soviet designed WWER plants, 5 Canadian designed heavy water reactors (HWR) under construction in Romania and also a Westinghouse pressurized water reactor (PWR) in operation in Yugoslavia.

The dependence of Central and Eastern European Countries on nuclear electricity is considerable; it is 50% in Hungary, 35.7% in Bulgaria, 28.4% in Czechoslovakia and 12.2% in the USSR.

At this time there are 10 first generation 440 MW WWER, model 230 reactors in operation. Two units in Armenia and four in the eastern part of Germany have been shutdown (Table I). Four of the operating units are located in Bulgaria, two are in Czechoslovakia and four are in the Soviet Union. All of these units lack safety design features basic to other pressurized water plants. The weaknesses include lack of containment to enclose the reactor systems, insufficient redundancy and separation of safety equipment, limited emergency core cooling capacity, insufficient fire protection, and deficient instrumentation and control systems.

The second generation of 440 MW WWER model 213 reactors have eliminated many of the design deficiencies of the model 230, particularly through the use of sealed chambers to localize accidents and a steam suppression system. Of the 16 units in operation (Table II), the two reactors located in Finland have undergone significant safety improvements particularly in manufacturing quality and the use of non-Soviet instrumentation, as well as a containment structure surrounding the reactor systems. At this time there are four Model 213 units under construction in Czechoslovakia. In addition, two WWER model 318 are under construction in Cuba. As with the units in Finland, the Cuban plant incorporates a containment structure as well as a number of additional safety improvements.

The safety concept of the larger and more modern Soviet designed 1000 MW WWER plants is similar to that of non-Soviet PWR plants in operation worldwide and include a full containment structure. However, some concerns related to design and operational problems remain, even for the more advanced 1000 MW units. Of the seventeen units in operation, only the one in Bulgaria is outside of the Soviet Union. One additional unit is undergoing pre-operational testing in Bulgaria. Nineteen other units are under construction in the Soviet Union and two units are under construction in Czechoslovakia (Table III).

TABLE I. WWER-440 MODEL 230 REACTORS IN OPERATION (OR SHUTDOWN)

Country	Plant	Unit	Start of operation
USSR	Novovoronezh	3	1971
		4	1972
	Kola	1	1977
		2	1980
	Armenia	1	1973
	(now shut down)	2	1975
Bulgaria	Kozloduy	1	1974
		2	1975
		3	1981
		4	1982
Czechoslovakia	Bohunice	1	1979
		2	1981
Germany	Greifswald	1	1974
	(now shut down)	2	1975
		3	1978
		4	1979

TABLE II. WWER-440 MODEL 213 REACTORS IN OPERATION

Country	Plant	Unit	Start of operation
USSR	Rovno	1	1980
		2	1981
	Kola	3	1982
		4	1984
Czechoslovakia	Bohunice	3	1984
		4	1985
	Dukovany	1	1985
		2	1986
		3	1986
		4	1987
Finland	Loviisa	1	1977
		2	1981
Hungary	Paks	1	1983
		2	1984
		3	1986
		4	1987

TABLE III. WWER-1000 REACTORS IN OPERATION AND UNDER CONSTRUCTION

Country	Units in operation	Units under construction
USSR	16	19
Bulgaria	2	—
Czechoslovakia	—	2

TABLE IV. RBMK REACTORS IN OPERATION AND UNDER CONSTRUCTION

	Units in operation	Units under construction
Chernobyl	3	—
Ignalina	2	1
Kursk	4	2
Leningrad	4	—
Smolensk	3	1
Total	16	4

In the Soviet Union there are also 16 large graphite reactors (RBMK) of the Chernobyl type in operation and 4 under construction, (Table IV) In 1990, RBMK plants generated 47.8% of the total nuclear electricity in the USSR. As of the beginning of 1991, RBMK installed capacity accounted for 45% of the total nuclear generating capacity in the USSR. Since of the Chernobyl accident the safety of these reactors has been a matter of international concern.

2. IAEA WWER 440/230 PROJECT

In response to requests from Member States operating Soviet designed WWER 440/230 nuclear power plants for assistance through of the IAEA's nuclear safety services, a major international Project was established to evaluate these first generation reactors as a complement to relevant on-going national, bilateral and multilateral activities. The Project is extrabudgetary and depends on voluntary contributions from Member States.

The objective is to assist countries operating WWER-440/230 plants in performing comprehensive safety reviews aimed at identifying design and operational weaknesses. The review should form the technical basis for the safety decisions which must ultimately be taken to improve safety.

An advisory group met early in September 1990 to establish the technical scope and a work programme. The advisory group agreed upon a programme involving:

(a) A review of the conceptual design in order to obtain an overall view of the safety aspects of WWER-440/230 plants;

(b) Safety review missions (each lasting about three weeks) by teams of some 15 experts to the individual reactor sites in order to evaluate plant-specific design deficiencies and the conduct of operations, maximum use being made of the IAEA's experience with the provision of safety services - particularly through OSART and ASSET missions; and

(c) Studies on matters of generic safety concern as reactor pressure vessel embrittlement, the applicability of such techniques for the early detection of leaks, accident analysis re-evaluations using modern computer codes and the conduct of probabilistic safety assessments.

A Steering Committee with specialists from Bulgaria, Czechoslovakia, Germany, France, Spain, Switzerland, the United Kingdom and the USSR has been established to monitor the Project and provide technical guidance to the IAEA on the resolution of safety issues and the prioritization of activities. The United States joined the Steering Committee in October 1991.

Observers from OECD/Nuclear Energy Agency (NEA), Commission of European Communities (CEC), World Association of Nuclear Operators (WANO), and the World Bank regularly attend meetings of the Steering Committee, and the International Nuclear Safety Advisory Group (INSAG) has a sub-group to provide advice.

Project coordination lies with the IAEA Secretariat. The schedule of activities through December 1991 is shown in Figure below.

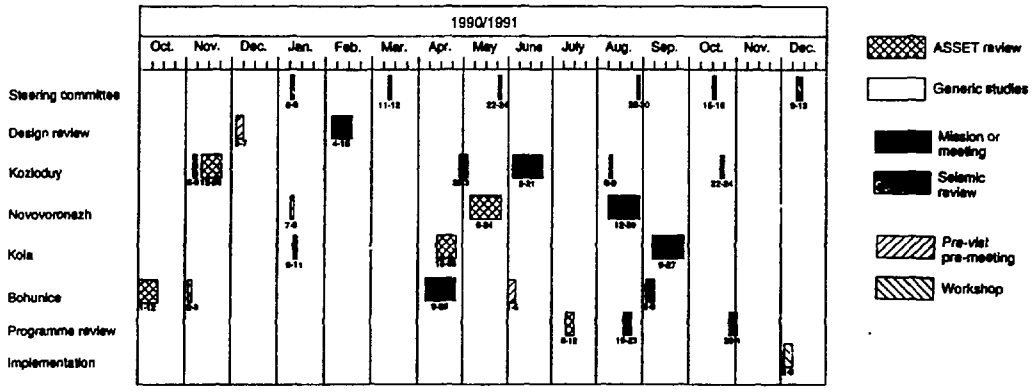

2.1. Concept Review and Missions

In February 1991, the IAEA conducted a review of the design concept of WWER-440/230 nuclear power plants. Thirty-two experts from ten countries and three international organizations participated in the review. Together with twenty-five Soviet specialists, they examined detailed information prepared by Soviet designers and operators. Use was also made of the results of other studies, including the investigation carried out in Germany for the Greifswald NPP in 1989 and the one performed in the USA.

The original design concept of these reactors was developed in the late sixties and early seventies in compliance with the USSR industrial codes, standards and rules which were effective at the time of design. The design basis accident (DBA) is the loss of integrity of the primary cooling circuit equivalent to a hole of 32 mm in diameter.

Overall, it was found that the degree of redundancy, diversity and segregation was low in some of the reactor systems, therefore making them susceptible to common-cause failures. Violations of single failure criteria have also been established. Other weaknesses were also found due to the fact that, at the time of design, specific nuclear standards had not been applied with regard to instrumentation and control and electric power supply. It was further noted that, compared to current practice in the case of most other nuclear power plant types, the design basis is very limited and that safety analyses had been performed of only a narrow spectrum of potential accidents. Confinement function was also found to have safety shortcomings.

There is, however, some built-in safety due to the large water inventory in the primary and secondary cooling loops as compared to other PWRs. Indeed, the fires which occurred at Greifswald (1975) and in Armenia (1982) caused a total loss of heat sink for about five hours without any damage to the reactor core. Another positive feature of the core is the low heat production with respect to fuel weight. The heat flux from fuel to coolant is so low that the safety margin to a heat transfer crisis (DNBR) is significantly higher than other PWRs.In addition, the design concept review pointed to differences between various WWER-440/230 plants, confirming the importance of plant-specific safety review missions. It has also provided a valuable checklist of problems to be investigated during the safety missions.

Safety Review Missions have been conducted to all four individual sites with WWER-440/230 plants in operation, namely: Bohunice, Units 1-2 (CSFR), Kozloduy, Units 1-4 (Bulgaria), Novovoronezh, Units 3-4 (USSR) and Kola, Units 1-2 (USSR).

This set of on-site reviews by teams of about 15 international experts each, have assessed not only the plant-specific design deficiencies but also the overall conduct of operations. The scope of the reviews conducted included:

-core design,
-system analysis,
-mechanical and component integrity,
-instrumentation and control,
-electric power,
-accident analysis;
-plant management and organization,
-quality assurance,
-fire protection,
-operator training and qualification,
-conduct of operations,
-maintenance,
-technical support, and
-emergency planning.

Basic design deficiencies were confirmed, although the value of a number of design strengths and specific plant modifications have also become evident. Moreover, there are major operational shortcomings. There are serious problems with the effectiveness of management in identifying and correcting nuclear safety issues; there are deficiencies in the material conditions of equipment; there are shortcomings in fire protection; vital operating procedures are frequently incomplete and their use is not enforced. Training programmes are insufficient and there is a lack of adequate simulators. Shortcomings in regulatory oversight, particularly with inadequate inspection capability and the lack of enforcement authority have been identified.

Of particular safety concern were the findings of the mission to Kozloduy Units 1-4 in Bulgaria. On the basis of the findings, the IAEA Director General wrote the Bulgarian Prime Minister and urged that he undertake the vitally needed steps to upgrade conditions to allow operation even on an interim basis. The major shortcomings observed in Bulgaria, particularly those related to the material condition of equipment, were not evident on visits to the similar type plants in Czechoslovakia and in the Soviet Union.

Assessment of Safety Significant Event Teams (ASSET) Missions

ASSET missions have also been carried out at all WWER-440/230 plants in operation and to Greifswald 1-4 to review the operational experience of 160 reactor years accumulated by these plants, and to assess the appropriateness and completeness of corrective actions taken by plant management to prevent recurrences of incidents.

In-depth root cause analyses have been performed of operational events which were selected either by their high safety significance or because they are of a recurring nature or corrective measures have not yet been implemented. Recommendations were made to:

-improve certain areas of equipment operability, personnel proficiency and procedural adequacy, and

-enhance plant programmes for prevention of incidents, i.e. quality control, preventive maintenance, surveillance and experience feedback.

ASSET findings confirmed design deficiencies and operational problems reported by the safety review missions.

Seismic Safety Review Missions

In addition, the IAEA has carried out missions to the Bohunice and Kozloduy sites to review the safety of these plants against seismic hazards, with emphasis on - inter alia - earthquake design acceleration and the seismic vulnerability of structures and components important for safety.

The original design of WWER-440/230 plants did not take into account external hazards, in particular earthquakes. For this reason, at least the two sites investigated have major seismic weaknesses.

As a consequence of the Romanian (Vrancea) earthquake in 1977 with estimated 0.1 g at the Kozloduy plant site and which caused some damage to the plant, a seismic upgrading programme was started. The same site was later affected by two other severe earthquakes with their origin at Vrancea in 1986 and again in 1990.

On the basis of the IAEA mission which conducted a plant walkdown to evaluate seismic safety it was concluded that the Kozloduy NPP has major seismic safety problems even for the minimum design acceleration of 0.1 g recommended internationally to all NPP sites (NUSS 50-SG-51, Rev. 1).

Recommendations include the replacement of some plant equipment, the installation of additional supports, and the establishment of a basis for prioritization of seismic safety upgrading. It should be noted based on the seismic walkdown that a number of simple improvements can be implemented immediately which can considerably impact the capability of the plant to withstand an earthquake.

A seismic safety review mission was also conducted at Bohunice to review the ongoing seismic upgrading programme. A maximum expected intensity of 8 on the MSK scale corresponding to a design acceleration of 0.25g was adopted for the seismic level corresponding to the safe shutdown earthquake. It was based on actual recorded earthquakes with maximum ground acceleration ranges from 0.14 to 0.30 g.

Measures recommended by the mission included a review of the anchorage of safety related electrical cabinets, seismic ruggedness of on-site emergency power (e.g. diesels, batteries), and a seismically protected service water cooling system.

2.2. Ranking of Safety Issues

An important part of the IAEA Project was the evaluation of the safety significance of the deficiencies identified during the conceptual design review and safety review missions.

Generally accepted current safety principles and objectives such as IAEA NUSS Codes and Guides and INSAG 3 together with the technical knowledge and experience of the international experts who participated in the Project formed the basis for the identification of specific deficiencies (i.e. safety items). Individual safety items related to the same major safety concern have been grouped in broader categories characterizing *safety issues.* Subsequent to their identification, safety issues are classified according to the potential impact in defense-in-depth. Finally, issues both related to design and operation are ranked according to their safety significance in four categories of increasing safety severity.

Category I: Issues in Category I reflect a departure from recognized international practices. It may be appropriate to address them as part of actions to resolve higher priority issues.

Category II: Issues in Category II are of safety concern. Defense in depth is degraded. Action is required to clear the issue.

Category III: Issues in Category III are of high safety concern. Defense in depth is insufficient. Immediate corrective action is necessary. Interim measures might also be necessary.

Category IV: Issues in Category IV are of the highest safety concern. Defense in depth is unacceptable. Immediate action is required to overcome the issue. Compensatory measures have to be established.

3. PROJECT RESULTS

To facilitate the analysis and consolidation of findings the results from the Conceptual Design Review and of the Safety Review Missions to the four plant sites have been compiled in a computerized database. This provides for easy interrogation and review of the available information. The database stores about 1,300 (records) items which reflect specific safety concerns.

Collectively the safety items in the IAEA database, the findings of the seismic safety missions, and the ASSET results provide a comprehensive and systematic evaluation of the safety of WWER-440/230 plants.

Table V presents a summary of the safety issues and their ranking. A detailed description of the findings is reported in IAEA TEC-DOC 640.

TABLE V . RANKING OF SAFETY ISSUES

Area	Category			
	I	II	III	IV
Design				
Core		4		
Systems		5	7	3
Components		2	5	5
Instrumentation and control		4	7	1
Electrical		1	2	2
Accident analysis		4	5	
Fire protection			3	
Total (design)		20	29	11
Operation				
Management	2	3	6	2
Operational procedures		2	1	1
Plant operations	1	2	3	
Maintenance	1	2		1
Training	1	1	3	
Emergency planning		2	3	
Total (operation)	5	12	16	4
Total	5	32	45	15

4. IAEA PROJECT FUTURE ACTIVITIES

The experience gained by the IAEA in the framework of the WWER Nuclear Safety Project together with its other regular safety services and activities place the IAEA in a unique position among the intergovernmental organizations to provide the technical advice necessary to ensure that the assistance programmes respond both to genuine safety needs and priorities are consistent with long-term safety requirements being developed at the international level.

The second phase of the IAEA Project will therefore focus on helping countries to review safety improvements required to WWER-440/230 NPPs and to make the best use of the assistance which they receive through - for example - the CEC and WANO. Such assistance should be in line with the recommendations resulting from the IAEA Project and should not duplicate work already completed or initiated internationally or within the framework of national programmes. An important feature of such assistance will be the strengthening of the technical capabilities and the role of national regulatory bodies.

It is also proposed for the IAEA to participate in the OECD Group 24 coordination as a special technical advisor for identifying priorities and providing technical recommendations.

The IAEA is also going to prepare in cooperation with the CEC a data bank on nuclear safety projects in Eastern Europe.

The actual programme implementation will take into consideration activities undertaken in the framework of other national or multilateral programmes to avoid duplication of efforts.

NUCLEAR SAFETY IN SMALL AND MEDIUM SIZED COUNTRIES

Rafael Caro

Consejo de Seguridad Nuclear

Madrid, Spain

SUMMARY

In this paper the Nuclear Safety and the Radiological Protection in Spain will be described. This country can be considered as a good example of that discipline in a small or medium size country.

The number of nuclear plants in Spain is nine, meaning a 38% of the net electrical production . The technology of those plants is American (Westinghouse and General Electric), and the Spanish participation in their construction and design ranges from the first one in 1970 which was a Turn-Key project to the last generation ones with a national participation of around 90%.

These plants being of American origin, the regulations are, too, very much influenced by the American legislation in this field. Even more, the structure of the Nuclear Regulatory Body is very similar to the U.S NRC. A brief description is given of it and of its tasks.

As for the industrial infrastructure, most of the components of NPP are built under license by Spanish companies. The European integration, though, is producing a certain unstabilizing effect on them.

Invited paper, presented at the 17th National Meeting of the Israel Nuclear Society, Beer-Sheva, Israel, May 4, 1992.

On the Accuracy of Benchmark Transport Calculations

R. L. Perel, U. Salmi, J. J. Wagschal
Racah Institute of Physics
The Hebrew University of Jerusalem
91904 Jerusalem, ISRAEL

Over the last quarter of the century quite a few benchmarks for the numerical determination of the space, time, angle or energy distribution of particles in an assembly have been published [1, 2, 3]. The purpose of utilizing such benchmarks varies according to the interest of the user. We are currently interested in the benchmarks for data testing of recent evaluated data files. When using a benchmark problem for data testing one has to keep in mind that the measurements of the critical mass in simple geometry (spherical for instance) are very accurate. Translating the experimental uncertainty to reactivity one gets that the typical uncertainty in the effective multiplication factor, k_{eff}, is about 1 milli-k (i.e. 1000*(k-1)=1). The specifications of a data testing benchmark problem should thus be such that residual calculational uncertainties due to the specification coarseness should not exceed a fraction of a milli-k.

The CSEWG benchmark book [2] has the following recommended mode of calculation for the one-dimensional transport calculation of a bare core:

a. S_{16} (angular quadrature)
b. 40 (spatial) mesh intervals
c. vacuum boundary at the surface
d. a 26 group structure with half lethargy unit width and an upper energy of 10 MeV.

For reflected spheres only 30 mesh intervals are recommended in the core. In both cases there is no recommendation for the treatment of anisotropic scattering.

Pazy et al. [4] have outlined, already almost twenty years ago, how to correct calculational results in order to overcome inaccuracies stemming from coarseness dictated by the computing technology limitations of that era. In particular they have shown that using an isotropic source with a transport correction rather than taking a few terms (L >= 3) in the anisotropic scattering source Legendre expansion, leads to a shift of 3 milli-k in reactivity calculations of bare spheres and of over 8 milli-k in reactivity calculation of thick reflected spheres.

As to the upper limit of the recommended group structure, the limit of 10 MeV leaves out over 0.2% of the fission neutron yield with energies higher than 10 MeV. Ignoring these neutrons results in lowering the effective multiplication factor, k, of Jezebel or Godiva by 3 milli-k. Even if one does not ignore these neutrons, and the fission spectrum is renormalized to unity, the resulting k is still lower by more than

1 milli-k when compared to a calculation with a 15 MeV upper energy limit. Realizing that the "missing" neutrons are the higher energy neutrons which are more potent, and accounting for them in the highest energy group still results in a k that is too low by more than half a milli-k. This lower k is the direct outcome of the simple fact that $\nu\sigma_f$ is an increasing function of energy in the MeV range and that the average group value did not take into account the $\nu\sigma_f$ value over 10 MeV.

Another shortcoming of the CSEWG specifications can be identified in the constant equal lethargy width of the energy groups. The refining of the group structure between 10 keV and 6 MeV reduces k by over one milli-k before convergence is reached. On the other hand the further refining of the energy groups above 6 MeV (but using the 15 MeV upper limit) or below 10 keV results in a change of less than 0.05 milli-k.

The recommended spatial mesh seems adequate since it is only 0.1 milli-k off the converged value. On the other hand, k calculated by S_{16} is still about 0.4 milli-k off the converged value. This should be modified by using a higher quadrature order.

In conclusion we would like to suggest that the recommended mode of calculation of the CSEWG benchmarks, which were clearly defined for data testing, should be modified taking into account that modern computing technology enables inexpensive detailed calculations with as few approximations as possible. Alternatively the recommended mode of calculation should be omitted entirely, leaving it up to the user to chose his mode of calculation (e.g. Monte Carlo or deterministic methods). It will be the user's responsibility to make sure he has achieved the proper convergence required by the problem at hand.

References

1. Argonne Code Center: Benchmark Problem Book, Argonne National Laboratory, ANL-7416 (1968) and later revisions.

2. ENDF-202, Cross Section Evaluation Working Group Benchmarks Specifications, BNL-19302, National Neutron Cross Section Center, Brookhaven National Laboratory, (1974) with later revisions and additions.

3. MCNP: Neutron Benchmark Problems, Los Alamos National Laboratory, LA-12212 (1991).

4. A. Pazy, G. Rakavy, I. Reiss, J. J. Wagschal, A. Yaari and Y. Yeivin, Nucl. Sci. and Eng., **55**, p. 280 (1975).

A PRELIMINARY ANALYSIS OF THE AP600 REACTIVITY CHARACTERISTICS AT B.O.L

B. Tavron and L. Reznik
Nuclear Engineering Department, Israel Electric Corporation

INTRODUCTION

The design strategy of the Westinghouse AP600 Advanced Light Water Reactor follows the objectives of the DOE and EPRI for ALWRs, where one of them is: "To use experience-based power generation components so that plant prototype or demonstration models are not required". According to this strategy the AP600 core design is based on a conventional Westinghouse 17 X 17 Optimized Fuel Assembly (OFA). However some modifications are introduced in the AP600 core: The reflectors employ stainless steel rods - to reduce core leakage and vessel wall fluence, also the advanced Wet Annular Burnable Absorber (WABA) rods are used. This 'nearly' conventional nuclear design allows us to use conventional PWR analysis tools to estimate the core characteristics. In this work we have evaluated the B.O.L fuel temperature reactivity parameter of this core by using the Pennsylvania State University LEOPARD-MCRAC code package. Calculational results show that the Doppler reactivity coefficient does not differ significantly from that of traditional designs.

The LEOPARD-MCRAC Computer code package

The LEOPARD code[1] is used to generate macroscopic cross sections for the various types of core assemblies. The code has a microscopic cross section library generated from ENDF/B-IV. The thermal spectrum calculations uses the Wigner - Wilkins[2] treatment with modified disadvantage factors (the ABH method[3]). The calculations are made for a cell consisting of the pellet, clad, moderator regions as well as an extra region compensating for presence of structural materials. The thermal energy group cutoff is at 0.625 eV and it contains 172 fine energy groups. In the ephithermal spectrum calculations the B-1 approximation is used as in the MUFT code. The resonance integral of U^{238} is calculated from the empirical formulation given by Strawbridge[4] and includes an iterative search for calculation of the spatial resonance shielding. Burnup calculations are made for a given time (or burnup) step at power level and soluble boron concentration. The resulting macroscopic cross sections depending on burnup and soluble boron concentration are given as polynomials and stored as a data library (the ADDs library) suitable for subsequent MCRAC code runs.

The MCRAC code[5] is used for diffusion and fuel management calculations. It employs a finite difference approximation to the 2 energy group, 2-dimension diffusion equation. The critical boron search option in MCRAC was used to determine the necessary soluble boron concentration.

AP600 Core Design and simulation

The AP600 core is of 157 in. diameter, containing 145 OFA assemblies, surrounded by reflector assemblies containing closed packed stainless steel rods. The active core height is 12 feet. This core design results in a low power density of 74 KW/l and relatively low neutron leakage. Selected fuel assemblies contain burnable poison rods with variable boron concentrations. Soluble boron and 45 control rod clusters are used for control. Lack of detailed design data forced us to estimate many core parameters. For example, the reflector region is assumed to contain 90% stainless steel and 10% water. The WABA were represented by an equivalent burnable boron concentration - the amount of the equivalent soluble boron and the burnable rod positions were estimated using design data from existing Westinghouse core designs[6]. The temperatures assumed for the analysis were: 310 °C - for moderator, 340 °C - for cladding and 690 °C for fuel. For this design, the MCRAC code criticality search has determined 940 ppm of soluble boron at B.O.L in order to reach criticality. Burnable boron rods were shuffled in the core and their concentrations were adjusted in order to get a reasonable power shape. The power distribution of the core at B.O.L is shown in Fig-1.

The fuel temperature reactivity coefficient is defined as the change in reactivity per change in effective fuel temperature, and depends primarily on the Doppler broadening of U^{238} and Pu^{240} resonance absorption. At B.O.L, with fully withdrawn control rods and no Xenon, the core has the highest (less negative) fuel temperature reactivity coefficient since in fresh fuel there is no Pu^{240}. The fuel temperature reactivity coefficient was calculated by changing the fuel temperature by 5°C and evaluating the resulting core reactivity change. This is a 'brute force' method which is commonly used in scopeing calculations.

Results and Discussion

The resulting AP600 estimated fuel temperature reactivity coefficient is compared with corresponding coefficients from Westinghouse and Framatome designs: The Westinghouse Sundesert nuclear power station design[6] (2775 MWt, 3-Loop, 157 assemblies of 17 X 17 older Westinghouse design) and Framatome standard 3-loop design[7] (2770 MWt, 157 assemblies, 17 X 17 Framatome design). These fuel temperature reactivity coefficients for effective fuel temperature of 700°C are listed in Table-1.

Table-1

	AP600 estimation	Westinghouse Sundesert 3L	Framatome Standard 3L
Fuel temp. coeff.	-2.3 pcm/°C	-2.75 pcm/°C	-2.85 pcm/°C

pcm = percent mille = 10^{-5} $\ln(k_1/k_2)$

The Doppler reactivity coefficient depends mainly on the fuel assembly design - the H/U ratio. Due to the different assembly designs and other design variations, we have obtained up to 17% difference in the fuel temperature coefficient. This result is within the design limits of nuclear plants and resembles traditional 17 X 17 OFA's design results.

Summary

In this work we have simulated the B.O.L AP600 core with the PSU LEOPARD-MCRAC code system. The Doppler fuel temperature reactivity coefficient has been evaluated. Estimated design data have been used in the simulation. As follows from our calculations, the new features in the AP600 design, lower core power density (large core), stainless steel reflector and WABA rods, do not influence significantly the fuel temperature reactivity coefficient. This work is however of preliminary character and it should be noted that other reactivity parameters should be calculated as soon as more design data becomes available.

Refrencese

1) R.F. Barry, 'LEOPARD - A Spectrum Dependent Non-Spatial Depletion Code', Westinghouse Electric Corporation, WCAP-3269-26 (1963).

2) F. R. Allen, 'Homogenisation of a Wigner-Seitz Cell in two Group Diffusion Theory', Atomic Energy Establishment Winfrith, United Kingdom, AEEW-R-594 (1968).

3) A. Amouyal, P. Benoist and J. Horowitz, 'Norevelle Methods de Determination du Factor d'Utilisation Thermique d'une Cellule', J. Nucl. Energy, 6, 79, (1957).

4) L. E. Strawbridge and R. F. Barry, 'Criticality Calculations for Uniform Water-Moderated Lattices', NS&E 23, 58-73 (1965).

5) H. Y. Huang, J. P. Colletti, Z. H. Kodah, S. S. Kim, 'MCRAC - Multiple Cycle Reactor Analysis Code', Pennsylvania State University, 315-497991 (1981).

6) Sundesert Nuclear Power Station, PSAR, San Diego Gas & Electric Company.

7) Standard 3-Loop, PSAR, Framatome.

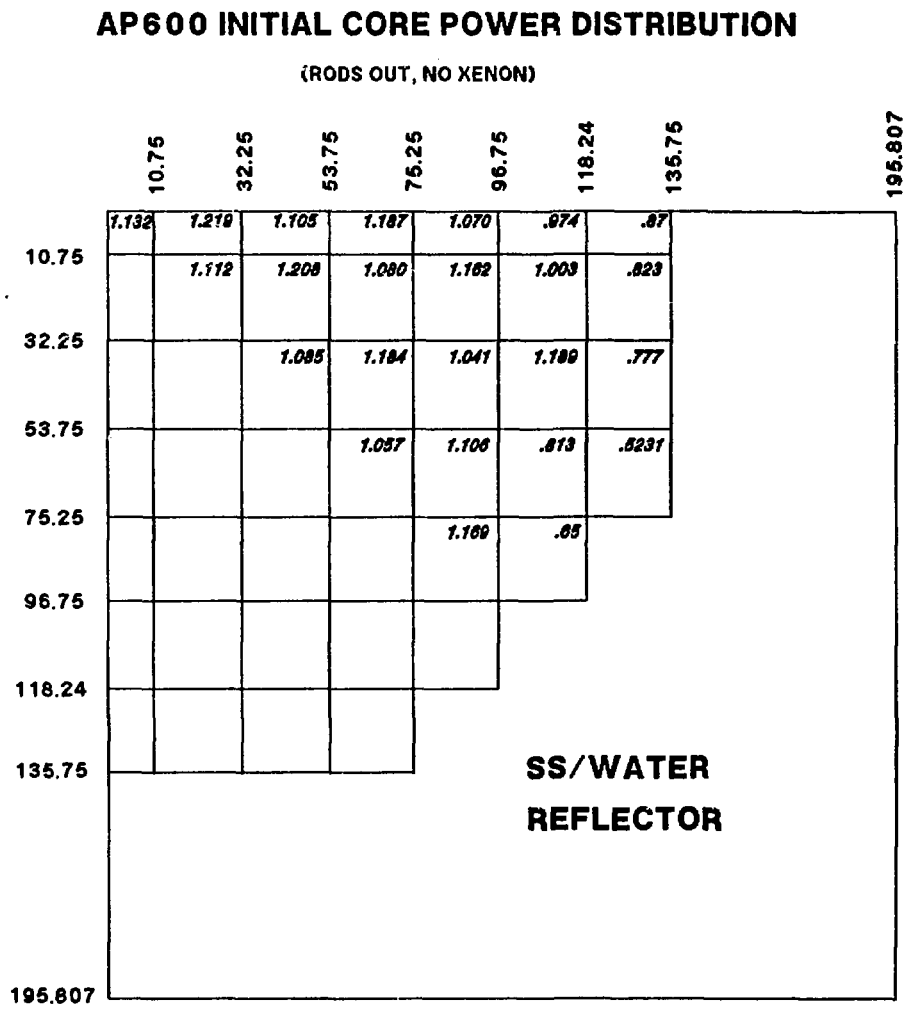

Fig - 1

Transport of Neutrons in Double Random Media

Yigal Ronen
Department of Nuclear Engineering
Ben-Gurion University, Beer-Sheva, Israel

1. INTRODUCTION

There is a growing interest in transport of neutrons in random media[1,2,3]. In a recent paper[1] it was demonstrated that for randomly nonhomogeneous media the uncollided flux density, which is calculated with the average density, is always underestimated . As a result, the leakage from a random medium is always greater than that of a homogeneous medium with an average density.

Two types of random media are of particular interest. The first type includes random media with voids. In this category we can include porous materials, boiling water and pebble-bed reactors. In pebble-bed reactors the random characteristic is a result of the voids between the pebbles.

The second type of media are those which include aggregates. The most common example of an aggregate medium is concrete.

Both these types of media are double random ones. Their first random feature is related to the size of the voids or the size of the aggregates. Their second random feature is related to the location of the void or the aggregate in the media.

Dealing with these types of double random media requires that the probability density function (p.d.f) of the voids, or the aggregates be known. Since there are many voids, or aggregate stones, in the media we are considering, a normal distribution of the voids, or the aggregates, is a good choice. Thus, in order to deal with one random aspect of these media, it is sufficient to know the average size of the voids, or the aggregates, and their related standard deviations. These two parameters can be determined, in most cases, experimentally for the required medium.
The second feature of the randomness will be discussed later.

2. THE APPROACH

In this paper, we will address the problem of the transport of neutrons in these double-random media. The key point in our approach lies in the assumption that random treatment is valid to these types of problems. By a valid random treatment, or our randomness assumption, we mean that two random media with the same random characteristics will yield about the same results with respect to the transport of neutrons. For instance, if we take two blocks of concrete with the same volume and shape, and the concrete is of the same type, we do expect that the transport of neutrons in these two concrete blocks will be about the same, although the location of their aggregates is different. We expect that this assumption will be valid if the medium is large enough, compared to the size of the aggregates or voids, and that there are many such voids or aggregates in the medium.

In those cases in which the randomness assumption is valid, we suggest that the problem of transport of neutrons in random media will be solved by solving the transport equation in a predetermined random media. In other words, we will calculate the density distribution of some random medium with the same characteristic properties as the actual random medium. Thus, by determining the

density of our theoretical medium, we can actually solve the transport equation in the known medium.

3. THE METHOD

As discussed in section 2, our approach to the problem of the transport of neutrons in random media is to predetermine n(**r**) in a random manner, and then to solve the integral transport equation with the known n(**r**).

The first stage in determining n(**r**) is to decide on the number M of different void volumes, or aggregate volumes. Denoting the volume of a void, or aggregate, belonging to a group i as V_i, the number of such voids in a given volume is N_i. Thus, the total volume of the voids, or the aggregates, in a given volume, or in the whole medium, is :

$$V_v = \sum_{i=1}^{M} N_i V_i = \text{total void volume.} \qquad (1)$$

The values of V_i and N_i are obtained from the given p.d.f. of the voids, or the aggregates. The total number of voids, or aggregates is :

$$\sum_{i=1}^{M} N_i = N_v \,. \qquad (2)$$

The second stage is to determine the geometry and the mesh size of our problem. If the voids are considered as spheres, a 3-D spherical geometry must be used. If the voids are considered as 3-D cubes or 2-D squares , Cartesian geometry must be used. In Cartesian geometry, the mesh interval should be smaller, or equal to the dimensions of the smallest void. The total number of 2-D or 3-D mesh intervals is N_t.

The third stage is to draw N_v random numbers between 1 and N_t. Each number will indicate a location. Thus, the total number of random locations is N_v. In each mesh location, a void will located. In this manner, N_v locations will determine N_v voids.This procedure can locate all the different voids. As a result, n(**r**) is explicitly determined by a random process. Knowing n(**r**), Eq. (1) can be solved numerically by standard procedures and transport codes.

4. A NUMERICAL EXAMPLE

As a numerical example we have considered a square reactor core with dimensions of 42 cm. The reactor core was calculated in two energy groups. The cross sections of this core represent a PWR one. The core was calculated with a 2-D integro-differential transport code DOT 4.2 [4]. For the calculations a quarter of the core was represented by 140 x 140 mesh intervals. Thus a quarter of the core was represented by 19600 squares. The boundary consitions used were reflective for the left and bottom sides and vacuum for the right and up sides.

We have considered two cases. In one case the core was unchanged but all cross sections were multiplied by 0.8. Namely, a reduction of 20% in the density of the core. The second case was that 20% of the meshes were voided and 80% of the meshes have the original density. The locations of the voided meshes were randomly chosen. We made two such random choices. The

differences in the random results were not large.The compasion between the homogeneous and the two inhomogeneous random results are given in Table 1.

From this numerical example we see that a reactor with a homogeneous core has less fast leakage about 0.7% and a higher k_{eff} of about 0.09% compared to a random inhomogeneous core. The differences are not large due to the fact that the core considered is large and the leakage is small. A more profound effect is expected in smaller cores.

Table 1.

Comparison between Homogeneous and Random Heterogeneous Transport Calculations

	k_{eff}	Group 1 Net Flow (%)*	Group 2 Net Flow (%)*
Homogeneous calculations 2.64 with 80% density	1.03	14.66	
Inhomogeneous calculations with 20% random voids. Run 1	1.036	14.76	2.68
Inhomogeneous calculations with 20% random voids. Run 2	1.036	14.78	2.68

* Right and bottom.

References

1. Y. Ronen, "A note on Particle Interaction with Randomly Inhomogeneous Medium"
Kerntechnik, **56**, 47 (1991)
2. G.C.Pomraning "Transport and Diffusion in a Statistical Medium", Transport Theory and
Statistical Physics **15, 773** (1986)
3. M.M.R. Williams *Random Processes in Nuclear Reactors*, Pergamon Press Oxford (1974).
4. W.A.Rhoades, D.B.Simpson, R.L.Childs, and W.W. Engle, Jr., "The DOT-IV Two
Dimensional, Discrete-Ordinates Transport Code with Space Dependent Mesh and Quadrature,"
ORNL/TM-6529, Oak Ridge National Laboratory (1978); see also "DOT-IV Version 4.2,"
CCC-320, Oak Ridge National Laboratory (1982).

VARIABLE SEPARABILITY IN FLUX MODES AS A BASIS FOR PIN POWER RECONSTRUCTION

M.Abudi AND M.Segev

DEPARTMENT OF NUCEAR ENGINEERING
BEN GURION UNIVERSITY IN THE NEGEV
BEERSHEVA

The expression

$$\underline{\phi}(x,y) = \underline{\underline{\underline{\chi}}}(x)\,\underline{\underline{\underline{Y}}}(y)\,\underline{f} \qquad (1)$$

("_" denoting a 2*1 column vector

"=" denoting a 2*2 matrix

"r" denoting a diagonal 2*2 matrix),

approximating a 2-group flux in a homogenised assembly, was used as a starting point for the development of the NOXER nodal core code [1]. presently the utility of this expression is demonstrated as concerns the reestablishment of the flux detail inside the assembly, namely 'pin power reconstruction'.

Usually [2,3] pin power reconstruction derives from describing the 2G fluxes with the following set

$$\left.\begin{aligned}\phi_1(x,y) &= \sum_{i=0}^{N} a_i\, x^{p_i} y^{q_i} \\ \phi_2(x,y) &= \sum_{i=0}^{N} b_i\, F_i(\kappa_i^F x)\, G_i(\kappa_i^G y)\end{aligned}\right\} \qquad (2)$$

where F and G stand for the cosh and sinh functions, and where the coefficients k are related to the diffusion coefficent and absorption cross section of group 2. The use of the hyperbolic functions was found necessary in order to properly account for the flux strong variability in the vicinity of assembly corners. The inaccuracy of pin powers based on eqs. (2) may typiccally reach 2% to 3% for assemblies not immediately adjecent to the reflector, and may be as high as 10% to 15% in pins adjecent to the reflector.

In the central portion of an assembly, away from the corners, separability in the form of eq. (1) indeed holds. Consequently a pin power reconstruction method based on set (1) for the center portion of the assembly, and on set (2) for the periphery of the assembly, is found to considerably reduce the inaccuracies incurred in a method base solely on set (2).

The table below exemplifies this improvement for the BOL of the ZION-II first cycle and for the BOC of TMI cycle 5. The accurate pin powers relative to which the comparisons are made, were calculatd with DOT4.2

REFERENCES

[1] M.SEGEV
TWO GROUP DIFFUSION THEORY BASED ON SEPARATION OF VARIABLES
Ann.Nucl.Energy 15,1988

[2] K. KOEBKE, L.HETZELT
ON THE RECONSTRUCTION OF LOCAL HOMOGENOUS NEUTRON FLUX AND CURRENT DISTRIBUTIONS OF LIGHT WATER REACTORS FROM NODAL SCHEMES
Nucl. Sci. Engn. 91, 1985

[3] K. SMITH, R.KEMPE
SIMULATE-3 PIN POWER RECONSTRUCTION METHODOLOGY AND BENCHMARKING
Nucl. Sci. Engn. 103, 1989

TABLE 1 : PIN POWER RECONSTRUCTION

ZION -II, CYCLE I, BOC

	set (2)	sets (1) + (2)
max pinpower error % in the core	11.6	10.7
average pinpower error % in the core	0.58	0.40
error in core hottest pin % pin (8,10) in assm. (1,5) hottest pinpower = 1.42	0.68	0.41

TMI - I, CYCLE 5, BOC

	set (2)	sets (1) + (2)
max pinpower error % in the core	8.7	7.9
average pinpower error % in the core	0.93	0.70
error in core hottest pin % pin (8,8) in assm. (1,1) hottest pinpower = 1.99	2.40	0.24

THE USE OF MODERN EVALUATED NUCLEAR DATA IN STANDARD LATTICE ANALYSIS CODES

by

W. Rothenstein* and B. Tavron**

Introduction

It is sometimes desirable to update the multigroup cross-section data of standard lattice analysis codes which are used in order to prepare few group parameters for the different regions into which a reactor core and the reflectors are subdivided. This is an essential preliminary step for the calculation of detailed flux and power maps, and for criticality studies. The most recent evaluated nuclear data (1) can then be used for the complete range of problems which have to be addressed, when the reactor behaviour is being investigated. Multigroup lattice analysis is carried out, in general, by codes which combine a certain measure of sophistication with the need for rapid calculations. The analyses must be made for many subregions of the reactor, in which the material composition may be different and in which different neutron absorbers may be present. In addition, temperature effects must be taken into account, possibly with feed back between the nuclear and thermal hydraulic aspects of the problem. The changes of composition with fuel depletion require numerous further runs of the analysis codes, as well as the need to include new actinides and fission products in different amounts. Consequently, updating multigroup data libraries may be a major task. An example is the VSOP code package (2) which is used for the analysis of High Temperature Reactors.

There is a conflict between the nature of the calculations made in the multigroup lattice analysis codes, and the philosophy underlying the most recent evaluations of the basic nuclear data of different isotopes, or of materials containing mixtures of isotopes, such as the ENDF/B-VI data which have recently become available. The basic evaluated data provide a very detailed description of the nuclear properties for a large number of different reaction types and for the complete range of energies of the neutrons which maintain the chain reaction, 10^{-5} eV to 20 MeV. The evaluators prescribe interpolation procedures which should be used between neighbouring energy points at which the data are given in the appropriate tables. They also provide precise information of the formalisms which are adopted to quantify certain nuclear properties, and for which the parameters are given as functions of energy. Examples are fission spectra, thermal scattering laws and resonance cross-sections.

* Nuclear Engineering, Technion

** Nuclear Engineering Department, Israel Electric Corporation

This volume of detail cannot, in general, be utilised fully in multigroup codes, which, as stated previously, should handle a single problem very rapidly. Only the most important neutron interactions can be treated for the different reactor nuclides; angular distributions of scattered neutrons are frequently handled only for linear anisotropy of scattering; and simple weighting functions have to be specified for averaging the basic point cross-section data over the individual fine energy groups. Resonance shielding effects are in many cases treated by somewhat drastic approximations. For all these reasons the basic nuclear data have to be adapted to the calculational models of the lattice analysis codes which are used, as it is not possible to change the codes in such a manner, that the full information contained in the nuclear data files can be taken into account.

The present report deals with a material which is used as a neutron absorber in High Temperature Graphite Reactors. There were no multigroup data for Hafnium in the thermal and epithermal libraries of the VSOP code. On the other hand, natural Hafnium is one of the materials for which ENDF/B-VI data are now available. Neutron absorption by Hafnium occurs at thermal energies, and in many resonances, most of which are above the thermal energy region. The preparation of multigroup libraries for natural Hafnium in the VSOP format from the ENDF/B-VI basic data is discussed. Special steps were taken to ensure that resonance shielding effects can be obtained with good accuracy for this absorber material by the Nordheim method of the ZUT code, which is routinely used in conjunction with VSOP to calculate the effective resonance integrals of the fertile nuclides in HTGR fuel elements.

ENDF/B-VI Data for Natural Hafnium. Preparation of Multigroup Cross-Sections

Natural Hafnium (Z=72) is material MAT=72000 in the ENDF/B-VI library; it is a mixture of 6 isotopes. The isotopic abundances as number fractions, their spin quantum numbers, dilute resonance integrals and 2200 m/sec neutron capture cross-sections are given in Table 1. Resonance parameters are given for numerous s-wave and p-wave resonances in the resolved resonance energy region which starts at 10^{-5} eV for all isotopes, the upper energy of this region being isotope dependent. They are continued into the region of the unresolved resonances which ends at 10^5 eV for all isotopes. Resonance parameters are given for the Breit-Wigner single level formalism and include the neutron, gamma, and total widths for each resolved resonance, as well as the energy of the resonance peak and the spin quantum number of the Compound Nucleus.

Table 1
Some Isotope Dependent Data for Natural Hafnium

Isotope	Spin I	Abundance (# fraction)	Dilute RI (barns)	$\sigma_{n,\gamma}$ (2200/msec)
HF-174	0	0.0016	446	391
HF-176	0	0.0520	337	21.8
HF-177	3.5	0.1861	7220	376
HF-178	0	0.2730	1747	84.6
HF-179	4.5	0.1363	451	40.4
HF-180	0	0.3510	29	13
Element		1.0000	1900	104.5

The basic data include, apart from the contributions of the resonances to the radiative capture cross-section at thermal energies, a 1/v additional thermal capture cross-section for HF-174, 176, 178, while this effect is given for HF-180 by the presence of a negative energy resonance.

The NJOY Code (3) was used to prepare Multigroup Cross-section Data sets for Natural Hafnium in the GAM Code group structure at epithermal energies, and in the THERMOS Code group structure at thermal energies as used in the VSOP Code package. In addition to the group structures the NJOY Code requires weighting spectra for cross-section averaging and a temperature at which the cross-sections are to the evaluated. For the former a 1/E weighting function together with the U-235 fission spectrum above about 0.1 MeV was used at epithermal energies; this choice is sufficiently accurate for fine energy groups with lethargy widths of 0.25 each, since the only assumption is that the weighting flux has approximately the chosen shape for the narrow energy range of any single group. The thermal spectrum for the THERMOS group cross-sections was replaced by a histogram, i.e. a constant weighting flux in each fine energy group. At epithermal energies 0°K was selected as the temperature, since resonance shielding is calculated in the ZUT section of VSOP at the temperature at which the Hafnium absorber is used. Room temperature was specified for the calculation of the THERMOS group cross-sections by NJOY for the use of Hafnium as an absorber in experiments performed at the KFA.

The problem was how to handle the large amount of resonance data for Hafnium as given in ENDF/B-VI for MAT = 72000, within the methodology of VSOP. There is no

justification to use the ZUT code for all of the 236 resonances for which resonance parameters are given in the Hafnium ENDF/B-VI data, and even less is there a need to estimate resonance shielding at the energies of the unresolved resonances. There are, however, some resolved resonances for which self shielding is so important that it must be taken into account just as in the case of the large resonances of the fertile isotopes in the fuel.

To this end the dilute resonance integrals of all the resolved resonances of Hafnium were calculated and weighted with the abundances of the respective isotopes. The values were then sorted and it was found that 8 resolved resonances contribute about 1800 of the total 1900 b dilute resonance integral. They included the 7.8 eV resonance of HF-176, the 1.094, 2.38, 5.892, 6.571 and 8.869 eV resonances of HF-177, the 7.78 eV resonance of HF-178, and the 5.68 eV resonance of HF-179.

In order to enable the VSOP multigroup code to calculate the resonance shielding of these resonances, whenever needed, in its GAM and THERMOS sections at epithermal and thermal energies, two Hafnium runs were made with NJOY. The first was for the natural Hafnium element, MAT=72000, of ENDF/B-VI. The second was for a pseudo Hafnium material for which the above 8 resonances were removed by deleting their resonance parameters from the ENDF/B-VI data, and re-entering them into the ZUT code library of VSOP with their appropriate g_J values. The total Hafnium absorption is then obtained by adding the shielded resonance cross-sections resulting from the ZUT calculations for Hafnium to the corresponding capture cross-sections in the pseudo Hafnium libraries, both at epithermal energies and in the thermal energy groups.

Analysis of the H1 Core of the KAHTER Assemblies

The H1 room temperature critical assembly of the KAHTER experiments (4) which contains Hafnium absorber spheres was analysed by the VSOP code package with the ENDF/B-VI group cross-sections for HF described here. The HF was in the form of kernels, 42 microns in diameter, in a graphite matrix of 4.6 cm diameter. The outer diameter of the absorber sphere was 6.0 cm, like the fuel spheres, including the graphite shell surrounding the matrix. Each absorber sphere contained 4.2 gm of Hafnium in the form of Hafnium Carbide.

The group data were those for natural HF in the VSOP group structure of the GAM and THERMOS sections of the code package, when resonance shielding was not taken in to account.

When resonance shielding was treated by the Nordheim method in the ZUTDGL section of VSOP, the pseudo HF group cross-sections were used; for this material the THERMOS library was corrected for the tails of the 8 missing resonances of the Hafnium isotopes. The ZUTDGL resonance absorption calculations were made in four runs, one for each of the isotopes of HF to which the 8 principal resonances belong. The run for the isotope of number fraction α was made with atom density (αN_{HF}) of the principal absorber, where N_{HF} is the atom density of natural Hafnium in hafnium-carbide of density 12.2 gm/cc. In accordance with the Nordheim procedure the first admixed material is carbon which has atom density $N_c/(\alpha N_{HF})$ relative to the atom density of the principal absorber. The second admixed material consists of the other HF isotopes which have atom density $(1-\alpha)/\alpha$ relative to that of the principal absorber.

The attached figures show the epithermal and thermal group cross-sections used for the analysis of the H1 critical assembly by the VSOP code package, without and with resonance shielding. The former consist of the group cross-sections obtained by the NJOY code for the ENDF/B-VI data of natural HF at infinite dilution in the resonance energy region. The latter are the corresponding group cross-sections of pseudo HF augmented by the shielded group cross-sections of the 8 principal HF resonances for the HF-C kernels in the graphite matrix using the Teuchert double heterogeneity treatment (2); the tails of the 8 resonances in the THERMOS energy groups are also included. The cross-section histograms at thermal energies show considerably higher values near the 1.094 eV resonance peak of HF 177 than the epithermal energy histograms, because the group widths of the THERMOS library are much smaller than those of the GAM code; on the other hand the total resonance integrals are of course the same, since they are the ones generated by the ZUTDGL code with flux depressions near the resonance peaks, and by NJOY without the flux depression.

In Table 2 the k_{eff} values calculated for the H1 critical assembly are shown together with the neutron leakage and absorption fractions. The 2D CITATION code was used in VSOP for the diffusion calculations. The assembly was modelled approximately as in reference 4, with a slightly reduced graphite density in the side reflector to allow for the control rod channels.

The resonance shielding increases k_{eff} by nearly 1%, using the double heterogeneity treatment of Teuchert. Treating only the heterogeneity between the separate spheres in the pebble bed changes the shielded resonance integrals by not more than one or two percent and has a negligible effect on k_{eff}. This was tested by Nordheim resonance absorption

calculations for hafnium carbide kernels of ten times smaller diameter, followed by few group diffusion calculations. The principal resonance shielding is therefore due to self shielding of Hafnium homogeneously mixed with graphite in the matrix of the absorber spheres, and a small interaction effect between neighbouring spheres.

Table 2
Criticality Calculations of the H1 Assembly of the KAHTER Experiments

	No Resonance Shielding	With Resonance Shielding
Effective Multiplication Factor	1.00666	1.01548
Leakage Fraction	0.30281	0.30446
Absorption Fraction	0.69719	0.69554

Conclusion

It has been shown how the most recent extensive evaluated nuclear files can be used in standard reactor analysis codes with particular emphasis on resonance absorption calculations. The multiplication factors resulting from the analysis of an HTGR critical assembly containing Hafnium Absorber spheres is consistent with the way the core and reflector were modelled for a straightforward application of the VSOP code package.

References

1) "Data Formats and Procedures for the Evaluated Nuclear Data File ENDF-6", edited by P.F. Rose and C.L. Dunford, ENDF-102, BNL-NCS-44945, 1990

2) "VSOP-Computer Code for Reactor Physics and Fuel Cycle Simulation", E. Teuchert, U. Hansen, K-A. Haas, JUEL 1649, KFA Juelich, 1980

3) "NJOY91.13, A Code System for Producing Pointwise and Multigroup Neutron and Photon Cross Sections from ENDF/B Evaluated Nuclear Data", PSR-171, Oak Ridge National Laboratory, 1991

4) "Heterogeneous Poisoning of Critical HTGR Test Facility KAHTER: A Study for the Initial Loading of Pebble Bed Power Reactors", V. Drucke et al., Nuclear Technology, 55, 549-564, 1981

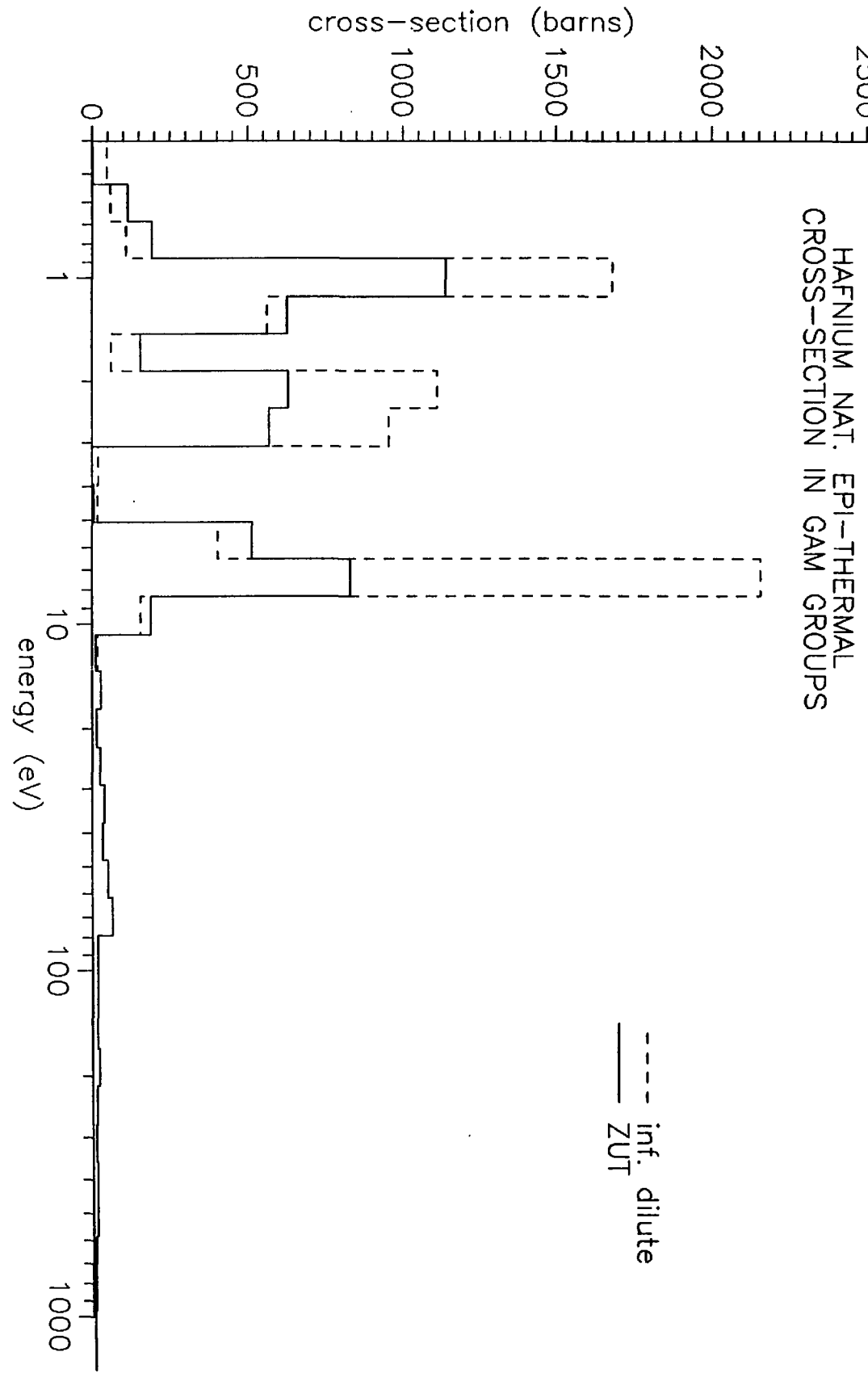
cross-section (barns)
0
500
1000
1500
2000
2500
HAFNIUM NAT. EPI-THERMAL
CROSS-SECTION IN GAM GROUPS
---- inf. dilute
—— ZUT
energy (eV)
1
10
100
1000

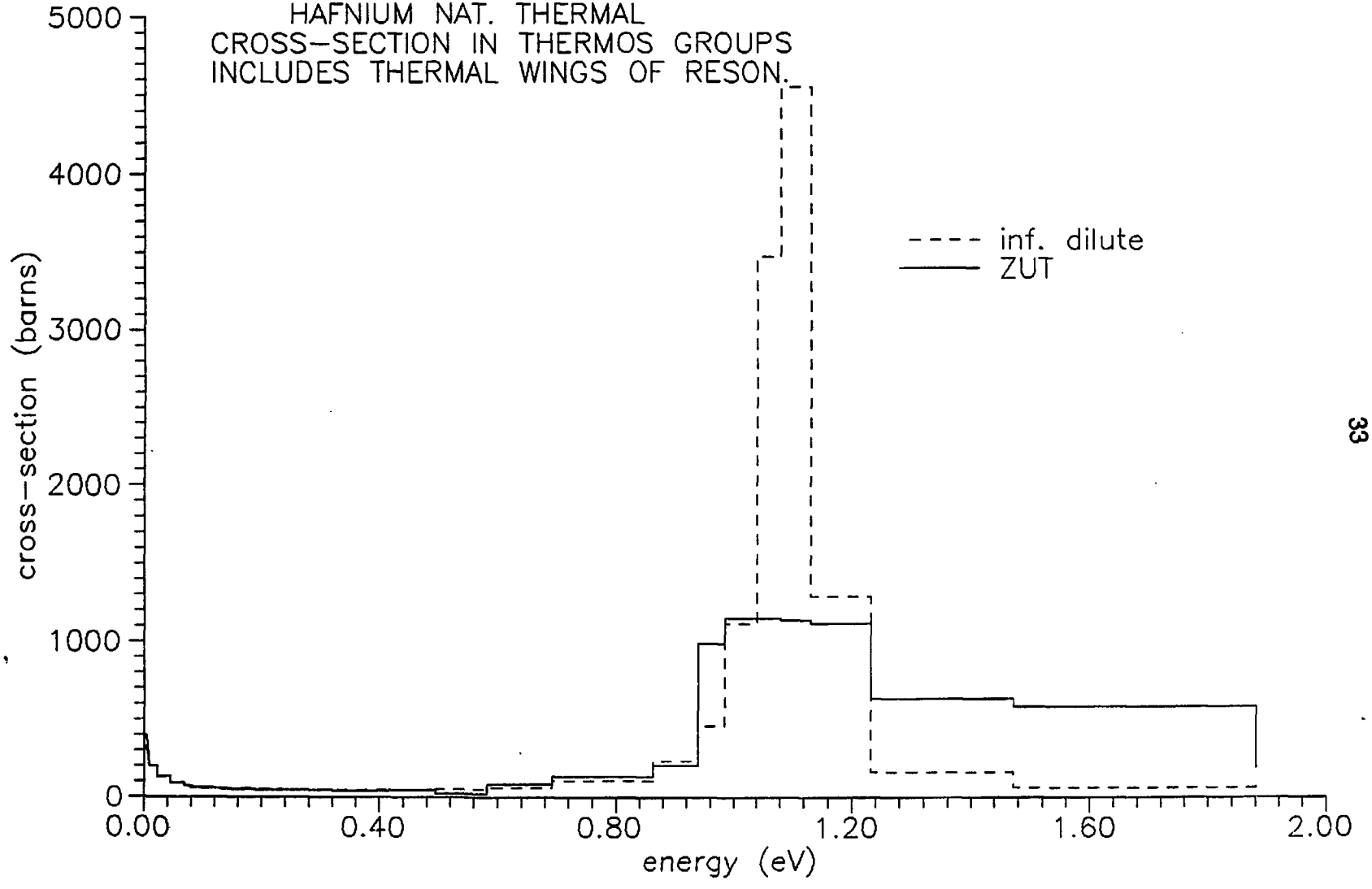
HAFNIUM NAT. THERMAL
CROSS-SECTION IN THERMOS GROUPS
INCLUDES THERMAL WINGS OF RESON.
inf. dilute
ZUT
cross-section (barns)
energy (eV)
5000
4000
3000
2000
1000
0
0.00
0.40
0.80
1.20
1.60
2.00

Energy Degradadation of Surface Sources in DSA based Geometrical Splitting Optimization Procedure

by

N.Gurvitz & A.Dubi

Abstract: The Direct Statistical Approach (DSA) can be utilized to obtain explicit rigorous expressions for the dependence of the variance and computation time on the splitting parameters. These functional dependencies have a general, problem independent form. The quality function, which is merely the variance of the estimator multiplied by the computation time per source particle, can adequately measure the efficiency of the MC calculation, for it is independent of the number of histories and it is proportional to the computation time required to achieve a PRSD of 1%. Once the quality function coefficients are known then the optimization problem is summed by finding the set of splitting parameters which minimize the quality function and thus maximize the efficiency of the MC calculation. According to the DSA theory the infinite set of the quality function coefficients can be constructed from a finite set of problem dependent parameters. The appropriate problem dependent parameters are the probabilities of a particle getting from one splitting surface to another, the average weights of the particles reaching the surfaces, the second moment of these weights and the average time to process a particle from one splitting surface to another. This approach was implemented by A. Dubi and A. Goldfeld into a prototype optimization procedure linked with the MCNP code (but not an integral part of the full MCNP calculation). The optimization procedure basically consist of three steps, namely the derivation of the appropriate problem dependent parameters, calculating the coefficients of the quality function and lastly finding the set of splitting parameters which minimize the function. The derivation of the problem dependent parameters in the prototype procedure was based on a surface to surface calculations in which the medium is "sprayed" with batches of particles emitted sequentially from each surface. In each surface calculation only next "neighbor" surfaces will be considered by terminating the particles on reaching the splitting surfaces. The advantage of this derivation process is that a full coverage of the problem medium can be obtained with a reasonable amount of computation time. Particles are generated deep in the medium and the need to transport particles from the source to "remote" and important regions is avoided. Thus, ensuring that the problem dependent parameters are calculated with the same precision for every surface. However particles emitted from a surface, must be correlated to the actual current crossing that surface, in their spatial,angular and energy distribution. otherwise the problem dependent parameters may be calculated with high precision and poor accuracy.

A systematic examination of the prototype procedure revealed a deficiency which caused inaccuracy in the optimization. The source assumed on each surface was found to be uncorrelated with the real current in problems consisting of slowing down mediums. The termination of particles upon the first crossing resulted in a harder spectrum of the surfaces sources which led to an

overestimation of the surface to surface transfer probabilities and consequently to underestimation of tne optimal splitting parameters. This effect is enhance enormously as the number of splitting surface in the problem is increased.

Two basic approaches were considered to account with the above deficiency. The fist was to obtain the problem dependent parameters directly (i.e. in the course of a regular MCNP calculation) by some additional tallying of the necessary estimators as the particles transport between consecutive surfaces. The problem of loosing important information or calculating the problem dependent parameters with poor accuracy is overcome by exploiting splitting guesses to "flood" the whole medium. The splitting parameters can be altered to direct the particles to different regions without loosing any information. The information gathered in this step can be accomedated in the regular MCNP calculation utilizing the optimal splitting parameters. This approach was implemented in a new procedure by K.W. Burn (ENEA, Italy). The second approach was the implementation of an additional iteration in which problem dependent parameters are derived solely with the "newly arrived" particles i.e. particles reaching the processed surfaces from succeeding surfaces. The final problem dependent parameters are calculated as combinations of the "new" and "old" parameters. Two combinations are considered. The first is based on the differences of the net currents crossing the surfaces when processed during the first iteration, and the net currents at the completion of the iteration. The second combination is more complex. The combination coefficients are proportional to newly recalculated net currents crossing the surfaces. The new currents are based on the problem dependent parameters derived in the first iteration and they are generated with Point MC. Two simple test cases demonstrate unequivocally the advantage of the direct approach over the two iterative approaches.

A Non-Algorithmic Approach to the In-Core Fuel Management Problem of a PWR Core

A. Galperin and Y. Kimhi

Department of Nuclear Engineering

Ben-Gurion University of the Negev

P. O. Box 653, Beer-Sheva 84105, Israel

The primary objective of a commercial nuclear power plant operation is to produce electricity at low cost while satisfying safety constraints imposed on the operating conditions. Design of a fuel reload cycle for the current generation nuclear power plant represents a multistage process with a series of design decisions taken at various time points. Of these stages, reload core design is an important stage, due to its impact on safety and economic plant performance parameters. Overall performance of the plant during the power production cycle depends on chosen fresh fuel parameters, as well as specific fuel configuration of the reactor core.The motivation to computerize generation and optimization of fuel reload configurations follows from some reasons: first , reload is performed periodically and requires manipulation of a large amount of data. second, in recent years, more complicated fuel loading patterns were developed and implemented following changes in fuel design and/or operational requirements, such as, longer cycles, advanced burnable poison designs, low-leakage loading patterns and reduction of irradiation-induced damage of the pressure vessel.

An algorithmic approach to the problem was generally adopted[1, 2, 3]. The research and development projects, reported in open literature, are characterized by a number of similar features, despite the differences in the formulation of the objective function and/or the mathematical tools applied.The optimization is carried out in a number of a sequential but separate steps while the control poison problem is treated separately from the fuel placement problem.The algorithmic methods which perform an optimization by modifying the initial state toward a higher object function

value can lead only a local optimum.

The nature of the reload design process is a "heuristic" search performed manually by a fuel manager. The knowledge used by the fuel manager is mostly accumulated experience in reactor physics and core calculations. These features of the problem and the inherent disadvantage of the algorithmic method are the main reasons to explore a non-algorithmic approach for solving the reload configuration problem.Several such attempts, reported in literature, computerized the manual process performed by the fuel manager [4 , 5]. The methods are based on "depth first search" guided by heuristic rules - an approach which generates an solution acceptable from the safety point of view but is far from the optimum (a longer fuel cycle length or other equivalence parameter). Several features of the "solutions space" (a collection of acceptable final configurations) are emphasized in this work: 1) the space contain numerous number of entities (> ~25!) that are distributed non-uniformly, 2) the lack of a monotonic objective function decrease the probability to find an isolated optimum configuration by depth first search or equivalent technics, and 3) the evaluation of the partial solutions, i. e. comparison of the partially loaded cores, is very difficult and has high level of uncertainty. These characteristics of the solution space guide a new approach for solving the problem, which are based on a "beam search" method. Using the beam search method allows to avoid the "back tracking" problem by choosing in each stage several partial solutions (determined by the heuristic rules organized in the knowledge-base). The solution space expansion is carried out by sequential generation of the horizontal levels (expanding only the preferred combinations) for each of the nodes visited. One of the main advantage of the presented method is the ability to perform an efficient "exhaustive search" and to explore solutions space by modification of the knowledge base.

Those principles were implemented in a computerized system containing few modules [6, 7, 8]. Three main elements are combined in the knowledge-based system which perform heuristic guided by search: control strategy, knowledge-base containing rulesets and data-base containing a description of the physical system.The control strategy is an implementation of a guided search algorithm similar to "beam search". The knowledge-base contains two rulesets in the IF-->THEN format and a loading sequence of fuel assemblies.Two sets of rules are designed to prevent combinatorial explosion of the solutions set. The first ruleset contains "forbidden" type rules for

elimination of the "obviously" unacceptable patterns, the second set contains "preference" type rules for choosing the "most promising" solutions from all the permitted ones. Finally, the physical description of the system under consideration, i. e., data describing the reactor core geometry and properties of the available fuel assemblies, is represented by using technics of "frames" and "objects". In addition to the three main modules described above, the package contains few other modules which provide the working environment for effective exploitation of the method. The user interface provides means for analysis of the generated result, connection with neutronic cycle evaluation module and graphical representation of the solutions space and loading patterns. An important module of the package a "rule editor", serves as an interface between the user and the knowledge-based search module.The rule editor provides the capability to display, create modify rules without programming. All the modules of the package except the nodal code were developed in COMMON LISP and implemented ton a SUN's SPARC workstation.

A self-learning mechanism was revealed in the process of running the prototype system. Analysis of the solutions parameters and corresponding loading configurations led to modifications and expansion of the knowledge base until a set of near-optimal solutions is obtained. The process starts with a "general" loading strategy and a wide spreading of the solutions in the space and gradually converges to the generation of the near-optimal solutions by introducing modifications of a "local" nature in the rulesets.The knowledge contained in the rulesets is transparent in the resulting configurations. This method provide the fuel manager with means to use his knowledge and experience in an efficient and consistent way.

It was shown by application of the heuristic search method, implemented as a knowledge-based production system, several near-optimal solutions are obtained[7].In addition it was shown that the solution set reflects the compiled knowledge contained in the rulesets.

In the first case some of the obtained solutions demonstrate superior performance compared with the reference solution an actual fuel reload of the TMI-1 reactor for the fifth cycle.

Using the knowledge-based system increases the efficiency of the fuel manager work by generating better solutions even without optimization.This advantage is demonstrated by performing a heuristic search based on the reference case strategy (rules) which results in a set of solutions in the vicinity of the reference configuration. Several solutions with a better performance were discovered.

The search strategy proposed in this work is based on the division of the solution space into families of solutions identified by the loading pattern of the fresh fuel assemblies. To identify promising or optimal families during the search execution, a heuristic evaluator may be used to assign the performance parameter to partially loaded core and allow an effective pruning of the search space. The heuristic evaluation parameter developed and demonstrated presents an example of quantification of a heuristic knowledge. Using the demonstrated parameter to reject the expansion of few families during the search execution may increase the speed of solutions generation.

Although a family of solutions identified by a partially loaded core of fresh fuel assemblies in some cases it was shown to be advantageous to perform a "secondary optimization" in order to explore "sub families". The knowledge-based system provides an ability to generate solutions bases on partially loaded core. The physical justification behind such an optimization is the non-monotonic feature of the objective function for the optimization procedure. The advantage of the method provides means to direct the search into any desirable region in the solutions space.

A large number of PWRs currently employ fuel reload patterns, which differ significantly from 3-batch out-in scheme. More complicated reload patterns were adopted due to increased demands on core performance such as : longer (than annual) cycles and low leakage cores. Both, longer cycles, with increased reactivity swing, and low leakage patterns with higher power peaking factors, necessitate utilization of BP rods. Several methods developed by different researchers suggest solution of this problem by a complete decoupling of the fuel configuration generation and BP design. Utilization of heuristic search method partially removes the disadvantage of decoupling the two problem and prevents the need of several approximations, which may lead to impractical solutions.The ability to perform an "exhaustive search" provided by the knowledge-based system may lead to generation of solutions without splitting the fresh fuel enrichment which is usually done by other methods. Many of the obtained solutions demonstrate superior performance compared with the reference solution, as for example - the loading pattern of ZION-1 reactor (ninth cycle) [8]. The results demonstrate the consistent improvement in quality of the results which can be achieved by using the proposed optimization methodology.

The application examples demonstrate a potential of the presented method to be developed into a practical computerized tool for the utilization in industry.

References

1. S.Levine, "Module 5 - Incore Fuel Management", Penn State University (1980)
2. J. Colletti, "Iterative Solution to the Optimal Control of Depletion Problem in Pressurized Water Reactor", Ph. D. Thesis, Penn State University (1981)
3. Y. J. Kim, T. J. Downar and A. Sesonske, "Optimization of Reload Design for Low-Leakage Fuel Management in Pressurized Water Reactors", Nucl. Sci. Eng., **96**, 85 (1987)
4. B. M. Rothleder , G. R. Poetschhat, W. S. Faught and W. J. Eich, "The Potential for Expert System Support in Solving the Pressurized Water Reactor Fuel Shuffling Problem", Nucl. Sci. Eng.U. **100**, 440 (1988)
5. A. H. Robinson, A. O. Heberlin and G. L. Wang, "An Automated Search Procedure for Fuel Shuffling in PWR's Including Rotation Effects",Proc. Topl. Mtg. Artificial Intelligence and Other Innovative Computer Applications in the Nuclear Industry: Present and Future, Snowbird, Utah, August 1987.
6. A. Galperin and E. Nissan,"Application of a Heuristic Search Method for Generation of Fuel Reload Configuration", Nucl. Sci. Eng., **99**, 343 (1988).
7. A. Galperin, S. Kimhi, and M. Segev,"A Knowledge-Based System for Optimization of Fuel Reload Configurations", Nucl. Sci. Eng., **102**, 43 (1989).
8. A. Galperin and S. Kimhi, "Application of Knowledge-Based Methods to In-Core Fuel Management", Nucl. Sci. Eng., **109**, 103 (1991).

ENDF/B-VI ^{233}U DATA TESTING

R. L. Perel, U. Salmi and J. J. Wagschal

Racah Institute of Physics
The Hebrew University of Jerusalem
91904 Jerusalem, ISRAEL

The release of a new data file calls for data testing by integral measurments. Clean integral experiments have always been a good tool for testing and/or improving neutron cross section data. The work presented here is part of an effort to generate a modern version of an adjusted cross section library. In earlier work[1] critical assemblies based on ^{233}U were considered, using ENDF/B-IV data. Since there are a few ^{233}U spheres surrounded by natural uranium shells or by highly enriched oralloy shells, these measurements can serve not only for ^{233}U data testing but they can also serve the improvement of ^{235}U and ^{238}U neutron cross sections.

The recent CRISY system[2] includes data on several critical mass measurement integral experiments involving ^{233}U. These include among others a bare metallic ^{233}U sphere, three spherical cores intimately surrounded by oralloy shells of various thickness, three surrounded by natural uranium shells, and two surrounded by tungsten. Some of these integral experiments are by now CSEWG data testing benchmarks[3] and all of them are well documented[4,5,6]. All relevant details of these experiments are given in Table I.

Table I. Specifications of U 233 Critical Assemblies

No.	NAME	CORE R cm	CORE DENS g/cc	CORE ATOMIC PERCENT U 233	U 234	U 235	U 238	W	REFLECTOR R cm	REFLECTOR DENS g/cc	REFLECTOR ATOMIC PERCENT U 234	U 235	U 238	W
1	U23_1	5.983	18.424	98.130%	1.240%	0.030%	0.600%							
2	U23-U_1	4.600	18.644	98.219%	1.096%		0.685%		6.589	18.800	1.025%	93.264%	5.711%	
3	U23-U_2	5.044	18.621	98.219%	1.096%		0.685%		6.266	18.800	1.025%	93.264%	5.711%	
4	U23-U_3	3.180	17.951	97.708%	0.894%		0.195%	1.202%	7.971	18.800	1.025%	93.234%	5.741%	
5	U23-U-Un_1	4.600	18.644	98.219%	1.096%		0.685%		9.909	18.920		0.720%	99.280%	
6	U23-U-Un_2	5.044	18.621	98.219%	1.096%		0.685%		7.346	18.920		0.720%	99.280%	
7	U23-U-Un_3	4.206	18.420	98.148%	1.235%	0.030%	0.587%		24.119	19.000		0.720%	99.280%	
8	U23-W_1	4.600	18.644	98.219%	1.096%		0.685%		10.391	17.210				100.0%
9	U23-W_2	5.044	18.621	98.219%	1.096%		0.685%		7.482	17.210				100.0%

The specifications in Table I were used as input to our one dimensional transport calculations. One should notice that for most of these experiments there is more than one reference. In case of inconsistency or incompleteness of the data, we had to use comparative considerations[2]. However, the typical uncertainty in the effective multiplication factor, k_{eff}, as derived from the reported experimental uncertainties is about one milli-k [(k-1)*1000], whereas the discrepancy between different specifications of the same experiment leads to a shift in k_{eff} which is smaller than this experimental uncertainty. One may further notice that the cores of some experiments are identical, and are part of a series of experiments performed by the same people using the same techniques both for the measurements and for the uncertainty analysis.

All calculations of k_{eff} were performed following guidelines similar to those appearing in the CSEWG Benchmark specifications, namely S_{16}, 30 (more than 24) energy groups, more than 40 mesh intervals in the core and a similar number of intervals in the materials surrounding it. All multi-group cross-sections were processed by NJOY[7] from ENDF/B-VI[8] files. The calculated reactivities, $1000*(k_{eff}-1)$, for these experiments are presented in Table II. One immediately notices that most calculated values are negative and much bigger in absolute value than the experimental uncertainties,and as usual[9] these deviations do not exceed ten milli-k. The ENDL-84[10] neutron cross section library was used to recalculate the ^{233}U multi group cross sections and all transport calculations were repeated with the substitution of <u>only</u> the ^{233}U cross sections. The new values are also presented in Table II. This time all results fall within five milli-k of the experimental value.

Table II

Calculated Reactivities (in milli k)

no.	name	^{233}U cross sections	
		ENDF/B-VI	ENDL-84
1	U23-1	-6.48	2.13
2	U23-U-1	-0.47	3.86
3	U23-U-2	-3.34	2.29
4	U23-U-3	-1.19	-0.12
5	U23-Un-1	-0.91	3.65
6	U23-Un-2	-2.66	3.27
7	U23-Un-3	2.05	4.88
8	U23-W-1	-8.58	-0.77
9	U23-W-2	-5.63	2.39

In our earlier work[1] using ENDF/B-IV data the reactivities have been too low by more than twenty times the experimental uncertainty. The improvement of the ENDF/B-VI ^{233}U data file can be attributed to the increase in the fission cross-section and in $\bar{\nu}$, the number of secondary neutrons per fission. Although the ENDF/B-VI ^{233}U fission cross-section is about equal to the corresponding ENDL-84 cross-section, $\bar{\nu}$ is still too low over the important energy range 0.3-2.3 MeV.

In conclusion the ENDF/B-VI data for ^{233}U were found to be still inadequate for reactivity calculations of fast assemblies. The ENDL-84 file on the other hand still leads to a better global agreement between measured and calculated reactivities, mainly due to changes in the neutron yield.

REFERENCES:

1. R. L. Perel, U. Salmi and J. J. Wagschal, "^{233}U Data Testing by Integral Experiments", Trans. Isr. Nuc. Soc. 15, p. 53 (1989).

2. U. Salmi, R. L. Perel and J. J. Wagschal, "CRISY: a **CRI**tical Assemblies Documentation **SY**stem", International Conference on Nuclear Data for Science and Technology, Juelich, Germany, (1991).

3. Cross Section Evaluation Working Group Benchmark Specifications, ENDF-202, Vol 1 (1981).

4. E. A. Plassmann and D. P. Wood, Nucl. Sci. and Eng. 8, p. 615 (1960).

5. G. E. Hansen and H. C. Paxton, Reevaluated Critical Specifications of Some Los Alamos Fast-Neutron Systems, LA-4208 (1969).

6. H. C. Paxton, Los Alamos Critical-Mass Data, LA-3067-MS, Rev (1975).

7. R. E. MacFarlane, D. W. Muir and R. M. Boicourt, "The NJOY Nuclear Data Processing System", Vols 1 to 4, LA-9303-M, (ENDF-324), LANL, (May 1982 to December 1985).

8. ENDF-102, Data Formats and Procedures for the Evaluated Nuclear Data File, ENDF, Revised by R. Kinsey, NNDC, BNL (1979).
   see also:
   ENDF-102, Data Formats and Procedures for the Evaluated Nuclear Data File ENDF-6, Edited by P. F. Rose and C. L. Dunford, NNDC, BNL, BNL-NCS-44945, Informal Report (revised edition Oct. 1991).

9. A. Pazy, G. Rakavy, I. Reiss, J. J. Wagschal, A. Yaari and Y. Yeivin, Nucl. Sci. and Eng. 55, p. 280 (1974).

10. D. E. Cullen and P. K. McLaughlin, ENDL-84, IAEA-NDS-II (1985), also DLC-120 of RSIC.

A New Artificial Neural Network–Based Methodology for Malfunctions Management in Dynamic Systems

M. Tramer, E. Wacholder and E. Elias
Department of Mechanical Engineering
Technion – Israel Institute of Technology
Haifa 32000, Israel

Introduction

Detection and isolation of malfunctions and abnormal events in complex, non–linear, dynamic systems are important for their safe and reliable operation. Malfunction isolation currently relies on quick interpretation of a large number of alarms by the operator. To assist and support the human decision, an extensive scientific and engineering efforts have been directed in the last two decades towards the development of an intelligent machine which could make correct decisions in a noisy environment. Artificial Neural Network (ANN) systems which are mathematical models to simulate a theorized mind and brain activity, have recently been suggested as a method for exploring and reproducing human information processing tasks.

One of the most popular and best examined and verified ANN is the multi–layered feed forward network which exploits the Back–Propagation (BP) learning rule. The BP learning rule has been mainly used, and proven to work for *static* pattern recognition [2]. In the present work the applicability of the BP algorithm is extended for malfunctions management in *dynamic* systems [4]. The feasibility of the proposed methodology is demonstrated using a numerical simulation of a High Temperature Gas cooled Reactor (HTGR) system [1] as a test case. The results show that ANNs using the Back–Propagation learning algorithm can be successfully employed for solving pattern recognition problems of time–dependent phenomena. The pattern recognition unit thus obtained is highly noise–tolerant and exhibits good generalization features.

The proposed methodology

The Back–Propagation Paradigm belongs to the group of supervised learning and feedforward recall systems. Namely, the elementary BP is a three–layer ANN with feedforward connections from the first (input) layer processing elements to the second (hidden) layer processing elements and feedforward connections from the second layer to the third (output) layer. In general, it is possible to have several hidden layers. In feedforward connection, each processing element of a layer is connected to each element of the layer above. A weight is allocated to each connection. The BP encoding algorithm performs the

input to output mapping by minimizing a cost function. The cost function is minimized by adjusting the weight connections according to the error between the computed and desired output processing element values [3].

High rate pattern recognition can be realized by dividing the transient analog signal of each sensor into a series of consecutive digital reading samples of time interval *dt* (Fig. (1)). For each scenario one can sample several state variables. In the present case the input to the neural network consists of two or three of the following measured variables: The He temperature in the core, core thermal power and the secondary loop inlet water pressure. A fixed length time "window" (Fig. (2)) is introduced consisting of several consecutive time intervals *dt* for each state variable and for each scenario. This "window" is moved along the time axis by adding the last measurement to the time series and eliminating the oldest one, thus keeping the length fix. In a typical scenario the transient period is finite. Thus, an input vector to the neural network consists of the concatenated "windows" (Fig. (1)) of all the measured variables for a given scenario. A scenario is characterized by several input vectors constructed by moving the "windows" from the beginning to the end of the time axis. This process is repeated for all the scenarios in order to complete the learning set of the network (Fig. (3)). In the learning phase, the learning set is used to adjust the connection weights of the networks as described in [3].

Figure 1. shows the concatenation process for three state variables. Each time–series consists of three intervals *dt*. Figure 2. demonstrates the moving "window" concept and Figure 3. describes a typical learning set with 8 scenarios and 5 input vectors for each scenario.

In the pattern recognition execution phase the already trained network receives input signals from the plant and should be able to isolate and recognize the progressing scenario. The pattern recognition process is carried out as follows: A sampling–unit is attached to each of the sensors. These units generate a signal for each measured variable at each time step (*dt*). The signals are input to a preprocessing unit where they are concatenated, namely, the first entries of the new vector are obtained from the translation of the previous vector entries by one location backwards, while the last entry becomes occupied with the most recent measured digital signal. These new vectors are further concatenated to a single measured vector which is introduced to the network, as an input for pattern recognition.

This approach enables an on–line continuous sampling and detection of variable patterns at high frequency. The main assumption underlining this method is that the network execution time is much shorter than the sampling time step. The theoretical earliest alarm of an incipient failure is delayed by no more than the sample's time interval. However, the verification criterion for a failure occurrence is typically met some time later.

Results and Discussion

The network was "trained" to detect and identify eight scenarios: $\pm$ 1 and $\pm$ 5% reactivity change; 20 and 60 % power drop to the primary coolant blower; $\pm$ 5 % change in steam generator inlet water temperature. Three state variables were sampled, with a sampling time of two seconds. The width of the measuring time "window" was 20 seconds. The learning set included three vectors, with an overlap of 15 sec between the vectors of each scenario, and the steady state vector.

The network output was a binary coded event number between 0 and 8 corresponding to the eight scenarios used in the training set. Dimensions of the network were 30, 10, and 4 processing elements in the input, hidden, and output layers respectively, and the network was fully connected. Sigmoid activation functions were used for all the neurons. The network weights were initialized with randomly selected values in the range of [-0.1,+0.1].

Figure 4. depicts the network performance in terms of the fraction of correct isolations versus the level of noise of the input vectors and the isolation time for scenario 2 (-1% reactivity change). The noise was uniformly distributed, with a given amplitude independent of the signal. Perfect correct isolation was achieved with noise levels of up to 8 % and isolation time of less then twice the length of the measuring window (26 *sec*). However, the network correctly isolated the event with a 15 % noise level and an isolation time of roughly twice the length of the measuring window. The network performance rapidly decreases with increasing noise levels and shorter isolation time.

In summary, the results provide encouraging preliminary evidence to support the feasibility of ANN based failure identification and isolation techniques as a diagnostic tool in complicated power systems.

Acknowledegment

This work is supported by the Israel Ministry of Science and Technology under grant number 034-962.

References

1. E. Elias, S. Kaizerman, B. Cohen, D. Hasan, and E. Wacholder, "HTGRSS - A Computer Code for Simulation of Transient Processes in HTGRs; Simulation of the THTR-300 Primary and Secondary System", Technical Report TNED/R-723, Technion, 1989.

2. M. Roh, S. Cheon, and S. Chang, "Power Prediction in Nuclear Power Plants Using a Back-Propagation Learning Neural Network", *Nuclear Technology*, 94, 270–278 (1991).

3. K. Simpson, "Artificial Neural Systems", Pergamon Press, 1990.

4. M. Tramer, "Signal Processing in Nuclear Reactors Using Neural Networks", M.Sc. Thesis, I.I.T.-Technion, 1992.

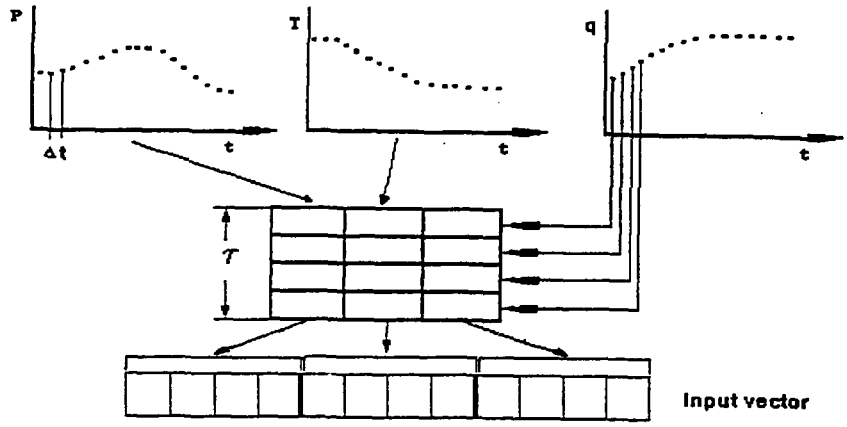

Figure 1. The Concatenation Process.

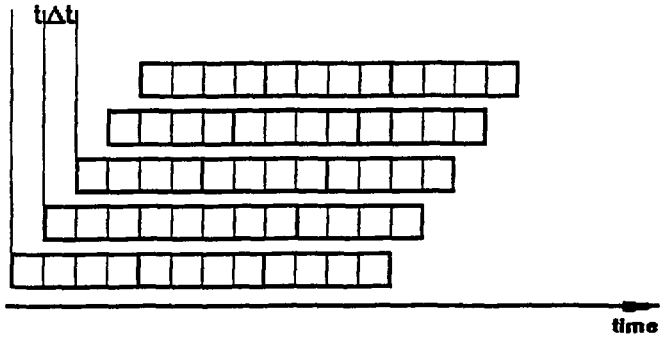

Figure 2. The Moving "Window" Concept.

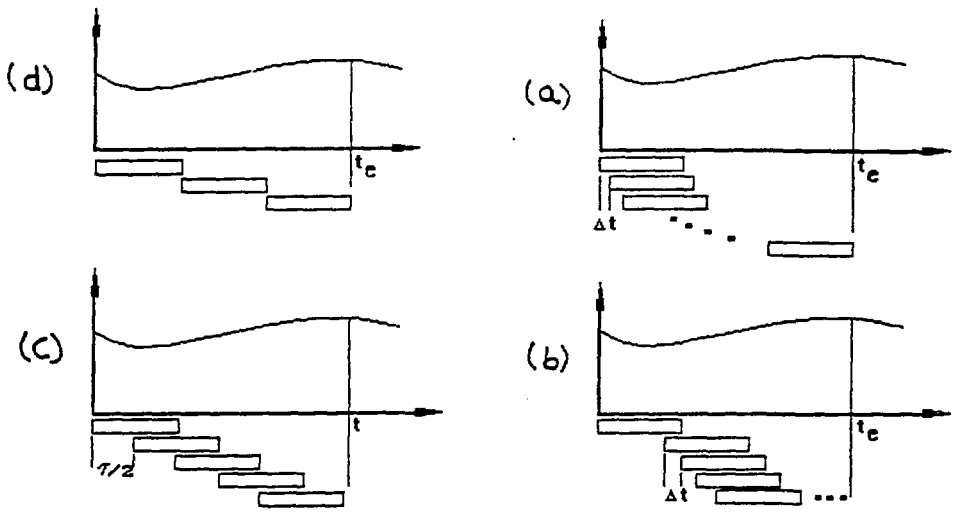

Figure 3. Typical Learning Set Configurations.

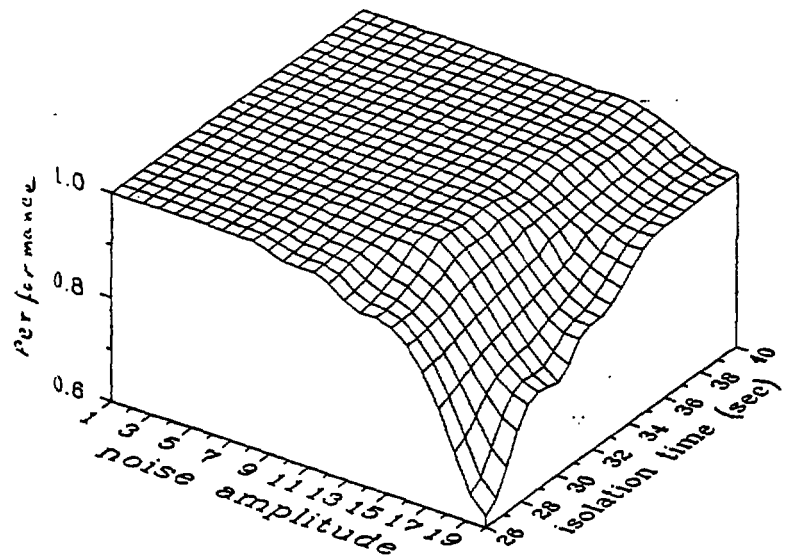

Figure 4. Network Performance for Scenario # 2 (−1 % Reactivity Change).

Some Interesting Aspects of Nuclear Power Economics

Dr. Amitzur Z. Barak
Israel Atomic Energy Commission

Without getting into the detailed basics of the economics of power production in general and nuclear power in particular, due to time and scope limitations, a few aspects will be focused on; these aspects are, naturally, interrelated.

An "expert" in economics wrote a paper a few years ago saying: "No more time should be wasted on analyzing the economics of nuclear- versus fossil-fuel power generation, as the statistics of last year show clearly that electricity from *coal-fired power plants was on the average cheaper by 45% than* that from nuclear plants".

Although this approach, based on factual data, may sound very logical it is also based on a few misleading (and probably inaccurate) hidden assumptions, such as:

1. The difference between the nuclear and fossil-fuel prices, in real terms, will remain essentially constant on the average for the next 50 years.

2. The power plants that will be installed according to our plan have the same characteristics as the average-equivalent plants covered by the referred past statistics, e.g. availability, specific-investment, heat-rate etc.

3. Financing elements and procedures will be similar to those relating to the plants covered by the mentioned statistics, e.g. discount-rate, interest-rates on long- or short-term loans etc.

In the following, the economical meaning of the factors mentioned in the above dubious assumptions will be discussed, in particular the plan duration, fuel prices forecast, discount-rate and time availability.

In addition, the limitations of the economical tools for evaluations and comparisons such as the cost of kWh or the generation system estimates (e.g. the "WASP" program) are discussed.

The main points are:

1. Plan duration and fuel price. The minimum scope of a nuclear power generation plan which is economically justifiable is above 2000MWe, namely 2 pairs of power units, at least. Preparations during a few years, then construction of the first unit during 7 years at least, plus quite a few years - probably 5 to 10 - between start-up of the first and the last unit under the plan in addition to 30 years of operation for each unit bring the fossil-fuel-saving-period of the plan to 35-45 years or even more, starting about 10 years from the decision to implement the plan. All considerations on fuel-cost saving should be based on the forecasts referring to this period.

2. Fuel price forecasts: At the moment several scenarios are possible for oil prices:

   (a) Fluctuations around an average, real constant value.

   (b) A new significant increase due to shortage following the slow development of new oil wells in the last 6 years.

   (c) Fluctuations around a gradual increase of a few percent per year. Coal prices may partially follow the oil prices.

3. Discount rate affects the power generation cost in three or four additive ways:

   (a) The gross initial investment increases with the discount rate due to interest during construction (AFUDC).

   (b) The levelized recovery of the initial investment increases with the discount rate.

   (c) The optimized design of some equipment items changes so that more fuel is consumed per kWh$_e$ generated, for a higher discount rate.

   These effects are more significant for nuclear power stations as the construction time is considerably longer. In addition:

   (d) In nuclear fuel fabrication, which starts a few years before burning-up, there is interest on the expenses of manufacturing the fuel.

4. Time availability and capacity factor have a strong effect on the cost of the kWh$_e$ wherever the specific investment (per installed KW) is high; nuclear units are characterized by specific investment which is twice or more, on the average, than fossil fuel units.

(5a) The limitation of the economical method of calculating the cost of a kWh$_e$ from a specified generation unit is that it does not consider indirect expenses, caused by this unit to other units (e.g. using nuclear units for base-load results in some lowering of the load factor of the coal and oil-fired units, increasing in turn indirectly their specific fuel consumption).

(5b) The limitation of the entire power generation system evaluation method is that it disregards some of the economical aspects that occur after the horizon time.

March 30, 1992

Recent Advances and Future Directions of Neural Networks Application in Nuclear Power Plants

Zvi Boger and Mordehai Ben-Haim

Nuclear Research Center - Negev
P.O. Box 9001, Be'er-Sheva 84191, Israel

Presented at the annual meeting of the Israeli Nuclear Societies,
Be'er-Sheva, May 1992

Extended Abstract

On-line applications of intelligent computation techniques, such as Expert Systems, Fuzzy Logic and Neural Networks (NN) are regarded as means to increase safety and plant reliability. The need to analyze the detailed behavior of the plant slows the successful implementation of some of these systems, and the derivation of the Expert Rules can be difficult in complex systems. In the 1990 annual meeting of the Israeli Nuclear Societies, ref. (1), NN techniques were shown to help in some tasks: Automatic learning of process and equipment behavior models; Extraction of Expert Rules from these models; Sensor fault validation by pattern recognition; enhancement of sensor sensitivity in noisy environments. In the years 1989 - 1991, several applications of the NN techniques to nuclear power plant operation were reported, summarized in two reviews, refs. (2), (3). This paper presents recent advances in this field, and discusses possible future directions.

Two main areas of research are persued in recent work. One is the on-line fault and abnormal situations pattern identification by NN. An example is given in refs. (4), (5), in which the aim is to diagnose early signs of degradation in PWR internals by analysis of available signals, such as power spectral density. In tests on "signal library" from Sequoyah-1 NPP. A NN with 15 inputs could detect and classify "features" in the spectra, connected to changes in the behavior of the reactor. It performed better than statistical methods that were previously employed. The second area is of modeling the dynamical behavior of reactor components. In one study, the dynamics of U-tube steam generator were modeled by a NN to relate the inlet steam flow to the SG water level, ref. (6). It behaved better than an elaborate computer model of the SG. In another study, the thermal power level of NPP was modeled by two NN's, one using 4 signals from the primary system, the second using 6 signals from the secondary system, ref. (7). Both NN predicted the thermal power with less than 1% error. When incomplete signal set was presented to the model, the error

increased to 1-2%. It shows also the possibility to use the NN for on-line signal validation. The most advanced study in this area was reported in refs. (8), (9), in which NN was used as part of the signal validation scheme of EBR-II automatic startup control system. Several simple NN's were used to predict the reading of plant signals, each based on few other plant signals. The control system was evaluated in simulated reactor startup, and the results seemed acceptable, although more elaborated NN designs were recommended.

Our experience with the Guterman-Boger fast teaching and network reduction and analysis algorithms, indicates that quick experimentation with NN for such purposes is possible, even with large nets of hundreds of inputs is possible. As we do not have a NPP in Israel, we cannot test directly our contention that these algorithms would solve most of the teaching problems encountered in the cited references. We can only point to the results gotten in similar complex systems in other fields, refs. (3), (10), (11). Some new results have been recently found by us in the area of expert rule generation that may be of interest to users of safety analyses of NPP operation.

One problem in preparing fault-tree analyses for the Probability Safety Analysis of a NPP is the tedious going through all possible paths of component failure, and their interactions with each other. Once prepared in the design stage, it would be helpful to use the information contained in them as on-line diagnostics and operator advisors. Such 'living' PSA have been prepared by researchers in France, ref. (12). We applied NN ideas to such expert system, used in on-line fault diagnosis of industrial plant, ref. (13). Deviations of sensors from the normal operating range were used as inputs to a NN whose output was the probability that the cause of these deviations was a particular fault, as estimated by an experienced expert. In one example, the deviations of 7 sensors were used to estimate the probability of over-pressure fault in an evaporator system (fig. 1). The NN was trained by 100 sensor patterns, and the results of estimating the fault probability in 36 other, previous unseen patterns, are shown in fig. 2. The significance of the fact that only in few cases the deviation from the human expert is greater than 10%, is that the NN was able to model the behavior of a complex system from relative few examples. It raises the possibility that a NN trained on partial PSA could generate automatically the complete analysis of the plant, ref. (14). The use of PSA related sensors as inputs for a NN that will provide on-line diagnostic operator help may be also possible.

It seems that the future role of NN in NPP operation is assured, at least in modeling, sensor validation and diagnostics. With NN beginning to be applied in closed loop control of complex systems such as combat airplanes and spacecraft, ref. (15), it's utilization in NPP control loops will come eventually.

References:

1. Z. Boger: Application of neural networks techniques to fault analysis. *Proceedings of the Annual Meeting of the Israeli Nuclear Societies*, Herzelia, December 1990, p. 217.

2. R.E. Uhrig: Potential applications of neural networks in the operation of nuclear power plants. *Nuclear Safety*, 32(1) pp. 68-79.

3. Z. Boger: Possible roles of neural networks in developing expert systems in the nuclear industry. Paper presented at the *IAEA Expert Meeting on Expert System Prototypes*. Springfields, UK, 1991.

4. K. Korsah and R.E. Uhrig: Investigation of neural networkparadigms for the development of automatic noise diagnostic/reactor surveillance systems. Paper presented at the 6*th Specialists Meeting on Reactor Noise*, Gatlinburg, Tennessee, 1991. CONF-910535.

5. K. Korsah and R.E. Uhrig: Analysis of neutron noise spectra using neural networks. Paper presented at the *Annual ANS Meeting*, Orlando, 1991. CONF-910603.

6. A. G. Parlos, A.F. Atiya, K.T. Chong and W.K. Tsai : Nonlinear identification of process dynamics using neural networks. *Nuclear Technology*, vol. 97. Jan. 1992, pp. 79-96.

7. M.-S. Roh, S.-W. Cheon and S.-H. Chang: Thermal power prediction of nuclear power plant using neural network and parity space model. *IEEE Transactions on Nuclear Power*. vol. 38(2), pp. 866-872.

8. B.R. Upadhyaya and E. Eryurek: Integration of multiple signal validation modules for sensor monitoring. *Proceedings of the 8th Symposium on Space Nuclear Power Systems*, Albuquerque, 1991, pp. 1126-1131.

9. R.C. Berkan, B.R. Upadhyaya, R.L. Bywater and R.A. Kisner : Advanced automation concepts applied to Experimental Breeder Reactor-II startup. ORNL/TM-11716, 1991.

10. Z. Boger and M. Ben-Haim: Solvent extraction knowledge acquisition by neural network modeling. Submitted to *Solvent Extraction and Ion Exchange*, 1992.

11. Z. Boger: Application of neural networks to water and wastewater treatment plant operation. *ISA Transactions*, vol. 31(1), pp. 25-33, 1992.

12. C. Anselin; A 'living' PSA based on use of expert systems. *Use of Expert Systems in Nuclear Safety*, Vienna, 1988, IAEA-TECDOC-542, pp. 109-108.

13. Z. Boger: Expert systems in nuclear power plants - how soon can they be implemented? *Use of Expert Systems in Nuclear Safety*, Vienna, 1988, IAEA-TECDOC-542, pp. 165-176.

14. M. Ben-Haim and Z. Boger: Neural networks as a fault diagnostic tool in process monitoring. Submitted to *Computers in Chemical Engineering*, 1992.

15. C.A. Robinson: Neural networks blossom in aerial vehicles. *Signal*, Feb. 1991, pp. 24-30.

Fig. 1: NEURAL NETWORK FOR PREDICTING THE OVER-PRESSURE FAULT

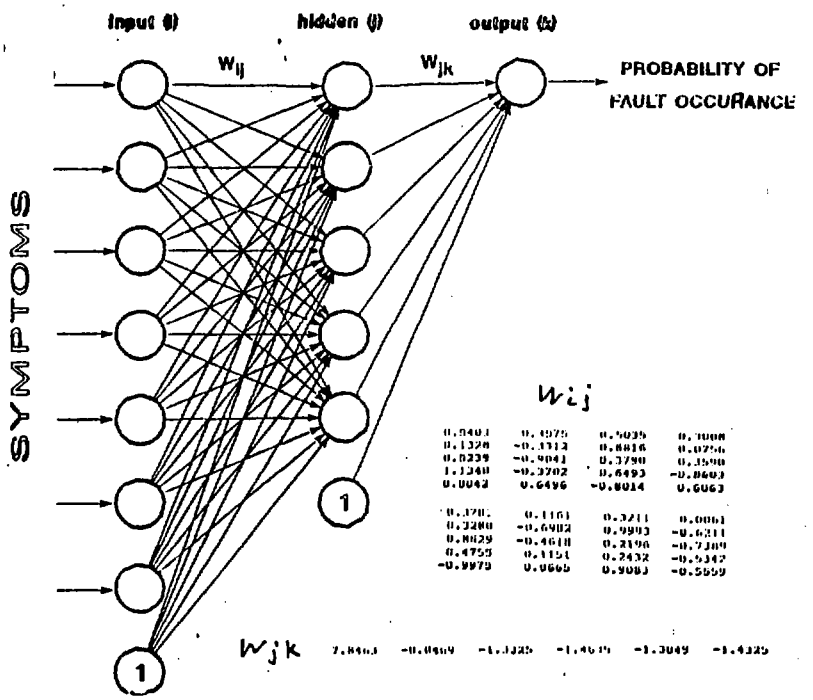

Fig2: Comparison of over-pressure fault probabilities (test set)

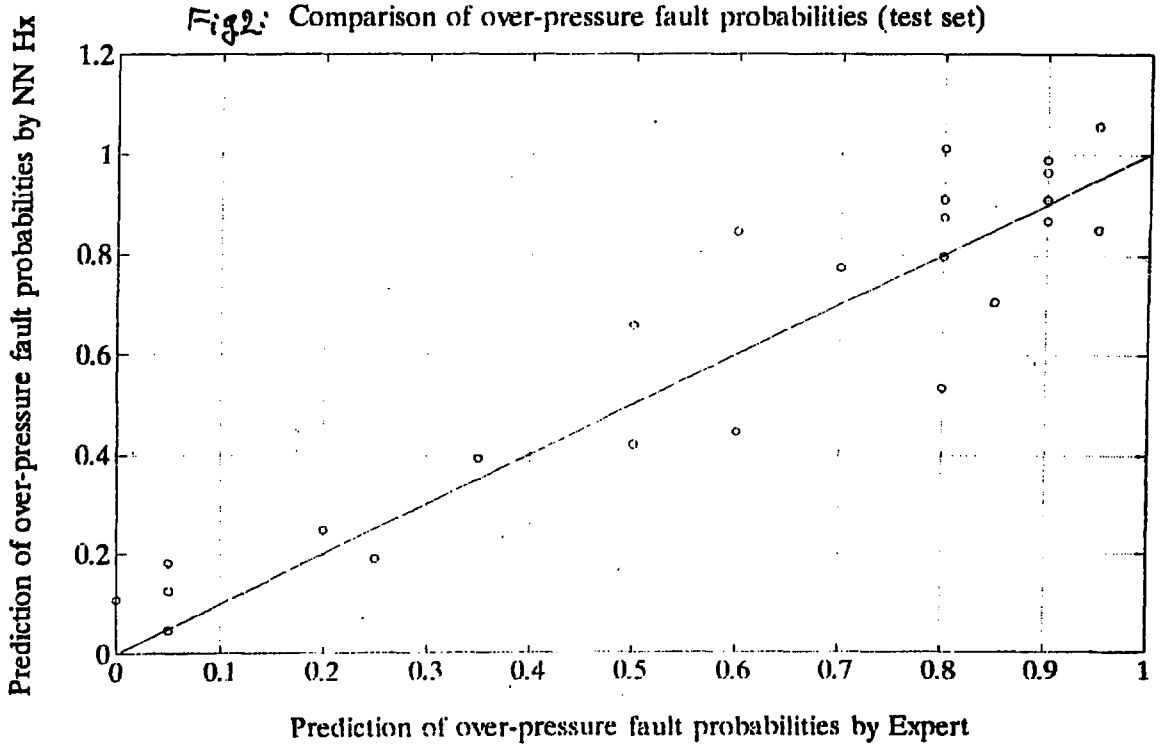

DYNAMIC STEAM-GENERATOR MODEL FOR GENERAL POWER PLANT APPLICATION WITH DSNP

M. Shapira, D. Saphier, D. Gal

Soreq Nuclear Research Center
Yavne 70600, Israel.

October 24, 1991

A reliable model for a Once-Through Dynamic Steam Generator is crucial for the safety analysis of most nuclear power plants. The Steam Generator is one of the most complicated component of the power plant due to the fact that a two phase flow occurs in different regimes of the secondary side of the Steam Generator. The secondary side can be divided into four main regions: subcooled region, nucleate boiling region, film boiling region, and superheated region. The boundaries between these regions depend upon the mass flow rate, the rate of the heat transfer and the thermodynamic properties of the secondary fluid. These conditions depend on the dynamics of the whole plant.

To get the solution for the dynamics of the Steam Generator, the energy, the momentum and the continuity equations, must be solved separately for the gas and the liquid phases for the four regimes. The locations of the boundaries between the different flow regimes should be a part of the solution as well.

In this study we assume a one dimensional flow and apply the approach where we solve one set of equations for the two phases and using a void fraction correlation to consider the fact that the two phases have different velocity and different thermodynamic properties. We use here a movable boundary formulation such that the locations of the boundaries between the different flow regimes are part of the dynamic solution.

Many void fraction correlations appear in the literature. The analysis with different correlations for the void fraction can yield different results. Various correlations need to be tested to find the best correlation for each region in this type of flow.

A Once-Through Steam Generator model for the DSNP (Dynamic Simulator for Nuclear Power-Plants) package was developed, where different void fraction correlations are applied by changing an input parameter of this model. In this model each flow regime in the secondary side is treated separately and can be divided into as many sub regions as necessary for the simulation. Solutions were obtained using the data from an operating HTGR power plant and comparisons between solutions with different correlations for the void fraction were made. The detailed descriptions of the model, the simulations results and comparisons between different void fraction correlations will be given in the full paper.

Incorporating New Experimental Data on Zircaloy Oxidation into the Thermohydraulic Analysis of Mitigated Severe LWR Accidents

L. Reznik

Nuclear Engineering Department, Israel Electric Corporation

Zircaloy oxidation phenomena are of high importance to the understanding of various timing and process aspects of severe accidents in the safety analysis of Light Water Reactors. This is due to the high heat generation rate of the exothermic reaction which may even exceed the fission product decay heat rate, and also due to the accompaning intensive hydrogen production, wich in turn carries the risk of in-containment explosure or fire.

During recent years many laboratories and organizations worldwide have taken part in research programs on severe fuel damage sponsored by the NRC, DOE and EPRI in the USA and by the OECD and KfK in Europe.

Several experiments among the recently conducted tests are especially important in regard to Zircaloy oxidation processes[1]:

- The FP-2 test performed at the Loss-of-Flow-Test facility (LOFT) at the Idaho National Engineering Laboratory (INEL),

- The PBF-ST test performed at the Power Burst Facility (PBF) at INEL within the NRC Severe Fuel Damage (SFD) program,

- The FLHT-4 and FLHT-5 tests performed in the Full - Length - High - Temperature facility (FLHT) at the Canadian Chalk River Laboratories.

The results of these and other recent experiments have been assessed and incorporated into the calculational procedures used in the IEC Nuclear Engineering Department for performing the thermohydraulic analysis of LWR severe accidents. The computer codes MAPCH2 and THALES serve us as the principal analysis tools.

These codes model the Zircaloy oxidation exothermic reaction

$$Zr + 2H_2O(steam) = ZrO_2 + 2H_2 + 6400\ J/g\ Zr \qquad (1)$$

As the temperature increases above 1500° K, oxidation of the Zircaloy cladding by steam becomes important. This exothermic reaction provides additional heating of the rods, and at ~1700° K a rapid autocatalytic reaction takes place, except where limited locally in the core by conversion of all available steam into hydrogen.

The MARCH2 code models the reaction rate as limited by the minimum of a gaseous diffusion rate or a solid diffusion rate. The gas - phase rate limitation by oxygen diffusion through a surface boundary layer of hydrogen is based on the hydrogen - blanketing model based on earlier experiments of Chung and Thomas[2]. The solid - phase rate limitation represents the process of oxygen diffusion through the growing ZrO_2 surface layer on the cladding resulting in parabolic rate kinetics. The solid - phase rate is also corrected in MARCH2 by using another hydrogen - blanketing factor to represent the steam - deprived region. The input options permit the user to chooze the parabolic rate constants from the Urbanic - Heidrick, Cathart or Baker - Just experimental data on cladding oxidation[2].

The Japanese THALES code[3] model developed by JAERI employs a more simplified approach using only the solid - phase rate limitation with the Baker - Just diffusion constants. While the oxidation reaction heat rate is calculated in MARCH2 internally, THALES requires a user - supplied input value of the isothermal specific heat of the Zr - H_2O reaction.

The in-vessel natural circulation is an important aspect of processes involving core - degraded accidents as it has a pronounced effect on the oxidation rate. While this aspect is not treated in MARCH2, THALES provides a better thermohydraulical frame to take partly into account effects of natural circulation in the vessel and in the primary system. Although THALES permits division of the primary system into many control volumes and connecting junction (where each control volume has the gas and the liquid regions separated by a movable mixture level), the model does not treat the local fluid movement due to the pressure differentials but rather provides a lumped-parameter approach. Similarly, gas and liquid temperatures, mixture levels and rates of flow between control volumes are calculated in THALES under the assumption of uniform pressure in the primary system and the thermal quasi - equilibrium in each region. Nevertheless, the two-phase multi-volume hydraulic analysis of THALES includes such models as the counter-current flow model for junctions, the liquid region void separation calculation based on a relative velocity and the quasi - static momentum balance model for the primary system loop (based on the gravity head effects due to the differences in the control volumes elevations). These models provide THALES with a much more accurate determination of the mixture levels and the core uncovery position in comparison with similar predictions by MARCH. These parameters have a direct impact on the oxidation rate, and are especially important in the analysis of mitigated severe accidents, (like those terminated by reflooding core debris).

Two major findings of the recent LOFT FP-2, SFD PBF-ST and NRU FLHT-4 and FLHT-5 tests thought as the most relevant to the phenomenology of Zircaloy oxidation at accident conditions may be summarized as follows[1]:

- concerning the question of fuel bundle reconfiguration and potential blockage effects - the data from the tests indicate the continued Zircaloy oxidation and hydrogen generation during and following melt relocation and inspite of creation of partial flow area blockages in degraded fuel bundles;

- with respect to oxidation during the initial stages of reflooding a severely damaged core the tests indicate that the exothermic reaction of hot Zircaloy is more likely to happen than immediate quenching of the core debris by reflood coolant.

In addition, experimental evidence from these and other tests and analyses[4] shows that modelling by MARCH2 of the "hydrogen - blanketing" rate limitation by steam diffusion through a hydrogen surface boundary layer is not valid under reactor accident conditions.

It has been also observed experimentally that the downward relocation of molten unoxidized Zircaloy limits the autocatalytic oxidation temperature rise and the hydrogen generation rate by removing unoxidized Zircaloy from the hotter regions of the core. (However, this unoxidized Zircaloy may become available in later accident stages). Since the MARCH modelling allows no relocation of unoxidized Zircaloy before an assumed slump of a core region at about 2500° K this may lead to a substantial overprediction of the hydrogen release in the autocatalytic oxidation stage of the accident.

Nevertheless, in many other aspects the tests' results show that the oxidation rates are underpredicted by both THALES and MARCH even for conditions in which a global steam starvation is calculated. The rate underprediction is mainly due to the fact that THALES ignores $Zr-H_2O$ reaction during the phases of the corium heat-up of the core support plate and in the vessel bottom head, and due to a similar approach is undertaken within the MARCH2 model.

In addition, there are many physical mechanisms of heat transfer which are neither modeled adequately in THALES nor in MARCH2 but may be responsible for enhanced steam generation during core uncovery. These mechanisms of heat transfer include:

- Thermal radiation from the uncovered region directly to the residual water;

- Axial conduction in the fuel rods from uncovered to covered regions;

- Thermal radiation or direct contact from uncovered materials to the surrounding structures and then by conduction to structures below the water level;

- Gamma-ray deposition in the residual water.

Incorporating the above experimental findings into the existing analytical tools may in general require a combination of direct modifications in the computer code source program and appropriate changes in the user-defined input parameters.

Mechanistic computer codes for the core damage analysis, such as the EPRI SCDAP or the NRC MELPROG are available at the IEC Nuclear Engineering Department. The non-mechanistic character of the available to us THALES and MARCH2 codes provides with a variety of input factors, control options for choice of different models and many user-defined parameters which could be otherwise computed internally by a mechanistic code. Although in general it is an obvious deficiency of THALES and MARCH2, this variety of input options and parameters assists to limit the code adjustments necessary to reflect the new experimental evidence by appropriate input modifications only.

A thorough analysis of the THALES and MARCH2 models has been performed in order to select groups of input parameters and controls which should be appropriately set up in order to overcome a general underprediction by the codes of the Zircaloy oxidation rate and the corresponding rate of hydrogen generation.

The following is the MARCH2 group of the input parameters and control options chosen to serve the above purpose:

FDCR=1.0 - Forcing the reaction to completion before core slump;

IMWA=1 - Continue the metal-water reactions at melting stage;

ICON=1 - Return the SG steam condensate back to the vessel;

MELMOD=1 - Choose the meltdown A-model for faster melt motion;

MWORNL=3 - Use the previous MARCH1 model for Zr-H_2O reaction;

TWOFF>3500.0 - Turn off the oxidation at greater temperature;

WZRCXX= 30000.0 - A deliberately increased Zr mass for HEAD;

MWR=4 - Use the previous MARCH1 model for reactions in cavity;

TQNCH=0.0 - No temperature limit for adiabatic debris heat-up;

IHOT=100 - "Fully-vaporized" model for debris-water interaction;

TMS>2700.0 - The maximum debris temperature for Fe-H_2O reaction;

A similar set-up of the THALES input parameters and controls chosen to correct the Zircaloy oxidation rate underprediction is:

ALFCLD=1.0 - Maximize the multiplier for cladding oxidation rate;

FDBR=1.0 - Maximize the debris oxidation factor;

FREAC=1.0 - Maximize the steam fraction reacting with Zircaloy;

HREAC=7000.0 - Increase by 10% the Zr oxidation specific heat;

FANN=1.0 - Maximize the fraction of intact/debris contact area;

FAMG=1.0 - Maximize the fraction of corium/support plate area;

FAMH=1.0 - Maximize the fraction of corium/bottom plate area;

FMLT(2)=1.0 - Maximize unoxidized cavity corium Zr content;

FMLT(6)=0.0 - Minimize the fraction of Zr_2O in cavity corium;

REFERENCES

1. A. W. Cronenberg, "Hydrogen Generation Behavior in the LOFT FP-2 and Other Experiments: Comparative Assessment for Mitigated Severe Accident Conditions", J. Nucl. Technol., 97, 97 (Jan.1992).

2. R. O. Wooton etc., "MARCH2 (Meltdown Accident Response Characteristics) Code Description and User's Manual", NUREG/CR-3988, (Sept.1984).

3. "The User's Manual of THALES Code System for Analyzing Progression of Core Meltdown Accident", JW219, JAERI, (Oct. 1987)

4. "Reactor Risk Reference Document", NUREG-1150, App. J-O, Vol. 3, (Nov. 1987)

Modeling of an AP600–Like Reactor Using RELAP5/MOD2

Y. Nekhamkin, D. Hasan, E. Elias, G. Gy. Halasz and E. Wacholder
Department of Mechanical Engineering
Technion – Israel Institute of Technology
Haifa, 32000 Israel

A simulation model has been developed for accident analysis in reactors conceptually similar to a Westinghouse advanced PWR 600 MWe (AP600) reactor. The model utilizes the IBM version of the computer code RELAP5/MOD2/CYCLE 36, which has recently been acquired through the IAEA. The code was prepared by JRC–ISPRA from the original CDC version developed at EG&G [1].

Modeling efforts at this phase have concentrated mainly on a realistic representation of the reactor coolant system (RCS) and its passive safety systems (PSS). The physical model consists of some 140 RELAP5 "components", each containing up to 10 "volumes", which are necessary for the joint modeling of both the RCS and the PSS. In previous papers by the present authors the RCS of the AP600 reactor was analyzed independently using the RELAP4/MOD6 code [2]. A few subsystems of the PSS were also analyzed using RELAP5/MOD1 [3]. The increasingly more powerful computer software and hardware currently available at the Technion, have enabled us to partake in the quantitative safety evaluation of advanced light water cooled reactors (ALWRs). This work complements a similar study performed at the Technion for a few types of presently commercially operating light–water–reactors (LWRs).

The AP600 system nodalization for loss of coolant accident (LOCA) analysis is shown in Figure 1. The model consists of hydrodynamic volumes (fluid control volumes), hydrodynamic junctions (momentum control volumes), and heat structures used to represent heat transfer surfaces which store energy such as fuel pins and the steam generator's tubes. The primary system model includes the reactor vessel, the core and two flow loops. Each loop contains a U–tube steam generator, a hot leg, a cold leg (representing two legs), a pump (equivalent of two main recirculation pumps) and flow paths. The first loop contains a pressurizer. The model also accounts for the passive residual heat removal system (PRHR), the in–refueling water storage tank (IRWST), the containment, the core make–up tanks (CMT) and accumulators. A point kinetics model, including reactivity feedback effects, is implemented for core power calculations.

The secondary system of the plant model is composed of several hydrodynamic components which represent the boiler region (tube region), steam generator upper and lower downcomer, steam separator, feedwater preheater section, steam dome and feedwater supply tank. Feedwater supply and steam flowrate were modeled by a time–dependent volume.

Design and operational data required for constructing the model were based on published information and complemented by engineering judgment. The verification of such a model is complex, and has to overcome some inherent limitations. The AP600 is still a reactor concept on a drawing board, compared to the broad experience and validation enjoyed by LWRs. Still, it has been conceived as a "natural" development of the Westinghouse series of two, three and four loop LWR designs. This was achieved by an effort to use proven LWR components to the largest extent possible. The evolutionary nature of the AP600 concept enabled us to substantiate the present model development on previous experience acquired over the years in modeling LWRs.

Model verification ranged from establishing the correct installation of the program [1] on the Technion's IBM 3081D MVS/XA system by running widely accepted sample problems such as the Edwards' blowdown tube case [4], through comparison to similar works in the literature [5], checks of model self-consistency and parametric evaluations. It is believed that such a verified computational tool will eventually enable an independent examination of vendors' data [5] regarding the capability of the AP600 plant and its PSS to mitigate a spectrum of postulated LOCA events, and its compliance with regulatory requirements.

Acknowledgment

This work is supported by the Israel Electric Corporation under project number 034-966.

References

1. V. H. Ransom et. al., RELAP5/MOD2 Code Manual, NUREG/CR-4312, EGG-2396, Rev. 1.

2. D. Hasan, E. Elias and E. Wacholder, "RELAP4/MOD6 Model for the AP600 RCS", Trans. Israel Nucl. Soc., 16, 155 (1990).

3. D. Hasan, E. Elias and E. Wacholder, "AP600 PSS Modeling Using RELAP5/MOD1", Trans. Israel Nucl. Soc., 16, 152 (1990).

4. A. R. Edwards and T. P. O'Brien, "Studies of Phenomena Connected with the Depressurization of Water Reactors", J. of the British Nucl. Energy Soc., 9, 125-135 (1970).

5. R. M. Kemper, C. M. Vertes, "LOCA Performance of the Advanced 600 MWe PWR", Proc. ANC Topical Meeting, Seattle, p. 750 (1988).

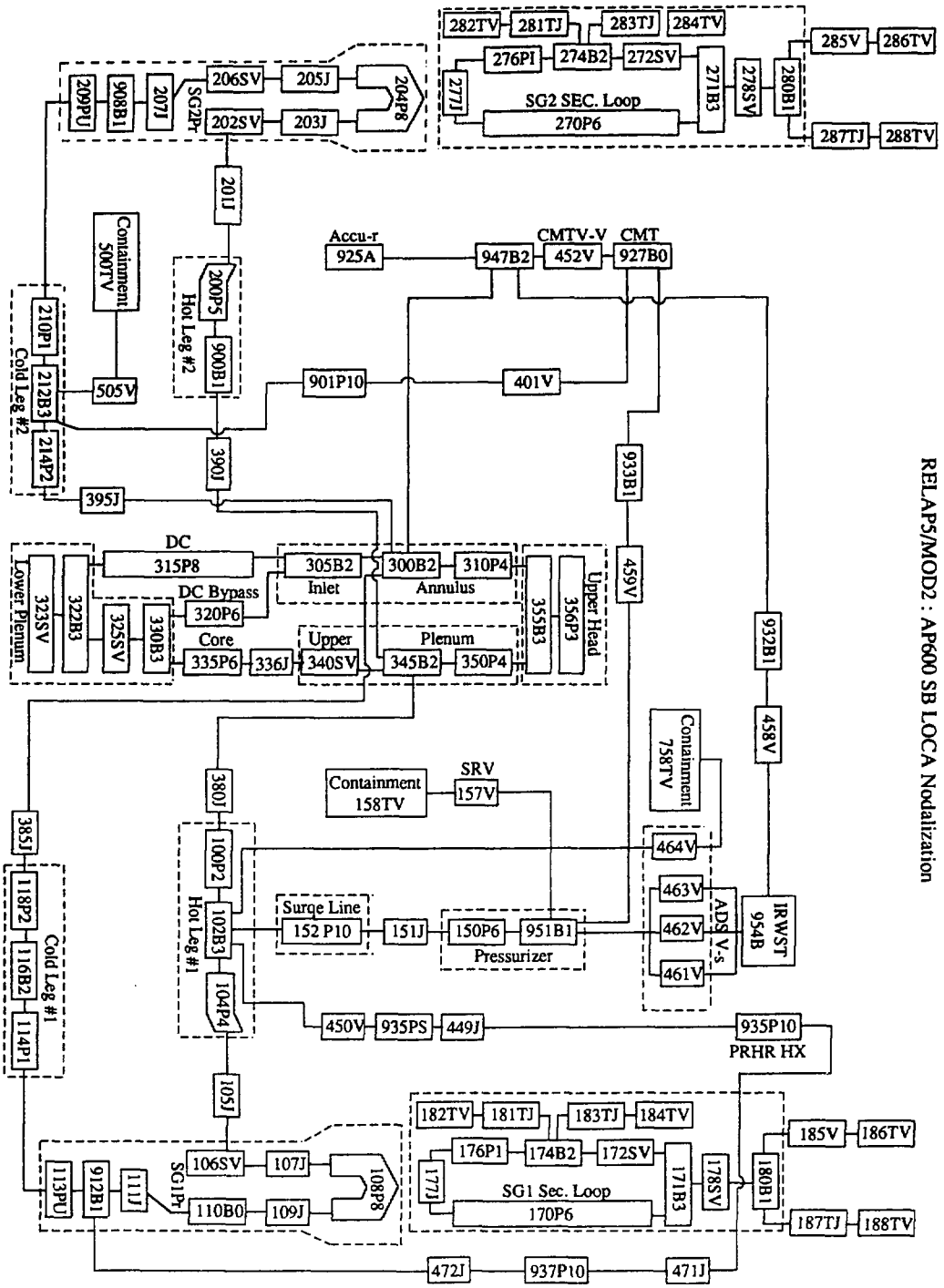

RELAP5/MOD2 : AP600 SB LOCA Nodalization

DYNAMIC MODELING OF GAS COOLED RECTOR THERMAL HYDRAULICS WITH DSNP.

D. Saphier, D. Gal and M. Shapira.

Soreq Nuclear Research Center
Yavne, Israel.

October 27, 1991

Several large scale simulations of various HTGR plants were developed at SNRC using the DSNP (Dynamic Simulator for Nuclear Power-plants). The DSNP is a special purpose block oriented simulation language. It is a modular modeling system by which a large variety of nuclear power plants can be simulated. HTGR phenomena simulated include forced and natural circulation, normal operational transients and accidents, pressurized and depressurized conditions, and decay heat removal by various operational modes.

Several models of HTGR components were developed an added as modules to the DSNP libraries. The DSNP system has four libraries. Three of the libraries include component models at increasing level of sophistication, and library four is a material property library including a large number of equations of state for different coolants as well as heat transfer and flow correlations.

The major components developed for HTGR studies include a one-dimensional, (1-D), and a two-dimensional, (2-D), thermal hydraulic pebble bed core models, a detailed 1-D once-through steam generator model, a 2-D solid conducting cylinder model to represent heat transfer through the prestressed concrete vessel (PCRV), an improved heat exchanger model to model the decay heat removal (DHR) unit, an improved circulator model, a 1-D gas chamber (Multichamber cavity module), and 1-D conducting block with centrally bored passage to represent the upper and lower graphite reflectors. All the other modules used in the HTGR simulations were previously available in DSNP. These include such modules as pipes, cavities, mixing plena, pumps, turbine, neutronics, Xenon poisoning, control elements, safety modules, valves and the many material property functions that are needed when a nuclear power plant is being simulated.

For each plant several DSNP simulations were developed - depending on the accidents to be simulated. In a depressurization accident with a total loss of flow a 2-D core model was used to investigate the detailed temperature distribution throughout the reactor. For reactivity transients the 1-D core model was sufficient, with a simple representation of the primary loop. For ATWS accidents in which natural circulation phenomena occurred with decay heat removal through a DHR or through the PCRV surface cooler, detailed modeling of the primary loop is necessary.

The major conclusion from these studies is that in the small modular reactor ($\sim$250MWt) the fuel temperature during a LOCA will be always below the critical value at which fission products will be released, even if no flow through the core exists - the heat will be dissipated through the PCRV into the environment. For the medium sized HTGR ($\sim$1000MWt) some mode of minimum natural circulation must be established in order to maintain the fuel temperature below its critical level.

Simulation details and results will be presented in the paper.

Heat Conduction in Reactor Fuel Elements

Shmuel Olek[+] and Eitan Wacholder[++]

[+] R & D Division, Israel Electric Corporation Ltd., Haifa

[++] Faculty of Mechanical Engineering, Technion-I.I.T., Haifa

Abstract

A new approach is offered for the solution of the heat conduction problem in a reactor fuel element, which has a general form of a heat source. A special eigenfunction expansion is derived for the temperature distribution, which treats the fuel and clad domains as though they are a single region with discontinuities. Numerical results obtained from the present analysis compare favorably with a previous analytical solution by Fourier series expansions.

1 Introduction

An accurate reliable solution for the heat conduction problem in a fuel-and-cladding configuration is of considerable importance in the nuclear industry. The relevant hot-channel factor may be reduced if axial heat conduction is accounted for.

Because of theoretical difficulties, this problem was solved mostly by numerical methods, and analytical solutions are rather scarce.

Some limited cases of axial conduction in fuel plates were solved in the past, e.g. Fagan and Mingle (1964) and Thorpe (1965).

Hetsroni et al. (1969) expanded the temperature distribution in a Fourier cosine series. Their solution is suitable for an arbitrary axial distribution of the volumetric heat generation. The results of a numerical example that they showed were in substantial agreement with those of Fagan and Mingle (1964) and Thorpe (1965), but they got different shapes for the temperature distribution at the centerline of the plate and for the heat flux distribution at the surface of the clad.

In this work we solve the temperature distribution in a reactor fuel element, where the fuel may have a heat source of a general form. The solution is obtained by an eigenfunction expansion for the temperature distribution, which is suitable for handling problems in composite media. The present method treats the fuel and the clad domains as though they are a single region with certain discontinuities. The heat generation is expanded in terms of the eigenfunctions. Thus, the problem is reduced from solving a nonhomogeneous partial differential equation to the solution of a nonhomogeneous second order ordinary differential equation. The formal solution of the latter equation is well known.

2 Analysis

Consider a reactor fuel element of either plate or cylindrical configuration. Let a dimensionless coordinate system (r, z) be placed at the centerline of the element and let $z = 0$ be the location of the bottom of the element at the coolant enterance (Fig. 1).

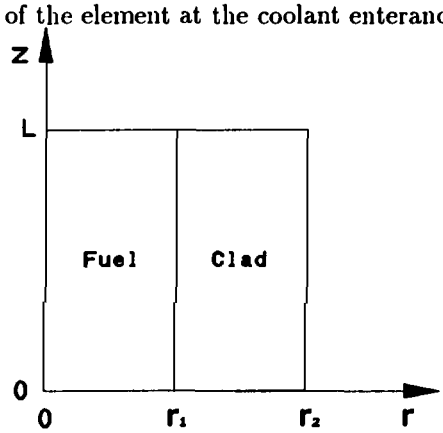

Fig. 1. The geometry and coordinate system used in the analysis.

In a unified formulation for both fuel and clad, we may write the steady-state heat conduction equation for constant thermophysical properties in the form

$$\frac{1}{r^\nu}\frac{\partial}{\partial r}\left(r^\nu \frac{\partial \theta}{\partial r}\right) + \frac{\partial^2 \theta}{\partial z^2} + q(r,z) = 0, \quad 0 < r < r_2, \quad 0 < z < L \tag{1}$$

where $\nu = 0$ for a plate configuration and $\nu = 1$ for a cylindrical one. The temperature θ is taken in excess of the liquid inlet temperature. The heat source is of a general form, and, for example, for a sinusoidal axial distribution in the fuel, we have $q(r,z) = q_0''' \sin(\pi z/L)$ for $0 \le r < r_1$.

The boundary conditions associated with Eq. (1) are

$$r = 0, \quad 0 \le z \le L \quad : \quad \frac{\partial \theta}{\partial r} = 0 \tag{2}$$

$$r = r_1, \quad 0 \le z \le L \quad : \quad \theta^- = \theta^+ \tag{3}$$

$$r = r_1, \quad 0 \le z \le L \quad : \quad \frac{\partial \theta^-}{\partial r} = \frac{k_2}{k_1} \frac{\partial \theta^+}{\partial r} \tag{4}$$

$$r = r_2, \quad 0 \le z \le L \quad : \quad \frac{\partial \theta}{\partial r} + B[\theta - \theta_f(z)] = 0 \tag{5}$$

$$z = 0, \quad 0 \le r \le r_2 \quad : \quad \frac{\partial \theta}{\partial z} = 0 \tag{6}$$

$$z = L, \quad 0 \le r \le r_2 \quad : \quad \frac{\partial \theta}{\partial z} = 0 \tag{7}$$

where θ denotes a dimensionless temperature, k_1 and k_2 are the thermal conductivities of the fuel and clad, respectively. The geometrical entities r_1, r_2, and L are shown in Fig. 1. The Biot number is denoted by B and $\theta_f(z)$ is the coolant temperature. The solution procedure consists of the following steps

Step 1: homogenize boundary condition (5) by introducing a new variable $\psi(r,z) = \theta(r,z) - \theta_f(z)$,

Step 2: use separation of variables and solve a Sturm-Liouville problem in the r direction over the interval $[0,r_2]$, for eigenfunctions whose derivatives are discontinuous in the interval,

Step 3: employ the theorem of Yeh (1980) to find a suitable weight function, with respect to which the noted eigenunctions are orthogonal,

Step 4: expand $q(r,z)$ in terms of the eigenfunctions, and derive a nonhomogeneous ordinary differential equation with z as the independent variable,

Step 5: solve the noted ordinary differential equation and determine the coefficients in the series expansion by using the boundary conditions at $z = 0$, and $z = L$, and by utilizing the orthogonality properties of the eigenfunctions.

Because of space limitations we present the final form of the solution only. The temperature distribution in both the fuel and the cladding is given by

$$\theta(r,z) = \theta_f(z) + \sum_{n=0}^{\infty} R_n(r) Z_n(z) \tag{8}$$

where

$$\theta_f(z) = W \cos \frac{\pi z}{L} \tag{9}$$

with

$$W = \frac{r_1 L q_0'''}{\pi \dot{w} c_p} \tag{10}$$

The eigenfunctions $R_n(r)$ are given by

$$R_n(r) = \begin{cases} R_n^- &= X(r) \\ R_n^+ &= A_n X(r) + B_n Y(r) \end{cases} \tag{11}$$

with

$$\begin{aligned} A_n &= \frac{k_1}{k_2} \frac{\frac{dX}{dr}(r_1)[\frac{dY}{dr}(r_2) + BY(r_2]}{\frac{dX}{dr}(r_1)[\frac{dY}{dr}(r_2) + BY(r_2)] - \frac{dY}{dr}(r_1)[\frac{dX}{dr}(r_2) + BX(r_2)]} \\ B_n &= -A_n \end{aligned} \tag{12}$$

where

$$X(r) = \cos(\lambda_n r), \quad Y(r) = \sin(\lambda_n r), \quad \text{for a plate geometry} \tag{13}$$

and

$$X(r) = J_0(\lambda_n r), \quad Y(r) = Y_0(\lambda_n r), \quad \text{for a cylindrical geometry} \tag{14}$$

and the eigenvalues λ_n are the positive roots of

$$\det \begin{bmatrix} X(r_1) & -X(r_1) & -Y(r_1) \\ \frac{dX}{dr}(r_1) & -\frac{k_2}{k_1}\frac{dX}{dr}(r_1) & -\frac{k_2}{k_1}\frac{dY}{dr}(r_1) \\ 0 & \frac{dX}{dr}(r_2) + BX(r_2) & \frac{dY}{dr}(r_2) + BY(r_2) \end{bmatrix} = 0 \tag{15}$$

The functions $Z_n(z)$ are given by

$$Z_n(z) = c_{1n} e^{-\lambda_n z} + c_{2n} e^{\lambda_n z} +$$

$$\frac{1}{\lambda_n^2}\left\{ g_n(z) - \frac{1}{2}\int^z [e^{\lambda_n(z-\tilde{z})} + e^{\lambda_n(\tilde{z}-z)}]\frac{dg}{d\tilde{z}} d\tilde{z} \right\} \tag{16}$$

where

$$g_n(z) = Q_n \frac{d^2\theta_f}{dz^2} + F_n(z) \quad n = 0, 1, \ldots \tag{17}$$

$$F_n(z) = \left[\int_0^{r_1} q(r,z) R_n^-(r) r^\nu dr + \frac{k_2}{k_1} \int_{r_1}^{r_2} q(r,z) R_n^+(r) r^\nu dr \right] \Bigg/$$

$$\left[\int_0^{r_1} R_n^{-2}(r) r^\nu dr + \frac{k_2}{k_1} \int_{r_1}^{r_2} R_n^{+2}(r) r^\nu dr \right] \quad n = 0, 1, \ldots \tag{18}$$

$$Q_n = \left[\int_0^{r_1} R_n^-(r) r^\nu dr + \frac{k_2}{k_1} \int_{r_1}^{r_2} R_n^+(r) r^\nu dr \right] \Bigg/$$

$$\left[\int_0^{r_1} R_n^{-2}(r) r^\nu dr + \frac{k_2}{k_1} \int_{r_1}^{r_2} R_n^{+2}(r) r^\nu dr \right] \quad n = 0, 1, \ldots \tag{19}$$

$$c_{1n} = \frac{G_n e^{-\lambda_n L} - H_n}{e^{\lambda_n L} - e^{-\lambda_n L}} \tag{20}$$

$$c_{2n} = \frac{G_n e^{\lambda_n L} - H_n}{e^{\lambda_n L} - e^{-\lambda_n L}} \tag{21}$$

$$G_n = \Gamma_n \frac{d\theta_f}{dz}(0) - \frac{1}{2\lambda_n^2} \left[\int^z (e^{\lambda_n \tilde{z}} - e^{-\lambda_n \tilde{z}}) \frac{dg}{d\tilde{z}} d\tilde{z} \right]_{z=0} \tag{22}$$

$$H_n = \Gamma_n \frac{d\theta_f}{dz}(L) - \frac{1}{2\lambda_n^2} \left\{ \int^z [e^{\lambda_n(\tilde{z}-L)} - e^{\lambda_n(L-\tilde{z})}] \frac{dg}{d\tilde{z}} d\tilde{z} \right\}_{z=L} \tag{23}$$

$$\Gamma_n = -\frac{1}{\lambda_n} \frac{\int_0^{r_1} R_n^- r^\nu dr + \frac{k_2}{k_1} \int_{r_1}^{r_2} R_n^+ r^\nu dr}{\int_0^{r_1} R_n^{-2} r^\nu dr + \frac{k_2}{k_1} \int_{r_1}^{r_2} R_n^{+2} r^\nu dr} \tag{24}$$

Summary

A new method was employed for the determination of the temperature distribution in a fuel-and-clad configuration. The solution method is based on an eigenfunction expansion, which treats the laminates as though they constitute a single region with discontinuities, due to their different properties. The eigenfunctions which do not form an orthogonal set with respect to the usual weighting function, are made orthogonal with respect to a special weighting function derived from Yeh's theorem (1980). This approach facilitates the complexity of dealing separately with the formal solution for the temperature distribution in

each laminate, then matching the temperature and heat flux at the common interface. The heat source, which may assume a general form, is expanded into a series in terms of the eigenfunctions, thereby reducing the solution effort from solving a nonhomogeneous partial differential equation to the solution of an ordinary differential equation, whose formal solution is well known. Numerical results (not shown) are in close agreement with a previous analytical solution by Hetsroni et al. (1969).

References

J. R. Fagan, and J. O. Mingle, 1964, Nucl. Sci. Eng., Vol. 18, p.443.

G. Hetsroni, E. Wacholder, and S. Haber, 1965, "Heat Conduction in Reactor Fuel Elements", Nucl. Sci. Eng., Vol. 37, pp. 329-336.

E. Kamke, "Differentialgleichungen, Lösungsmethoden und Lösungen, I, Gewöhnliche Differentialgleichungen", Leipzig, 1959.

J. F. Thorpe, 1965, Nucl. Sci. Eng., Vol. 23, p. 329.

H.-C. Yeh, 1980, "An Analytical Solution to Fuel-and-Cladding Model of the Rewetting of a Nuclear Fuel Rod, Nucl. Eng. Des., Vol. 61, pp. 101-112.

Experimental Study Heat and Mass Transfer During Quenching of Hot Surfaces

Y. Barnea and E. Elias
Department of Mechanical Engineering
Technion – IIT, Haifa
I. Shai
Department of Mechanical Engineering
Ben-Gurion University, Beer-Sheva

An experimental program has been carried out in order to study the flow and heat transfer regimes during quenching of a preheated annular vertical channel with subcooled water at atmospheric pressure. The quenching process is typically accompanied by a moving narrow boiling front (quench front) which divides the surface into dry and wet zones. This study is directed mainly to improve the current physical understanding of the microscopic heat transfer processes taking place in the precursory cooling region downstream of the quench front.

An experimental loop was constructed which simulates a typical fuel channel in small research reactors. The test section consists of an annular flow channel with an electrically heated rod at its center and an outer surface exposed to the ambient. The test section was heated to a predetermined temperature before flooded by cold water from a constant pressure feed vessel. The experimental program covers five different feed-vessel pressures, three initial hot surface temperatures in the range of 400 to 575 °C and two inlet water temperatures: 30 °C and 60 °C . Measurements include inlet conditions (fluid temperature, flowrate and static pressure), outlet conditions of the two separated phases (temperature and mass flow rates) and local measurements along the test section such as surface temperatures, coolant temperatures, void fraction and liquid head. The data was acquired and processed on-line by a microcomputer at high cycling rate (≈50 Hz). Detailed description of the test section is reported in [1, 2]. The rewetting phenomena is reviewed in [3] and [4].

As the quench front progresses along the flow channel, it removes heat from the hot surface by several heat transfer mechanisms such as axial conduction and radial convection and radiation to the coolant. At typical medium inlet flowrates (5–15 cm/sec) two flow regimes are prominent downstream of the quench front, namely the inverted annular flow (IAF) and the inverted slug flow (ISF). The two phase mixture which typically exists downstream of the quench front acts as a precursory cooling, which gradually decreases the surface temperature prior to quenching. Figures (1a) and (1b) show typical temperature traces along the heated surface at two opposing azimuthal angles. Initially

the surface temperature at a given elevation remains constant. At that period the liquid is far from the measurement point and does not affect the surface temperature. Latter as the precursory cooling mixture reaches the specific thrmocouple, the temperature starts to decrease gradually. The arrival of the quench front is accompanied by a sudden drop of the surface temperature at a rate of more than 500 °C /s. Shortly after quenching the surface reaches the local liquid temperature. Careful examination of the temperature traces at the two azimuthal angles reveals that the quench front progresses along the hot surface in a wavy manner. Circumferential temperature gradients are observed near the quench front.

Quench front velocities can readily be determined by measuring the time interval between the quenching of successive thermocouples. Generally, The quench front velocity was found to be affected by the the initial wall temperature and by the precursory cooling heat transfer which is in turn a function of the liquid inlet conditions. Measured values of the quench front velocity (u_Q) were fitted as a function of the initial wall temperature, T_o, the inlet water temperature, T_{in}, and the inlet water velocity, u_{in}.

$$\frac{u_Q - 1.5}{u_{in} - 2} = 0.61 - 0.0875\frac{T_o - T_s}{T_s - T_{in}} + 0.032\left[\frac{T_o - T_s}{T_s - T_{in}}\right]^3 \qquad (1)$$

where T_s is the saturation temperature corresponding to the ambient pressure. Equation 1 fits the data within about 12 percent in the liquid subcooling range of 40 °C to 70 °C T_o in the range of 400 °C to 575 °C and u_{in} in the range of 2 to 9 cm/s.

The detailed experimental results are graphically presented in [2]. the systematic wide data base obtained in this work enables the evaluation of many existing theoretical models. the particular configuration of the present test section allows a direct utilization of the results for improving the design of emergency core cooling systems in research reactors.

References

Barnea, Y., Elias, E., & Shai, I., "Experimental Apparatus for Quantitative Measurements in Precursory Cooling Regime during Bottom Reflooding", Trans. 22nd Conf. on Mech. Eng., p. 3.2.3. (1988)

Barnea Y., "Precursory Cooling during Bottom Reflooding of Hot Surfaces with Subcooled Liquid", D.Sc. Thesis, Technion – IIT (1991).

Elias, E. & Yadigaroglu, G., "The Reflooding Phase of the LOCA in PWRs, Part2: Rewetting and Liquid Entrainment", Nucl. Safety, 19, 160 (1977).

Olek, S., "Analytical Models for the Rewetting of Hot Surfaces", Paul Scherrer Inst. (PSI) Report No. 17, Würenlingen and Villigen, Switzerland (1988).

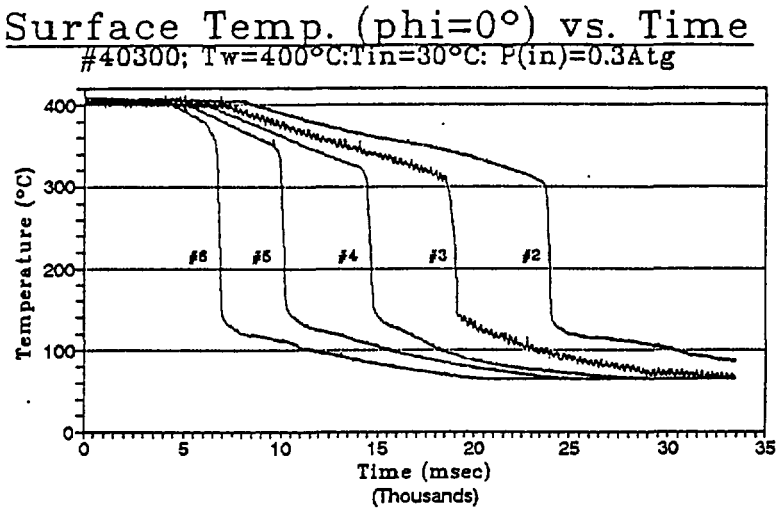

(a)

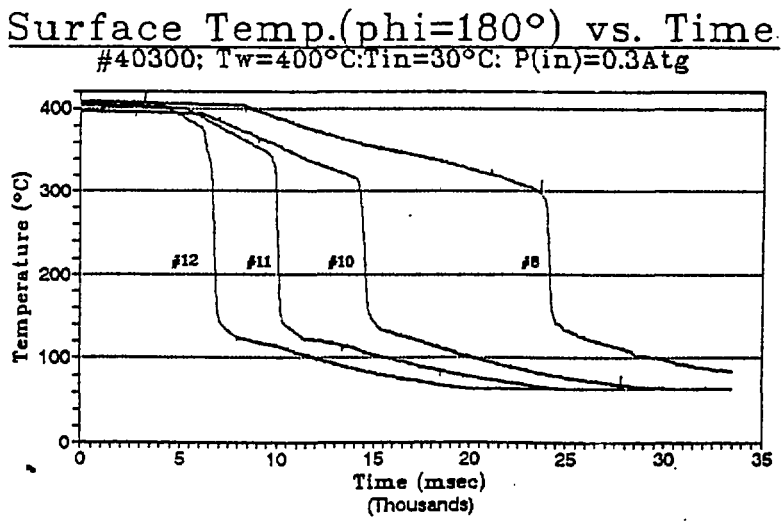

(b)

Figure 1 Surface Temperatures vs. Time at Two Azimuthal Angles

ON THE CONTROL VOLUME FINITE ELEMENT METHOD–TREATMENT OF CONVECTION

Sorin Dickman[+], Shmuel Olek[++], Eitan Wacholder[+] and E. Elias[+]

[+] Faculty of Mechanical Engineering, Technion-I.I.T., Haifa

[++] R & D Division, Israel Electric Corporation Ltd., Haifa

ABSTRACT

The control volume finite element method (CVFEM) is less known and employed by engineers than more conventional methods like the finite difference or the Galerkin finite element method. In this paper we intend to draw the attention to this method as an attractive tool for the solution of PDE arising in fields such as fluid dynamics and heat transfer. A brief description of the method is provided. Emphasis is placed on the treatment of the convection term. As an example, a well known convection type test case is analyzed.

INTRODUCTION

A new numerical scheme was introduced for the solution of the flow and heat transfer problems in a high temperature gas cooled reactor. The scheme is based on the control volume finite element method. In the present work, however, we restrict ourselves to demonstrating the performance of this method in a well known convection type test case.

The control volume finite element method may serve as an alternative to the Galerkin finite element method (GFEM), particularly for Dirichlet problems, because of the higher accuarcy resulting from a physically based way of setting up each CVFEM nodal equation [1]. In the approach of the CVFEM, the algebraic equations, used to represent the continuum system, are formed by performing conservation balances for the appropriate entity, mass, momentum, energy, etc., on defined control volumes distributed throughout the domain. This is in contrast to the more conventional weighted residual or variational approaches to the finite element formulation.

The CVFE method has several advantages. First, the resulting scheme can be made strictly conservative. Thus, when a specific quantity of a conserved variable is transported out of the

control volume, the same quantity is transported into the adjacent control volume. As a result, there is no artificial creation or destruction of a conserved variable. Inaccuracies that arise in coarse meshes, therefore, are due solely to approximation errors.

Second, the fact that the discretization of the governing equations is based on a balance of entities, whether diffusive, convective, or other, means that the terms in the resulting algebraic equations have a specific physical interpretation. For example, an algebraic term could represent a mass flow or the convection of a scalar entity. The modeling of the various terms in the algebraic equation then becomes a problem for the developer's understanding of the physical processes as opposed to his or her agility in handling abstract mathematics. This can lead to very fruitful insights and can be of great assistance in the development stages of program evolution.

Finally, the implementation of a control-volume-based discretization process is straightforward and cost-effective. The calculations of flows at the surface of the adjoining control volumes need be performed only once since the expression is the same for both control volumes, differing only in sign. This leads not only to cost reduction but also to algorithmic simplicity [3].

The convective tranport component in the discrete formulation considerably complicates the numerical modeling. The difficulties can manifest by the presence in the solution of instabilities, false diffusion or oscillations ("wiggles"). In the present study skew upwind and partial skew upwind methodologies in the framework of the CVFEM are analyzed.

DISCRETIZATION OF EQUATIONS

The basis of the control-volume-based finite element procedure is that an algebraic statement which represents conservation for each of the conserved quantities (mass, momentum, and energy) is applied at every control volume. The resulting algebraic equations will, for convection and diffusion problems, express a balance between the convective and diffusive flows of the variable in question, and, if present, the transient and source terms. The solution to the resulting equation system will then satisfy exactly the conservation balance, although an error in the solution will still result due to the approximations that will be employed for the entities. The exact satisfaction of the discrete conservation balance equations is in contrast, however, to most other finite element formulations wherein a weight residual or variational approach is taken.

The discrete control-volume equations can be derived in either of two ways. In the first, the governing differential equation is integrated over the extent of the control volume. This results in a net surface flow balance with the source and storage volume integrals. In the second, the physical conservation balance is applied directly to the finite discrete control volume. While the results of both methods are identical, the second approach does not require a priori knowledge of the actual partial differential equation [3].

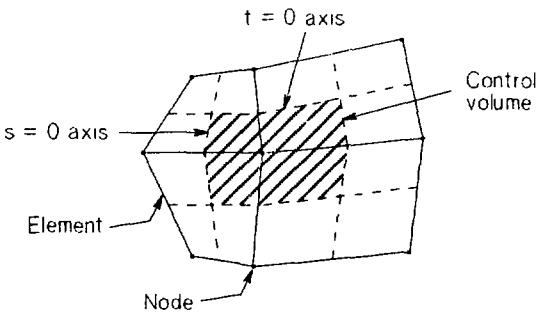

Fig.1. Definition of control volume.

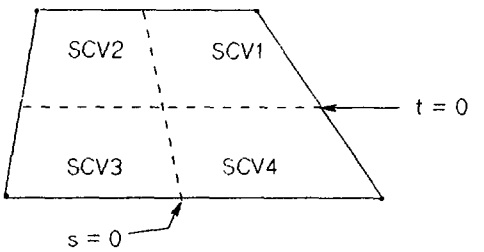

Fig.2. Definition of sub-control-volume and integration point.

CONTROL-VOLUME DEFINITION

In order to obtain a well posed, discrete algebraic problem, there must be one equation for each unknown used to approximate the solution over the domain. The method used to ensure this in a control-volume-based finite element method is to apply a conservation balance to each control volume throughout the domain, there being one control volume corresponding to each node in the solution domain. There is a variety of element configurations possible for use in a finite element discretization. However, in the following we restrict ourselves to the four-noded quadrilateral finite element for reasons of simplicity. Control-volume edges are identified by the lines $s = 0$ and $t = 0$ within each element surrounding a given node, as shown in Fig.1, with the effective control volume formed, upon assembly, as the assemblage of contributions from all elements having that node in common.

The particular choice of $s = 0$ and $t = 0$ for control-volume edges yields a symmetric

distribution of control-volume edges and areas in local coordinates. More important, however, this choice guarantees alignment of the contributing control-volume edges when the elements are assembled, irrespective of the orientation of these elements prior to assembly. This is an important characteristic necessary to retain the full geometric flexibility of the method and to enable all calculations to be performed at element level.

The lines defined by $s = 0$ and $t = 0$ then devide each element into four quadrants. These quadrants are called sub-control-volumes (SCV) and are illustrated in Fig.2. Each SCV boundary surface, internal to the element, contributes terms to the conservation balance through consideration of flows across this surface. In the assembled control volume of Fig.1, where four elements share a common node, there are eight SCV boundary segments defining the control-volume extent. For each such surface, an integral is required to determine the corresponding flow.

At the basic computational level we use one point of integration for the calculation of the convective flux ($\iint_\Gamma \vec{n} \cdot \rho T \vec{V} d\Gamma$) through one side of a SCV. The value of the entity T used in calculating the convective flux is $(1 - W_T)T_u + W_T T_{ip}$, where subscripts u and ip stand for the upwinding point and integration point, respectively. In the skew upwind formulation the value of the scalar entity T is determined at the point of intersection of the velocity direction calculated at the integration point and the boundary of the SCV.

In the partial skew upwind formulation the value of T is calculated at the intersection point of the opposing side of the SCV and the side of the SCV which intersects the direction of the velocity (evaluated at the integration point).

TEST CASE

The problem of convective transport of a step change of the scalar entity T (Fig.3) has often been used to characterize the cross-wind diffusion of numerical schemes [4]. The velocity distribution is uniform, and a discontinuity exists in the value of the transported quantity T across the sreamline a-b, which passes through the center of the square domain. In the particular case where the diffusion term is not present, the discontinuity in T must propagate through the computational domain along a-b. However, due to cross-wind diffution, any numerical scheme will produce some smearing, the extent of which is a measure of the false diffusion introduced.

RESULTS AND DISCUSSION

Fig.4 presents the best possible numerical and presently computed results for the skew upwind method. The best results are obtained for y_c=5, where the solution coincides with the best possible numerical result. For $y_c = 0$ the present solution is given for two mesh refinements

(10 × 10 and 20 × 20) and for y_c=0. In the latter case, it can be seen that numerical diffusion and over/undershooting is present. One way to reduce these inaccuracies is refining the mesh. In this case accurate solutions are obtained at the expense of a greater computational effort. Another way of eliminating the "wiggles" is by employing partial skew upwinding (not shown here because of space limitations) with the drawback of an increase in the numerical diffusion. This shortcoming can be reduced by increasing the value of the weight function W_T.

In summary, possible methodologies for the treatment of the convective term have been presented and the relative merits of each alternative for reducing false diffusion and "wiggles" have been analyzed.

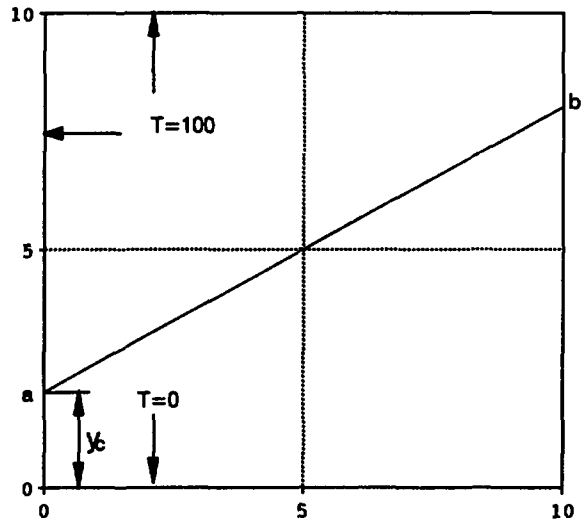

Fig.3. Schematics of the test case.

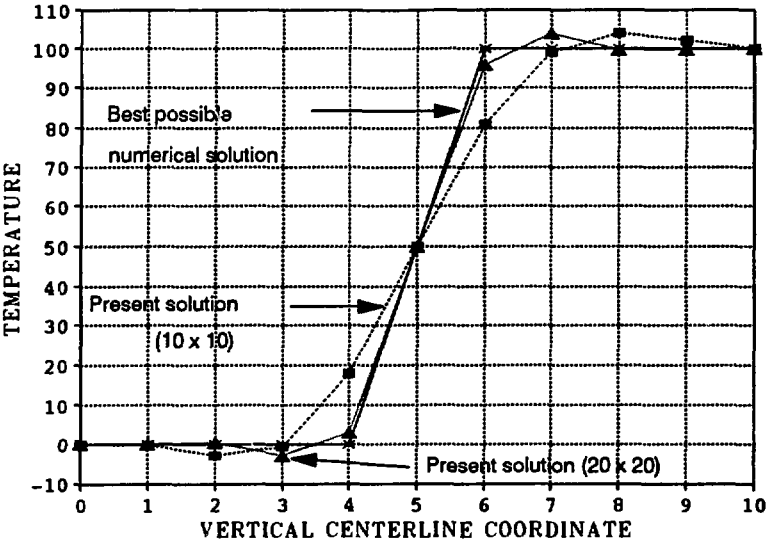

Fig.4. Computed and best possible numerical profiles along the vertical centerline for the skew upwind method. Results are presented for different velocity directions and mesh refinements.

REFERENCES

1. J. Banaszek, "Comparison of Control Volume and Galerkin Finite Element Methods for Diffusion-Type Problems", Numerical Heat Transfer, Part B, Vol. 16, pp. 59-79, 1989.

2. S. Dickman, "Thermohydraulic Analysis of HTGR Pebble Bed Core", PhD. Thesis (in work).

3. G.E. Schneider, "Elliptic Systems: Finite Element Method I", Handbook of Numerical Heat Transfer, Ed. W.J. Minkowycz, p. 379, Wiley-Interscience, ,New York, 1988.

4. C. Prakash, "Examination of the Upwind Formulation in Control Volume Finite Element Methods for Fluid Flow and Heat Transfer", Numerical Heat Transfer, Vol. 11, pp. 401-416, 1987.

ABSTRACT

The Canadian National Calibration Reference Centre for *In-Vivo* Monitoring: Its functions and its role in estimating the radioactive contamination of people in the Canadian Northwest Territories and the Russian Immigrants to Israel.

Gary H. Kramer
Human Monitoring Laboratory
Bureau of Radiation and Medical Devices
Department of National Health and Welfare
775 Brookfield Road, Ottawa, Ontario
CANADA K1A 1C1

BACKGROUND

In Canada, protection of workers and the public from ionizing radiation is a responsibility shared between the Atomic Energy Control Board (AECB) and the Department of National Health and Welfare. The AECB controls the exposures through its licensing process, under which licensees are required to determine the radiation dose received by workers and to ensure that the doses are below the regulatory limits. Doses to the public from licensed facilities are regulated through environmental, not human monitoring.

The Department of National Health and Welfare has a general mandate to protect and preserve the health of Canadians. At the Bureau of Radiation and Medical Devices (BRMD) a national external dosimetry program, and bioassay and *In-Vivo* measurement programs for internal dosimetry are conducted in addition to the national environmental monitoring programs.

FUNCTIONS

The determination of the radiation dose is generally a two-part process. The first part is the basic measurement such as a whole body count, a thyroid count or analysis of a thermoluminescent dosimeter which involves the use of an instrument. The second part of the process is the conversion of the measurement into a dose and is beyond the scope of this presentation.

The first, or measurement stage, requires calibration of the measuring instrument to ensure that the measurement is accurate. The calibration process must involve comparison either directly or indirectly with an appropriate standard. The process also requires appropriate documentation to demonstrate that the measurement accuracy is traceable to the standard. Without this tracing process, the estimate of the doses received may not be accurate, increasing the hazard to workers and the public. Standardization of radiation dose is not only a regulatory concern but is a worker and public concern also, as evidenced by the great interest shown by labour unions and by the public.

In 1983, the Atomic Energy Control Board (AECB) decided that a formal program of calibration for all forms of dosimetry was required. Three working groups were set up to determine the requirements for comprehensive calibration programs for external dosimetry, internal dosimetry and dosimetry of radioactive atmospheres. The Working Group for Internal Dosimetry recommended that the BRMD administer the calibration reference program for that aspect of dosimetry as a development of its existing informal calibration program.

In 1984, funding was obtained for this development and a reference centre was established at BRMD; part of the Reference Centre is the Human Monitoring Laboratory (HML). The HML has now been designated as Canada's National Calibration Reference Centre for *In-Vivo* Monitoring. The HML is a unique facility in North America. It provides external calibration sources to Canadian facilities to either confirm that their in-house calibration is accurate or provide sufficient information so that the facility can confidently implement a new calibration data set. Currently this service is free of charge.

Since 1987 the HML has been improving and expanding the design of the phantoms used in the inter-calibration; recent advances have been greatly influenced by the recommendations of the Workshop on Standard Phantoms (1).

The benefit to a user of the BRMD standard phantom program is two-fold. First, facilities can compare their results to other Canadian facilities and judge their performance based on the results. Second, and more importantly, the participation in the HML's Inter-Calibration Program allows the facility to demonstrate that their in-house calibrations are accurate and that their quality assurance program is performing as expected. The use of an outside independent standard gives any quality assurance program more credibility than it would otherwise have if all quality control results were based on in-house data.

POPULATION MONITORING

The accident which took place at the Chernobyl reactor site in the Commonwealth of Independent States (CIS; formerly known as the USSR) in 1986 spread radioactive fallout over the entire Northern Hemisphere. The amounts deposited in North America were not great but reports of contaminated reindeer herds in Scandinavia caused the Department of National Health and Welfare to examine the amount of fallout that was deposited in the Northwest Territories.

This was of particular concern because it was known that the fallout from the atmospheric atomic weapons tests in the 1960's had a very short pathway to human uptake. Many of the local residents hunt caribou and these animals subsist mostly on lichens during the winter period. The fallout deposits radionuclides on the lichen which is in turn consumed by the caribou and then the hunting population.

Radiocesium uptake by consumers of caribou meat had been a topic of concern in the

1960's. During the years 1966 to 1969, the Department National Health and Welfare Canada carried out a large number of radiocesium measurements in people from various Arctic communities. The levels in some individuals close to 100 kBq, with corresponding radiation doses were approaching 5 mSv, the maximum dose recommended for members of the public.

In 1986, this Department began a two year program of measurements on the various caribou herds in the Northwest Territories, the Yukon, and Northern Quebec. In no case did the radiocesium levels approach those reported for the Scandinavian reindeer. However, only 25% of the radiocesium in Canadian caribou originated from the Chernobyl accident; the remainder was residual fallout from the earlier atomic weapons testing.

Three factors prompted the Department to send a small team into Northern Canada to get accurate estimates of the internal radiocesium content of the hunting population. These were the realization that the Northwest Territories hunting population had been chronically exposed to radioactively contaminated meat over some 30 years, a great deal of media exaggeration of the problem in Northern Canada by a few outspoken activists and the fact that no model calculation can be validated without real data.

In contrast to the Northwest Territories project, the problem with the Russian Immigrants in Israel was not one of a prolonged chronic exposure but an acute exposure to possibly much higher levels of internal contamination. Most (if not all) of the Russian immigrants to Israel had not been tested by the teams sent to the CIS by the International Atomic Energy Agency (IAEA) and, therefore, had no idea what their internal burdens of radiocesium might be. Although it was expected that the internal burdens would be low, there was no way of demonstrating this expectation to the concerned population without actually performing the measurements.

The Department of Health and Welfare was asked to assist the Soroka Medical Centre and the Ben Gurion University in carrying out this project. The concern and anxiety of the immigrant population was very high; over 1200 persons were monitored in the three week period that the whole body counting was carried out and all of the participants were volunteers. Furthermore, all of the available appointments for whole body counting were filled before the actual measurements began.

The results obtained have not yet been fully analyzed at the time of writing this abstract but preliminary analysis of the data indicates that the internal burdens of the immigrant population are less than those measured by the IAEA. Reasons for this will be discussed during the course of the presentation.

1. Kramer GH, Inn KGW. A Summary of the Proceedings of the Workshop on: Standard Phantoms for *In-Vivo* Radioactivity Measurement. Health Physics 1991;61(6): 895-902

Occupational Exposure to Ionizing Radiation in Israel during the decade 1981 - 1990

T. Biran, S. Malchi
Radiation Safety Department
Soreq Nuclear Research Center

A statistical analysis of the occupational radiation exposure of radiation workers in Israel in the decade 1980 - 1990 was carried out using the central data base of National Personnel Dosimetry Service. The analysis refers to whole-body exposure to external penetrating ionizing radiations: X-ray, gamma, thermal neutrons, fast neutrons. Radiation doses were measured by TLD badges (chest, hand, leg, head). TLD rings or CR-39 nuclear track etch detector.

The data were compiled according to the questionaire of the United Nations Scientific Committee on the effects of Atomic Radiation (UNSCEAR). Statistics on annual doses were obtained for three main occupational categories: medical uses of radiation, industrial uses of radiation and education (including research) establishments.

Tables 1, 2 and 3 summarize the number of monitored workers, number of measurably exposed workers, collective effective doses (man Sv), Annual average individual effective dose per monitored worker (mSv)' measurably exposed worker fraction of the work force exposed above 15mSv annual individual dose (NR15) and fraction of the annual collective dose delivered at annual individual doses exceeding 15mSv (SR15 or MR15). Classification of the data follows the UNSCEAR guidelines.

As can be seen from the tables the annual average individual effective dose for a monitored worker of medical staff is in the range of 0.2-1.0mSv. Industrial workers are exposed to 0.1-0.7mSv/year while educational and research establishments radiation workers are exposed to much lower values: 0.06 - 0.23mSv/year.

Of course the annual average individual effective doses per measurably exposed worker (above 0.15mSv) are much higher: 1.3 - 3.8 mSv/year for medical staff, 1.8-3.7mSv/year for industrial workers and much lower values for educational and research radiation workers : 0.8 - 1.8mSv/year (excluded 1984).

As also can be seen from the tables the fraction of the workforce exposed above 15mSv is very low for all three categories while the fraction of the collective dose delivered exceeding 15mSv is quite high. This indicates that a large fraction of the collective dose is due to the small number of individuals exposed above 15mSv.

The statistical data of the medical staff were classified into 4 sub groups: diagnostic radiology (all), dental radiology, nuclear medicine and radiotheraphy.

The annual average individual effective doses of diagnostic radiology and radiotherapy staffs are between 0.1-1.0mSv/year per monitored worker, for dental radiographers: 0.02 -0.2mSv/year while nuclear medicine radiation workers are exposed to 0.5 - 1.0mSv/year per monitored worker.

On the other hand the annual average effective dose equivalent per measurably exposed worker do not differ significantly for differnt categories of medical employees.

Extremely Low Frequency Electromagnetic Fields (E.L.F. E.M.) Inside Infant Incubators.

E. Grubstein *, H. Shabtai*, E. Zemora** and A. Kushelevsky+

* Nuclear Research Center, POB 9001 Beer Sheva

**Department of Neonatology, Soroka Medical Center, Beer Sheva ,Israel

+ Department Of nuclear Engineering Ben Gurion University , Beer Sheva ,Israel

Until recently, it was assumed that E.L.F. E.M. radiation may pose health hazards only at very high intensities due to possible thermal effects. However work published in the last decade indicates that low levels of E.L.F. E.M. radiation can cause biological changes on a cellular level [1] and may even be associated with leukemia particularly in children, who appear to be in greater danger to E.L.F. E.M. radiation than adults [2].

These findings have focused attention on the need to monitor the E.L.F. E.M. emissions from electrical equipment.

In this paper we report on E.L.F. E.M. field levels measured inside infant incubator units. Infant incubators are used for the care of premature infants. They provide a controlled temperature and humidity environment which is obtained by means of electrical blowers and heaters underneath the mattress on which the infant lies. The importance of monitoring them is obvious considering that many of treated infants remain inside these units for long periods. Measurements were made at 50 Hertz using a magnetic flux density mete (Radiation Technology) calibrated in milliGauss(mG) units. They were carried out in the neonatal units of the Soroka and Beilinson Medical Centers in Beersheva and Petach Tikva respectively.

Results and Discussion

Much higher than background EM intensities were found inside the incubators at the mattress level, close to the control panel immediately above the blower and heater units, in nearly all of the incubators examined. In over 30 percent of the cases the fields exceeded 50 mG. In a few cases the levels were even higher than 100 mG. Further away from the the blower and heater units but also inside the incubator on the mattress the EM levels were found to be lower, but still higher than normal hospital background levels which are less than 1mG , and in most cases even higher than the Swedish recommended safe level [3] of 2.5 mG. .

As infants are generally more susceptible to the effects of radiation, we recommend that steps be taken to reduce the EM levels in the incubators.

Reduction of EM emission can be achieved by using less 'noisy' electrical components, placing them as far as possible from the mattress and by enclosing them in adequate magnetic shielding.

References.

1. Byus CV, Kartun K, Adey WR; Cancer Research1988;48:4222-4226
2. Savitz DA, Wachtel H, Barnes FA, John EM, Tvrdik JK AM. J. Epidemiol 1988 ;128:21-38
3. Tomenius L. Bioelectromagnetics 1986;7:191-208

Radon in Israel-1991

M. Margaliot, T. Schlesinger, M. Israeli, Y. Shamai, R. Duchan, O. Even, A. Aharony, U. Vulkan and A. Tal.

Soreq Nuclear Research Center, Yavneh 70600, Israel

and

A. Kazir

Tel-Aviv University, Ramat-Aviv, Israel

Introduction:

The exposure of the human tracheobronchial tract to ^{222}Rn (Radon) progeny, is widely accepted[1] to be the main environmental contributor to the general public's exposure to ionizing radiation. Consequently, measurements of ambient atmospheric radon concentrations are performed in many countries.[2]

Radon measurements in Israel are presently conducted mainly by a few commercial bodies. One of these (I.T.M. Ltd) employs the services of the dosimetry laboratory of the SNRC radiation safety department, and the information gathered within this framework, is the basis for the present study.

This information includes results of nearly 9,000 radon measurements performed in various regions of Israel, in which ~85% of Israel's population live, during the period May 1990 -December 1991.

Some features of interest, derived from this vast amount of raw data, are presented below:

a. Methods of measurement:

The information in the present work was gathered by both short-term (one week) and long-term (3-18 months) radon measurements.

1. Short-term radon measurements: These were conducted mainly (95%) with electret ionization chambers (Rad-Elect Inc.)[3].
   In the rest of the short-term measurements, activated charcoal canisters (F&J Products Inc)[4] were used.

2. Long-term integrative radon measurements (3-18 months): these were conducted with a Solid State Nuclear Track Detectors (SSNTD) system, developed by the dosimetry laboratory at SNRC.[5].

All three kinds of detectors were calibrated in the same radon chamber (2900 Bq/m^3 of radon, in a 2.7 m^3 chamber, inter-calibrated with the US EPA radon calibration facility in Las Vegas).[6]

b. Selection of measurement site and method:

The radon measurements were performed at the request of the occupants of the dwellings, and the detector(s) were deployed at the sites (within the dwellings) in which the occupants spend most of their time (main living room, bedroom etc.).

The typical radon measurement consisted of a one week electret exposure, (which is preferred to charcoal canisters due to its superior integration properties[3]).

Charcoal canisters were used only when it was suspected that high gamma radiation levels were present at the measurement site (since electrets are sensitive to gamma radiation). The majority of the measurements were conducted under normal ventilation conditions, as this was convenient to the dwellings occupants

When the radon levels thus detected, exceeded 40-50 Bq/m^3, it was recommended that a long-term measurement (>3 months) be conducted. (the basis for setting this threshold is discussed later).

As a result, ~10% of the short-term measurements were actually followed by long-term SSNTD measurements.

c. Radon levels in the populated regions of Israel.

The arithmetic and geometric averages of the radon levels measured in the various regions of Israel are presented in table 1 below. (the values in parenthesis are the corresponding standard deviations)

It should be noted that these are the results of the short-term measurements conducted in those regions.

The short-term results were chosen for this presentation, rather than the long-term ones, as the latter are probably biased, since the selection method of the measurement site, described above, tends to prefer locations with higher-than-average radon level, as sites for long-term measurements.

Table 1.
Radon levels in Israel-1991. (Bq/m^3)

location	arithmetic average	geometric average	population (% of total)	No. of cases (% of total)
Even-yehuda	59 (58)	39 (2.2)	0.03	2.7
Ashdod	69 (75)	46 (2.7)	2.5	13
Be'er-Sheva	50 (50)	35 (2.1)	5	1.7
Herzelia	44 (39)	30 (2.0)	3	3
Haifa	79 (90)	60 (2.8)	19	5.6
Tveria	60 (70)	40 (2.6)	2.4	1.3
Jerusalem	72 (81)	47 (2.6)	20	9
Carmiel	100 (121)	71 (3.0)	1.3	8.5
Naharia	62 (57)	40 (2.2)	1.3	20
Omer	40 (25)	28 (1.8)	0.05	0.3
Arad	90 (95)	72 (2.5)	0.8	10
Petach-Tikva	39 (37)	30 (2.0)	3	1.8
Kiryat-Gat	31 (21)	27 (1.8)	1.4	0.7
Kiryat-Tivon	66 (78)	45 (2.6)	1.2	0.6
Rechovot	40 (32)	30 (1.9)	3.3	0.8
Ramat-Gan	57 (65)	39 (2.3)	8	3.1
Ra'anana	68 (65)	46 (2.1)	2.5	2
Tel-Aviv	60 (70)	40 (2.5)	25	15.9
average of all measurements	68 (81)	43 (2.5)	------	100
population weighted aver.	64 (70)	40 (2.5)	100	-----

Notes to table 1:

1. The average radon levels presented above, are higher than the 33 Bq/m^3 cited as arithmetic indoors average, by the ICRP[7]. This fact is attributable to a bias which is introduced by the non-randomal selection of measurement sites: usually, measurements are ordered only for first floors and basements, which are expected to have elavated radon levels. In addition, people neighbouring a place in which a high radon level was detected, tend strongly to measure radon in their homes too. Such a bias has been reported[10] in the US, where radon measurements are also conducted commercially. **It can thus be assumed that the actual average radon level in dwellings in Israel (and the resulting human exposure) is lower than that indicated by the data in table 1.**

2. The fact that the standard deviation from the arithmetic average, is larger than the average itself (i.e. 64 ± 70), while negative radon levels are meaningless, is an indication that the data itself is

un-symmetric and not normally distributed. It appears that the data follow a log-normal distribution, and this becomes evident when the data distribution is presented on a logarithmic scale (fig. 1). The significance of the last observation is that a relatively small number of houses with excessively high radon levels, cause the elavation of the average. Remedial steps should therefore be aimed mainly at these places

Regarding the frequency distribution of the radon levels, it should be noted that ~20% of the results are higher than 100 Bq/m^3, ~7% are higher than 200 Bq/m^3, about 2% exceed 300 Bq/m^3 and 0.2% exceed 800 Bq/m^3.

3. The data regarding the population distribution in the table, is based on the 1990 annual publication of the Israel central bureau of statistics. In most cases, locations are referred to by the name of a central town, but the town's vicinity population is also included. (i.e."Ramat-Gan" refers to Ramat-Gan, Givaataim and Bnei-Braq).

4. The highest radon levels occur in Arad (arithmetic av.=90 Bq/m^3 , geometric av.=72 Bq/m^3) and in Carmiel (a.av.=100 Bq/m^3, g.av.=71 Bq/m^3). The elavation of radon levels in these two places is statistically highly significant (the null hypothesis probability for both places is $<10^{-3}$).

Arad is located in a phosphate rich area, and the uranium concentration in the phosphates in this area is ~100 PPM[8]. The elavated radon level in this region is thus to be expected.

The ground in the Carmiel region (chalk rocks) was not known formerly to be uranium rich.

Following the detection of high radon levels in this region, the uranium concentrations in a few ground samples from this region were examined by the dosimetry laboratory in SNRC (by delayed neutron analysis), and were found to be in the range 27-65 PPM (this is to be compared with the 1.8 PPM cited as the average soil concentration of uranium[9]). The radium concentration in these samples was also examined and was found to be nearly in equalibrium with the uranium. Additionnal measurements of radioactivity in the groud are needed in this region. (ground sampling was conducted by the SNRC field applications dep.)

It is noteworthy that while the arithmetic average radon level in Carmiel is higher than in Arad, the geometric average level is lower.

This apparent discrepancy is probably due to the difference in the distributions of radon levels in these two regions: while the elavated average in Arad is due to an abundance of cases of moderately high levels (150-200 Bq/m^3), the high arithmetic average in Carmiel is due to a few extremely high results.

In fact, the highest radon levels measureded by our laboratory in dwellings in Israel- 6650 Bq/m^3, were recorded in this region. Altough the reasons for the occurance of these high radon levels, have not been yet examined in detail, it appears, that at least in the few cases examined so far, the entry path of the radon into the buildings is via the underground tubing of the electricity network. (a feature

unique to Carmiel). This assumption has yet to be verified on a larger scale.

Fig. 1

Radon levels in Israel-1991.

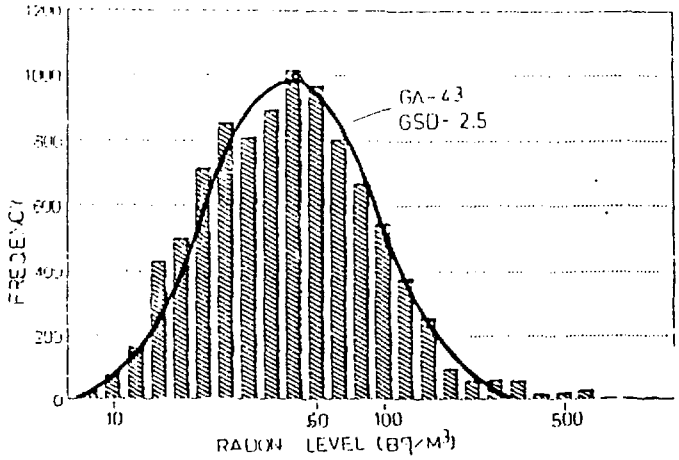

Note to Fig. 1: the bars represent the actual frequency distribution of the measurements. the continuous line represents a log-normal distribution with the same parameters (g.av=43, gsd=2.5).

d. Comparison of short-term to long-term radon measurements.

As stated above, ~10% of the short-term measurements were followed by long term measurements in the same locations. It is thus possible to compare the readings of these two different measurement methods. The frequency distributions of 850 short and the 850 parallel long-term measurements are shown in Fig. 2.

Fig. 2: Short versus long-term radon measurements. (850 cases each)

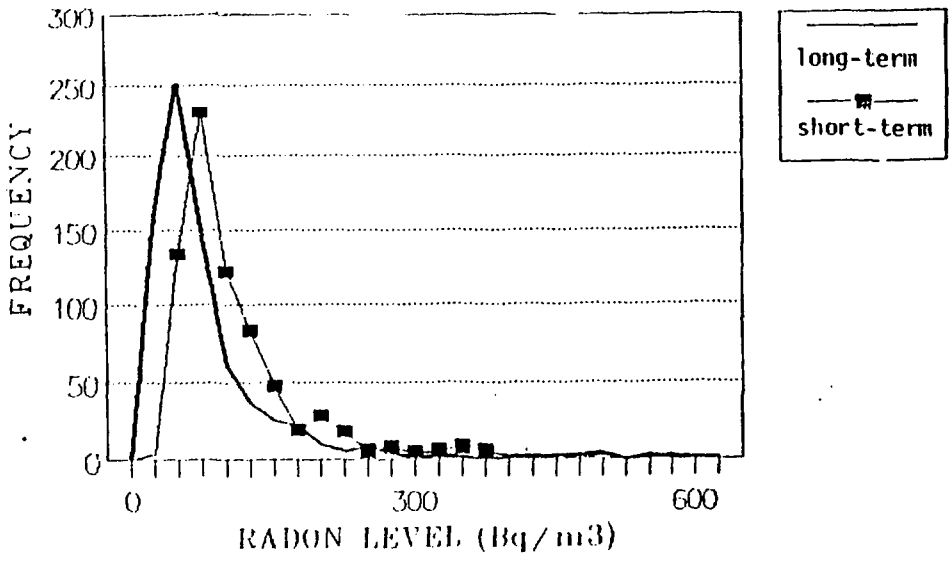

Notes to Fig 2:

1. It is evident that the short-term detectors show higher results than the long-term detectors. As the two types of detectors were calibrated in the same radon chamber, the discrepancy is due probably to a real difference in the measured quantity: The radon level is known to fluctuate in time, and hence, a high result of a short-term measurement might represent an upwards fluctuation, rather than a real high average radon level.
As only a "high" (> 40 Bq/m^3) reading of a short-term detector leads to a recommendation to conduct a long-term measurement, (which is less given to fluctuations) the average readings of the short-term detectors, are expected to be higher than those of the long-term detectors.

2. Comparing the results of the short and long-term measurements it appears that in ~60% of the cases the short-term results are higher than the long-term results. in ~20% of the cases the short-term results are lower by a factor of >1.5 than the long-term ones, and in ~5% of the cases the short-term results are lower than the long-term readings by a factor of 2.5 or more. It is the last detail which is the basis for selecting the short-term result of 40 Bq/m^3 as a threshold for performing long-term measurements: the Israel Atomic Energy Commission recommends presently 100 Bq/m^3 as the maximal radon level in dwellings[11]. It follows that if the short-term result does not exceed 40 Bq/m^3, it is probable (at the 95% certainty level), that the average long-term radon level will not exceed the $40*2.5=100$ Bq/m^3 recommended level.

REFERENCES

1. *IAEA: Facts about low-level radiation.* IAEA/PI/A14E, 1989.
2. Natural Radiation Exposure in UK Dwellings; NRPB-R190, 1988.
3. Kotrappa P. and Dempsey J.C.; An Electret Passive ^{222}Rn Monitor, Based on Ionization Measurement. Health Phys. 54:47, 1988.
4. Cohen B.L. and Cohen E.S.; Practical espects of radon detection with Charcoal Canisters. Health Phys. 45:501, 1983.
5. Margaliot M., Schlesinger T., Even O. and Kazir A. A Laser Scanning System for NTD Dose measurements. Isr. Nucl.Soc.Trans. 16:83, 1990.
6. Margaliot M. Schlesinger T. Even O. Duchan R. המאמר על תא הכיול and Shamai Y. A Small Radon Calibration Chamber, Properties and Mode of Operation. Isr.Nucl.Soc. Trans 16:204, 1990.
7. ICRP Pub No. 50, 1987.
8 Mazor E., and Molcho M.; J. of Hydr. 15:37, 1972.
9 *NCRP Rep. No 77. NCRP, 1984.*
10. Nero A.V. Airborne Radionucleides and Radiation in Buildings: a Review. Health Phys.45:303, 1983.
11. SNRC Rep. No 2029.

STUDIES IN ISRAEL OF RADIOCESIUM IN AN IMMIGRANT POPULATION COMING FROM AREAS OF THE UKRAINE, BYELORUS AND RUSSIA NEAR CHERNOBYL

M. R. Quastel[1], G.H.Kramer[2], L. Noel[2], R. Gorodisher[3], S. Polliak[1], E. Kordysh[4], R. Cohen[4] and J.R. Goldsmith[4]

[1]Institute of Nuclear Medicine, [3]Dept. of Pediatrics A, and [4]Dept of Epidemiology, of the Soroka Medical Center and Faculty of Health Sciences, Ben Gurion University of the Negev, Beer Sheva, Israel; [2]Bureau of Radiation and Medical Devices, Health and Welfare Canada, Ottawa, Ont., Canada.

During the period 1990-91, about 400,000 new immigrants from the former Soviet Union came to Israel. Of these, it is estimated that more than 40,000 came from areas of the Ukraine, Byelorus and the Russian republic which had been contaminated with radioisotopes from the Chernobyl accident in April 1986. Part of the total radiation exposure of these individuals has been due to radiocesium (physical T 1/2 of 30 years) which is ingested with the food. This radionuclide is distributed throughout the soft tissues of the body by an active transport mechanism similar to that of potassium, leaving the body mainly via the urine with a biological half time of about 100 days in adult males, and somewhat less in women and children.

As part of an effort to assess the total radiation exposure of these people, we carried out measurements of total body radiocesium in over 1,200 men, women and children using a portable whole body counter provided by Health and Welfare Canada. The population studied consisted of volunteers of all ages, generally in family groups. They had been in Israel from 1 week to almost 2 years and came from many urban centers in the CIS, but Gomel and Kiev were the largest sources of immigrant volunteers.

Most persons who had been in Israel more than 6 months had lost virtually all the radiocesium that they had accumulated prior to leaving the former USSR, and their body burdens had fallen below levels measurable with the portable whole body counter. However, individuals who had been in Israel less than 3 months still retained sufficient levels to allow an approximate back projection of body burden to the time before their immigrantion. For this back projection, we used arbitrary biological half times of 90 days for men, 65 days for women, and 36 days for children (1).

Since many of the persons examined had radiocesium body burdens below measurable levels, it was found useful to express the whole body counting results in terms of the proportion of subjects with radiocesium levels above a certain value (selected at 50 Bq). Figure 1 illustrates the differences between Gomel and other towns in the contaminated regions, in comparison to communities such as Kiev located in less contaminated areas. In figure 1, the values are calculated for different periods of residence in Israel, that is, without back projection to the time of arrival.

These data show that former residents of Gomel and other towns with substantial ground contamination with radiocesium are more likely to have detectable body burdens than do people coming from less exposed areas such as Kiev. We also found evidence of an exponential decrease with passage of time after arriving in Israel.

Figure 2 shows Cs-137 levels in persons who had come to Israel not more than 3 months before the date of measurement in November 1991. All body burden measurements were calculated after subtracting the contribution of environmental radon to the Cs-137 peak. The figure shows the proportion of subjects according to their Cs-137 levels expressed as log (Bq/kg), after back projecting to the time of departure from the CIS using the biological half times already mentioned.

The levels of radiocesium in Jews who emigrated from the Chernobyl regions in 1991 were lower than those observed during the 1960's as a result of fallout from atmospheric nuclear testing (2). Our back projected estimates for adults from the Gomel region having detectable levels gave average body Cs-137 concentrations of about 5 Bq/kg. In contrast, average body burden estimates reported from the Gomel area in the 1960s (4) were 2.6-4.2 kBq with concentrations up to 92 Bc/kg for children and 41 Bq/kg for adults. In Canada, at the same time, body burdens of healthy male adults were 6-30 Bq/kg (unpublished data).

We are aware of substantial measurements carried out by the IAEA in 1990 in smaller villages in the Chernobyl regions, but these results have not yet been cleared for publication.

It is important to point out that the total radiation exposure to this population was due not only to radiocesium but also to short lived agents such as I-131 which were present in the environment during the first few weeks after the accident. In addition there are longer lived alpha and beta emitters some of which are bone seekers and difficult to detect. The present measurements, made 5 years after the accident, were restricted to Cs-137 with a biological half time of 100 days or less, and are inadequate to provide an overall assessment of cumulative dose. Estimates of health hazard due to overall radiation exposure will depend on further measurements of the body content of other long lived radioisotopes, biologic markers and the analysis of epidemiologic data.

(1) Schwartz, G. and Dunning, D.E. (1982) Imprecision in estimates of dose from ingested Cs-137 due to variability in human biological characteristics. Health Physics 43, 631-645.

(2) Marei, A.N., Barkhudarov, R. M., Novikova, N.J., Petukhova, E.V., Dubova, L.D. and Briganina, V.M. (1972) Effect of natural factors on cesium-137 accumulation in the bodies of residents in some geographical regions. Health Physics 22, 9-15.

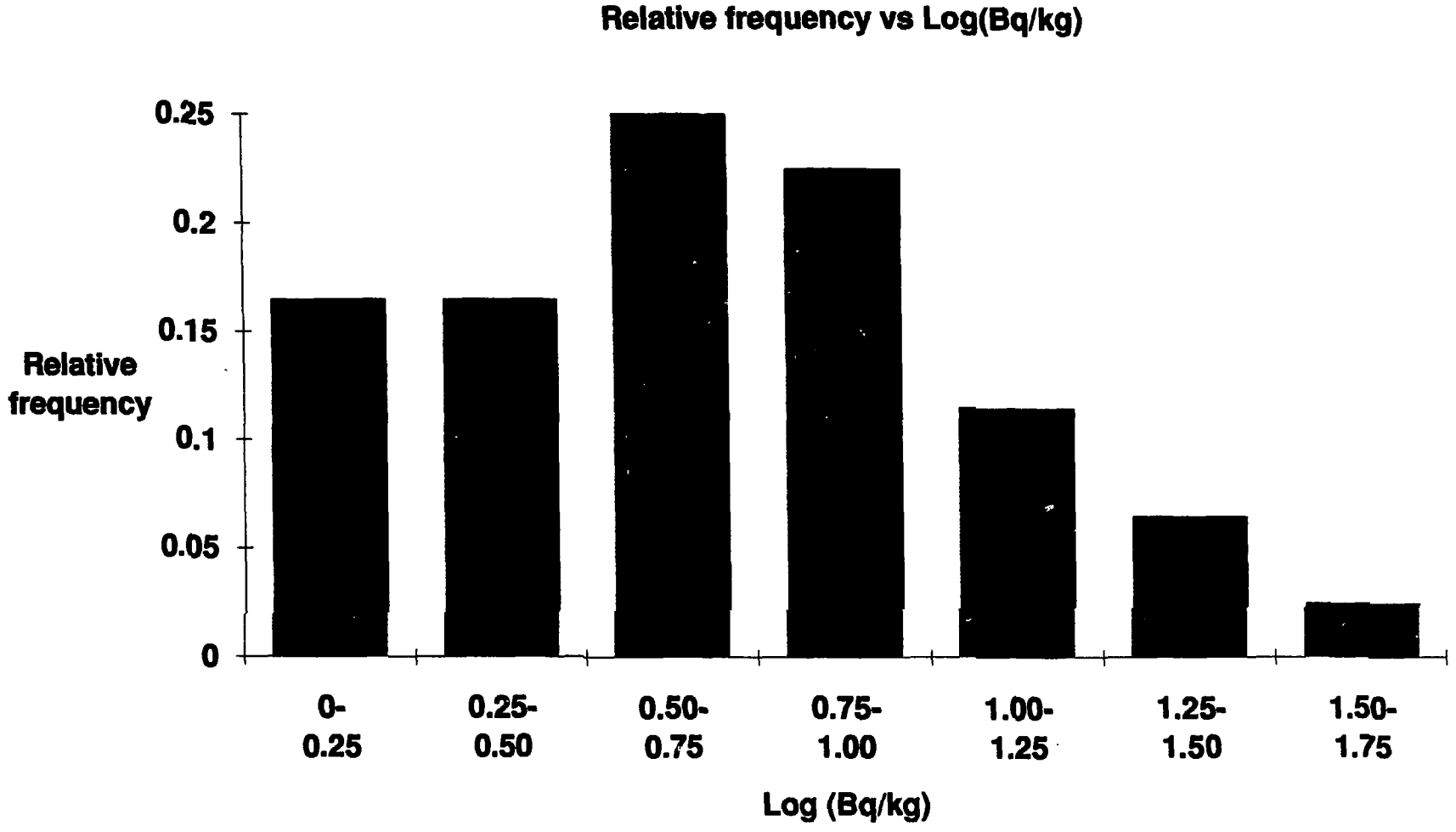
Relative frequency vs Log(Bq/kg)
Relative frequency
0.25
0.2
0.15
0.1
0.05
0
0-0.25
0.25-0.50
0.50-0.75
0.75-1.00
1.00-1.25
1.25-1.50
1.50-1.75
Log (Bq/kg)

RADIOCESIUM, > 50Bq, OLIM BY RESIDENCE, AND INTERVAL SINCE ALIYAH, PERCENT

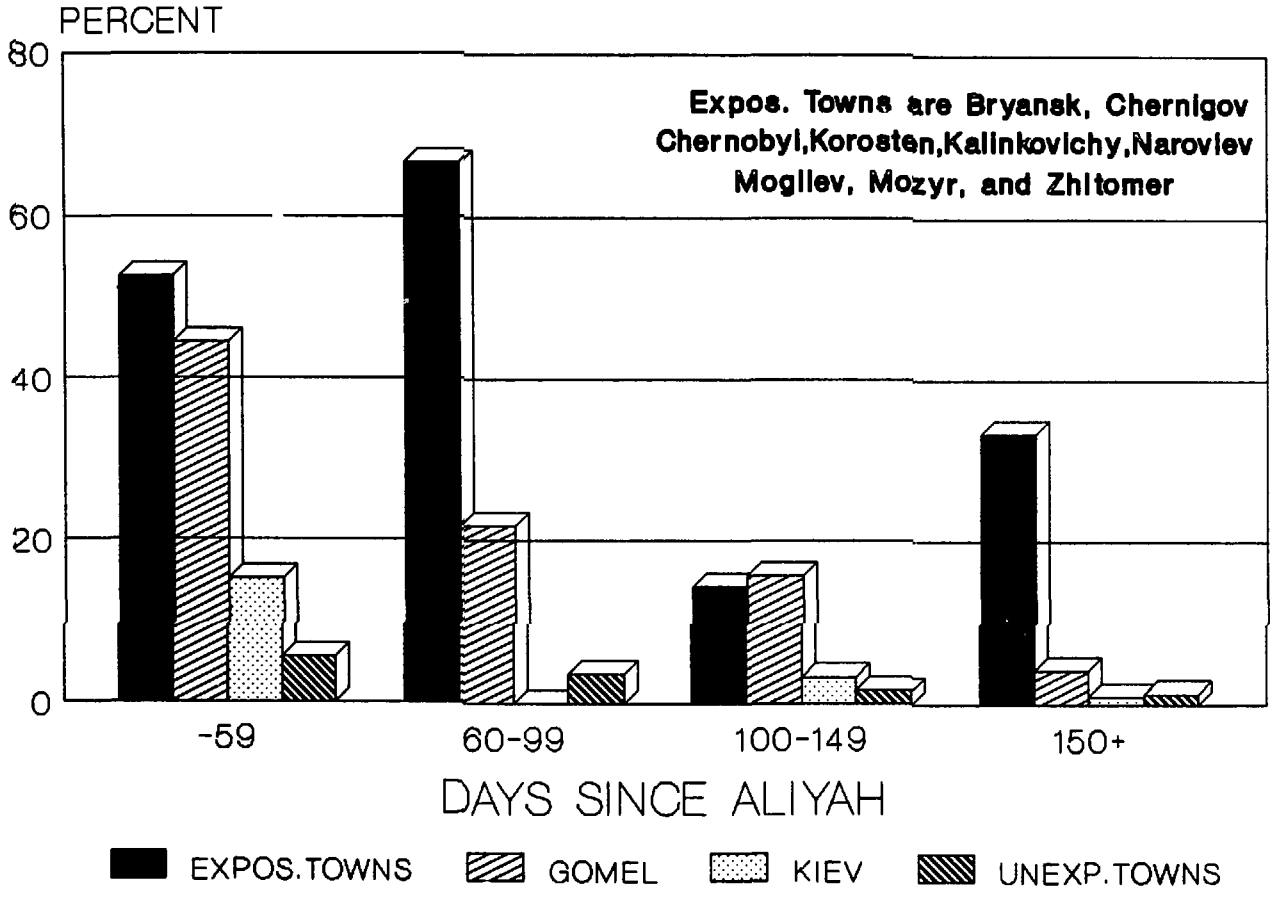

CALIBRATION OF TLD BADGES TO BETA RAY SPECTRA FROM ^{32}P.

U.German, B.Ben Shachar, E.Naim
Nuclear Research Center - Negev

1. Introduction.

The results of TLD chips readings are received in nanocoulomb units. Experimental calibration factors, also called beta factors, must be used to evaluate the penetrating and non-penetrating doses, but these calibration factors differ according to the spectral distribution of the various radiation sources [1]. No specific calibration factor can be evaluated for each case for a system based on a two chips card, and a compromise factor has to be found that will overestimate some exposures and underestimate others. It is of practice to use uranium as the beta reference source for the calibration factor determination as this source is most likely to be encountered and will overestimate the exposures in most cases. However, when more accurate evaluation of the exposure has to be made, specific calibrations have to be performed. The present work presents the evaluation of the beta factor of the TLD badge used at NRCN for ^{32}P beta source.

2. Theoretical evaluation.

The theoretical approach uses the theory of interaction of electrons with matter to develop a dose distribution function. Loevinger [2] used empirical data to derive a dose distribution function from a point beta source. The Loevinger expression has been widely used in beta dosimetry evaluations and some revisions of its parameters were also published. The average dose absorbed in the dosimeter is given by :

$$D=D_o*(1-e^{-\mu r})/(\mu r)$$

$$\mu= 18.6*(E_{max}-0.036)^{-1.37}$$

where:

μ - absorption coefficient of the dosimeter (cm^2/g)
E_{max} - maximum energy of beta ray (Mev)
r - dosimeter thickness (g/cm^2)
D_o - the zero thickness dose
D - the average dose absorbed in the dosimeter

The beta factor is calculated dividing D by D_o. For a ^{32}P source (E_{max}=1.71 Mev) and for a TLD-100 crystal thickness of 0.9 mm (230mg/cm²) we obtain a beta factor value of 0.41.

3. Experimental evaluations.

The measurements were performed with G-1 standard manufactured TLD cards, each containing two TLD-100 chips. An NRCN badge contains one TLD card. In order to detect penetrating and non-penetrating doses one of the crystals in the badge is covered by a 1.25mm Al filter. The cards are read in an 2271 Automatic Harshaw reader.

3.1 Two calibrated beta sources

Standard TLD badges were irradiated by two calibrated beta sources : ^{204}Tl (E_{max}=0.766 Mev) and $^{90}Sr/^{90}Y$ (E_{max}=2.28 Mev). The measurements were performed at the SSD Laboratory at a distance of 30cm. The beta factors for the two sources were evaluated from the ratios between the TLD readings and the known beta doses at the dosimeter position. The beta factors for the ^{204}Tl and $^{90}Sr/^{90}Y$ sources were found to be 0.043 and 0.74 accordingly. An approximate evaluation of the beta factor for ^{32}P can be made by interpolation at E_{max}=1.71 Mev . A value of 0.53 is obtained.

3.2 Uncalibrated ^{32}P source

Standard TLD badges and bare TLD cards were exposed to radiation from a ^{32}P source at three distances. The readings of the two TLD chips of the badge are due to the penetrating and the non-penetrating components of the radiation. The bare TLD cards represent the total exposure dose. Subtracting from the reading of the bare cards the penetrating radiation component gives the non penetrating contribution. The beta factor can be evaluated by dividing the TLD badge non-penetrating response by the bare card response. The different values are given in table 1. The values for the distances 38cm. and 50cm are almost similar, with an average value of 0.54 . For the distance of 10 cm the value of the beta factor is lower. This lower value can be attributed to the softer beta spectrum expected near the source and to geometrical uncertainties.

Distance (cm.)	TLD badge readings (nC)		Bare card reading (nC)	Beta factor
	Penetrating	non-penetrating		
10	0.29	58.5	136.2	0.44
38	0.10	5.8	11.5	0.51
50	0.06	2.9	5.1	0.57

Table 2. The results for uncalibrated ^{32}P source.

4. Conclusions

The values of the beta factors for ^{32}P when using the NRCN badges were estimated by different methods. The results are summarized in table 2. The ratios of the beta factor for ^{32}P to the beta factor for $^{90}Sr/^{90}Y$ are given as well.

Evaluation method	Beta factor P-32	Beta factor P-32 / Beta factor Sr-90/Y-90
Loevinger expression	0.41	0.78
Two calibrated sources	0.53	0.72
Uncalibrated P-32 source	0.54	0.75

Table 2. Beta factor values evaluated by different methods.

The beta factors for ^{32}P evaluated by the two experimental methods are similar for distances over 30cm. The calculated value and the experimental value at 10cm are lower. It seems that these lower values are due to a softer beta energy spectrum and to geometrical factors. The beta factors ratio of ^{32}P to $^{90}Sr/^{90}Y$ is similar for all evaluations. For the general case of exposure from a ^{32}P source a beta factor value of 0.54 is proposed for the NRCN TLD badge. This value is significantly different from the value 0.29 which is used for uranium.

References

[1] "Applied Thermoluminescence" , M.Oberhofer, A.Scharman ed. Adam Hilger Ltd., Bristol,1979

[2] R.Loevinger , Radiology 66 (1956) 55-62

EVIDENCE OF EXCESS BONE CANCER IN THE VICINITY OF U. S. AND U.K. NUCLEAR INSTALLATIONS

GOLDSMITH , JOHN R. M.D., M.P.H., PROFESSOR
and
KORDYSH, ELLA, M. D.,Ph. D., ENVIRONMENTAL SCIENTIST

EPIDEMIOLOGICAL AND HEALTH SERVICES EVALUATION UNIT,
SECTION ON OCCUPATIONAL AND ENVIRONMENTAL EPIDEMIOLOGY
FACULTY OF HEALTH SCIENCES
BEN GURION UNIVERSITY OF THE NEGEV
P.O.B. 653, BEER SHEVA, ISRAEL

SUMMARY

U.S. Mortality data were examined in counties containing or adjacent to nuclear installations, and in matched comparison counties before and after initiating operations. While no excess childhood leukemia was found as had been sporadically the case in the U.K., the data allowed us to look for excess of other cancer and in other age groups. RESULTS: We found for bone and joint cancer at ages 10-19 and 20-39 that standard mortality ratios (SMRs) were greater than 100 significantly more frequently than expected near facilities involved in research, fabrication, armaments, and reprocessing, when expected mortality was based on US data. When the data for these counties was compared with data for comparable counties not near such installations, the resulting Risk Ratios (RRs) were significantly more frequently above 1.00 than less than 1.00. We then re-examined data for comparable sites in the U.K., based on microfiche, which had data for age 0-24, and we considered locations for which 1/3 of the population lived within 10 miles of the nuclear installation, as well as comparison areas. The data, tabulated for five-year periods, (1959-1980) in terms of observed numbers and the SMR, showed no overall excess mortality, but for the most recent five-year period tabulated (1976-1980), there is excess for both morbidity and mortality of borderline statistical significance. Since radiation is known to cause bone tumors, the findings have biological validity , and justify a case-referent study of exposures for cases of bone and joint cancer in young persons living near nuclear installations.

Keywords: Bone and joint cancer, radiation, perinatal radiation, occupational radiation.

TABLE 2

BONE TUMOR MORTALITY IN AREAS WITH 1/3 OF THE POPULATION LIVING WITHIN 10 MILES OF A BRITISH NUCLEAR INSTALLATION,(INS) AND IN COMPARISON AREAS (COM) AGE 0-24

LOCATION		1959-1965 OBS	1959-1965 SMR	1976-1980 OBS	1976-1980 SMR	1959-1980 OBS	1959-1980 SMR
SELLA-FIELD	INS	2	165.0	1	148	5	133.0
	COM	1	125.7	0	0	4	140.9
SPRING-FIELDS	INS	1	16.4	3	110.4	9	49.4
	COM	8	121.3	2	65.2	22	110.3
CAPEN-HURST	INS	4	56.0	7	152.5	20	91.5
	COM	2	26.9	6	130.9	18	79.9
AMERS-HAM	INS	8	111.9	10	161.9	25	103.7
	COM	3	45.7	8	117.8	20	82.2
ALDER-MASTON	INS	4	119.0	5	144.2	15	120.0
	COM	4	109.6	5	167.2	14	114.7
HARWELL	INS	1	79.3	3	256.3	5	112.4
	COM	1	81.4	1	88.1	5	116.1
WINFRITH	INS	0	0	0	0	2	49.7
	COM	0	0	2	23.0	2	47.4
TOTAL	INS	20	76.3	29*	154.3	81	83.6
	COM	19	72.4	24	129.5	85	94.8

* $P = 0.017$, (one-sided) for INS OBS vs EXP based on SMR

0.18 (One-sided) for INS OBS vs COM OBS

TABLE 1

DEATHS FROM BONE AND JOINT CANCER IN COUNTIES INCLUDING OR ADJACENT TO NUCLEAR FACILITIES IN THE UNITED STATES AND IN COMPARISON COUNTIES AFTER START OF OPERATIONS

FOR AGES 10-19 AND 20-39

FACILITY	Installation or ADJACENT COUNTIES 10-19		20-39		COMPARISON COUNTIES 10-19		20-39	
	#	SMR	#	SMR	#	SMR	#	SMR
HANFORD	10	1.53	6	1.29	31	1.13	19	0.99
OAKRIDGE	5	1.04	6	1.86	10	0.87	19	2.32
MOUND	36	0.99	35	1.22	62	0.89	39	0.77
INEL	5	2.12	3	2.32	1	0.21	4	1.43
PADUCAH	6	2.24	1	0.54	9	0.56	5	0.40
SAVAN. RIV	10	1.72	9	2.46	11	0.73	11	1.10
FERNALD	46	1.05	44	1.32	54	1.05	40	0.95
PORTSMOUTH	0		1	1.92	0		2	1.28
ROCKY FL.	22	1.51	13	1.08	11	0.91	11	1.04
NUCL. F. S.	4	2.10	0		2	0.41	3	0.97
ALL DOE INSTALLATIONS	144	1.20	118	1.31	191	0.89	153	0.95
RR	1.34**		1.37*					
ALL UTIL	218	0.93	214	1.08	449	0.96	357	0.98
RR	0.99		1.21*					

* 0.01 < p < 0.05
** 0.001 < p < 0.01

"ALL UTIL"REFERS TO NUCLEAR POWER PLANTS,"ALL DOE"TO OTHER TYPES OF INSTALLATION

THE FADING OF LiF:Mg,Ti - IS IT REALLY LOW ?

Barak Ben-Shachar
Department of Scientifical and Technical Information
NRC-Negev, P.O.B. 9001, Beer-Sheva, 84190, Israel.

1.Introduction.

One of the most important characteristics of integrating thermoluminescence (TL) detectors used as ionizing radiation dosimeters is the stability of the stored TL signal. In most TL materials the TL signal decreases as a function of storage time due to the thermal escape of trapped charge carriers and this characteristic is, therefore, usually referred to as "thermally induced fading, or simply "fading". Lithium fluoride doped with magnesium and titanium is the most commonly used radiation dosimeter (1) and has been available commercially in the form of TLD-100 (Harshaw) since the 1960's. The most glaring disadvantage of this phosphor is its extremely complicated glow curve structure (approximately 10 glow peaks between room temperature and 400ΦC, many of them overlaping) which had led to great difficulty in arriving at a universally accepted characterization of its fading properties (2). The routine measurement of this phosphor includes its heating to a temperature of 250-300 ΦC. The main glow peak (and the most important for dosimetric applications) is the peak 5, vastly overlaping with peak 4.

A quick partial review of the data concerning the fading, as presented in six reference texts is highly illustrative: 7% in two weeks (3), 10% in one month (4), 5±3 % after 84 days, 5% after 50 days, 5% after 20 days and 0±2 % after 50 days (5), 5-10% in one year (6), approximately 5% in one year (7) and 1% per year (8). The extremes in the reported fading rates thus differ by approximately two order of magnitudes.

One of the possible reasons of the great variability (especially the high fading rates for the short storage intervals) is the inclusion of the rapidly fading peaks 2 and 3 in the TL signal, when the

measurement of the signal is performed by integrating the total glow curve (without peaks separation). Another reason could be the application of different kind of annealings: pre-irradiation annealing of 400ΦC/1h and different low temperature pre- and/or post irradiation annealings (5). At the other extreme, the comparative low fading rates are presumably based on some combination of peaks (4+5) or peak 5 alone (the main peaks used for the routine dosimetry). Some authors (9,10) even reported an increase in the intensity of peaks 4 and 5 in unannealed material, due to trap migration and aggregation.

The present research includes 2 parts:

A. The measurement of the fading of TLD-100 cards by integrating the total glow curve (without glow curve separation) for a large range of storage time (from several hours to 90 days).

B. The measurement of the fading of peak 5 alone or peaks (4+5) in annealed and unannealed TLD-100 chips, following gamma ray, alpha ray and thermal neutron irradiation, when the glow peaks in the glow curves are separated by the CGCD method, in order to find out a possible growth in peak 4 and/or peak 5 and to establish the possible role of LET in any observed differences in the stability.

2.Materials and methods.

The first part of the experiments were performed with the standard Harshaw G-1 cards, each of them containing 2 TLD-100 chips. The integral TL signal was measured by a 2271 automatic Harshaw manufactured TL reader and the TL cards were irradiated by a calibrated Sr-90 source, built in the TL reader. No pre- or post- irradiation annealings were performed. All the dosimeters were individually calibrated by irradiating them 5 times to the same dose (1 mGy).

The second part of the experiments were performed by TLD-100 hot pressed chips (Harshaw). The annealed materials were heated in air to 400ΦC/1h immediately prior to every irradiation followed by a natural "air cool" at approximately 75ΦC/min to room temperature. All dosimeters were calibrated individually and the unannealed materials were read-out prior to the irradiation and calibration so as to standardize their response. Gamma ray irradiations were carried out using a Co-60 source, alpha particle irradiations were performed in air on a sealed Am-241 source yielding approximately 4 MeV alpha partices

and the neutron irradiations were carried out with the KANDI-II neutron diffractometer facility at the IRR-2 and the energy of the neutrons employed was 81.0 meV. The TL glow curves were annalysed using a computarized glow curve deconvolution technique (CGCD) described elsewere (11,12).

3.Experiments and results.

A.The measurement of the fading by integrating the whole glow curve.

Six G-1 cards were calibrated by irradiating each one five times to a dose of 1 mGy. The standard deviation of each chip was less than 2%. The fading of the phosphors was measured by the following way: irradiation of the six cards to a dose of 5 mGy, storage in dark at room temperature to the relevent period (2 hours - 90 days), evaluation, and then again irradiation to the same dose and evaluation immediately after the irradiation. In table 1 the fading of the LiF:Ti,Mg cards, after different periods of time, are presented; the left part of the table includes the short time measurements (several hours) and the right part presents the fading from 2 to 90 days.

Table 1: The fading of TLD-100 by integrating the whole glow curve.

Storage time (h)	Fading (%)	Storage time (days)	Fading (%)
2	4.38±0.84	2	12.3±1.7
3	3.33±1.62	3	16.7±1.9
5	3.39±1.62	4	17.8±1.8
6.5	5.53±1.89	5	18.4±2.0
8	5.19±2.03	7	18.5±1.1
16	8.42±2.06	10	24.6±3.3
24	12.03±1.93	15	26.8±2.15
		22	30.2±3.2
		30	31.3±3.0
		45	32.9±2.1
		90	34.9±1.72

From the results of table 1 we can conclude the followings:

1. The fading is significant even a few hours after the irradiation (~4% after a few hours and ~8% after 16 hours).
2. Most of the fading occurs in the first 10 days (~25%), because the rapidly fading peaks 2 and 3. For longer storage in dark room, the fading is increasing slowly, up to ~35% after 3 months.

B. The measurement of the fading by separating peak 4 & 5 via CGCD.

The individually calibrated TLD-100 chips were irradiated by a Co-60 gamma ray source to a dose of 5 mGy, stored in the dark at room temperature for a period of 30 days and evaluated. The same chips were irradiated again to the same dose and evaluated immediately. The measurements were performed with annealed and unannealed materials. The same experiments were performed for alpha and thermal neutron irradiation. The results of the fadings of peak 4, peak 5, peak (4+5) and the fading of the whole glow curve are presented in table 2.

Table 2: The changing in the sensitivity of different peaks in TLD-100 via the CGCD.

Irradiatic	peak 4	peak 5	peaks (4+5)	whole glow curve
alpha (annealed)	-23.0	-5.2	-10.0	-19.9
alpha (unannealed)	-38.0	-5.2	-17.0	-27.6
neutron (annealed)	-5.6	-10.9	-9.9	-10.0
neutron (unann.)	+43.2	-4.9	+3.3	+2.8
gamma (annealed)	+11.1	-3.6	+0.7	-10.8
gamma (unannealed)	+32.0	-2.9	+6.3	-24.5
over all rad. (both types)		-5.5±2.6	-4.4±8.3	-18.8±12.8

From the results of table 2 we can conclude the followings:

1. We have received a growth of peak 4 after a period of 30 days for irradiation of both annealed and unannealed gamma rays and for irradiation of thermal neutrons for unannealed chips. Similar results are reported by Johnson (9) and Booth (10).

2. The fading of the whole glow curve is very different for different types of radiation (gamma rays, alphas or thermal neutrons) or different materials (annealed or unannealed).
3. No evidence of LET dependance of the whole glow curve fading was found (for example, for unannealed material, the results of the fading of alpha and gamma are very similar, and different from the fading of thermal neutrons; for the annealed one, the results of the fading of the gamma is almost iddentical to the fading of thermal neutrons, and different from the fading of alphas).
4. A well behave fading rate (-5.5±2.6) was obtained for peak 5 after 30 days, for both types of materials and different irradiations.

4. Conclusions.

A. When we are integrating the whole glow curve, the fading is far to be negligible (see table 1). Most of the fading occurs in the first days, due to peaks 2 and 3. It can be reduced by different pre- or post- irradiation annealings (not available for the G-1 cards) or by different preheatings.
B. Great care must be taken to correct the fading in the routine personnel and environmental dosimetry, when the exact time of the exposure is not known.
C. The fading of peak 5 or peak (4+5) is significantly less than the fading of the whole glow curve (see table 2).
D. We found a growth in peak 4 after 30 days (in accordance to references 9 and 10), but no evidence of growth of peak 5 in either material, for any of the types of irradiation.
E. No evidence of LET dependence of the fading was found, neither for annealed and not for unannealed phosphors (see paragraph 3).
F. A well behaved fading rate per month was found for peak 5 (-5.5±2.6) for all radiation types in both annealed and unannealed materials.

Thus we believe that these results convincingly demonstrate the advantages of using only peak 5 in dosimetric measurements, where fading corrections are of importance.

5.References.

1.Portal,G., "Review of the principal materials available for TLD", Rad. Prot. Dosim., 13, 351 (1986).

2.Ben-Shachar,B. and Horowitz,Y.S., "Annomaleous thermally induced fading of annealed and unannealed LiF:Ti,Mg (TLD-100 Harshaw) using computerized glow curve deconvolution", J. Phys. D:Appl. Phys.

3.Becker,K., "Solid state dosimetry", CRC-Press, Cleveland, OH, 1973.

4.Mahesh,K., Weng,P. and Furetta,C., "Thermoluminescence in solids and its applications", Ashford, Nuclear Technology Publishing, 1969.

5.Horowitz,Y.S., "General characteristics of thermoluminescent materials", in: "Thermoluminescence and thermoluminescent dosimetry", ed. Y.S. Horowitz, Boca Raton, CRC-Press, vol 1, 1984.

6.Oberhofer,M. and Scharmann,A., ed. "Applied thermoluminescence dosimetry", Bristol: Adam Hilger LTD, 1981.

7.McKeever,S.W.S., "Thermoluminescence of solids", Cambridge: University Press, 1985.

8.De Werd,L.A., "Application of thermally stimulated luminescence" in "Thermally Stimulated Relaxation Luminescence", ed. P. Braunlich Springer Verlag: Berlin, 197°.

9.Johnson,T.L., "Quantitative analysis of the growth and decay of the thermoluminescent peaks in LiF TLD-100", in Proc. International Conference on Luminescence Dosimetry, Krakow, p. 197 (1974). Edited by Niewiadowski.

10.Booth,L.F., Johnson,T.L. and Attix,F.H., "Lithium fluoride glow peak growth due to annealing", Health Phys., 23, 137 (1972)

11.Horowitz,Y.S.,Moscovitch,M. and Wilt,M., "Computarized glow curve deconvolution applied to ultra low dose LiF TLD", Nucl. Instrum. Meths., A244, 556-564 (1986).

12.Horowitz,Y.S. and Moscovitch,M., "Computarized glow curve deconvolution applied to high doses (10^2-10^5 Gy) TL dosimetry" Nucl. Instrum. Meths., A243, 207-214 91986).

A CONTROLLED DATA COLLECTION SYSTEM FROM A TLD READER.

U.German - Nuclear Research Center Negev

1. Introduction

The dosimetry laboratory of NRCN employs a 2271 Harshaw automatic TLD card reader. The system logic performs only basic parity checks of the data which is sent to the peripheral equipment, besides the upper and lower dose limit alarms. Other errors may remain undetected until the data analysis stage. A PC computer was connected to the automatic card reader system. The PC computer controls the operation of the system while receiving, checking and recording the data on magnetic media. A serial number is given to each record and other specifications as date, unit and type of analysis are also added to the data file.

2. The checks performed

The TLD cards in use at NRCN contain two TLD crystals. The first one is unfiltered and accumulates penetrating and non-penetrating doses, while the second is filtered by 1.25mm Al and accumulates the penetrating dose. Each complete record received from the tld reader consists of 28 characters. All characters should be numbers or spaces in the format given below:

x xxxx x x xxxx x x xxxxxx

The first group of three numbers concerns the reading of the first crystal. The first number in the group is a numeric character specifying the data being read (TLD-1, sensitivity check, etc.). The second number is a 4 digit integer specifying the charge which was accumulated and the third number specifies the range. The second group of three numbers concerns the reading of the second crystal in the same format. The last number is the card identification number and the character before it indicates its parity check.

The record is received as a string and before decoding it the following checks are performed:

- record length
- presence of only numerical characters and spaces
- numbers and spaces in the expected pattern

After decoding the data, the following checks are performed:

- expected control and parity numerical characters
- card identification number in a declared range
- ratio between the filtered and unfiltered crystals
- exposure less then minimum threshold
- exposure over specified limits
- card belonging to the unit being read

When any of the tests fails alarm is sounded and the system is stopped. The full record including the alarm cause is displayed, recorded an printed. The operator must check the alarm cause and has the possibility to correct errors. As the reading is still displayed and the card number is directly available, an error correction is a simple and short procedure. The corrected record is rechecked and passed only when all tests are positive or the specified instruction is given by the operator. Both the original information and the edited one are recorded for future control.

All the records are expanded by the following additions:

a. A one character symbol which defines the record (dose reading, card calibration, etc.)
b. The period - a four character string which defines the month and the year.
c. A serial number - advanced which each record read
d. The error specification, if any
e. Operator instruction, if any
f. A check number - the addition of all ASCII values in the record. The check number is recalculated when the record is read again at the analysis stage and compared to the original value

A sample print of the output is given in fig 1.

```
                09:16:55      : TIME
                15-12-91      : DATE

*OPERATOR ----R  / drive:D
+TITLE:       151291   3.............1291 / ORDER=HA / FIRST NR=1

*/            UNIT : 999

-1291.     1 -2 0118 1  2 9564 0  0 015504 PARITY 1  *COMMAND=n  1254
.1291.     1 -0 0118 1  2 9564 0  0 015504  UNIT      *COMMAND=go 1252
.1291.     2 -0 0126 1  2 0103 1  0 014333                       1231
-1291.     3 -0 4743 0  2 0521 0  0 017446  L O W     *COMMAND=n  1250
.1291.     3 -0 4743 0  2 4521 0  0 017446                       1254
.1291.     4 -0 2602 0  2 4039 0  0 017292 RATIO-OK              1249
-1291.     5 -0 0179 1  2 0161 1  0 ??????  CHAR      *COMMAND=n  1004
-1291.     5 -0 0179 1  2 0161 1  0 026530  CARD      *COMMAND=n  1243
.1291.     5 -0 0179 1  2 0161 1  0 016530                       1242
-1291.     6 -0 6600 0  2 4.............. LENGTH    *COMMAND=n   562
.1291.     6 -0 6600 0  2 4749 0  0 004654                       1257
-1291.     7 -0 8370 0  2 0105 1  1 013871 PARITY 3  *COMMAND=n  1248
.1291.     7 -0 8370 0  2 0105 1  0 013871 RATIO-OK              1247
-1291.     8 -0 6954 0  2 6394 0  0 0 4168  SPACE     *COMMAND=n  1267
.1291.     8 -0 6954 0  2 6394 0  0 014168                       1268
.1291.     9 -0 0110 1  2 9660 0  0 015867                       1253
.1291.    10 -0 0104 1  2 0122 1  0 011879                       1240
```

Fig. 1 A sample print of the program output

3. Conclusions

The computer system presented here improves significantly the reliability of data collection from the TLD reader. The various errors can be handled on-line, which greatly simplifies the errors detection and suppression. The system is operated routinely by the dosimetry laboratory at NRCN .

Exemption of Certain Radioactive Sources and Devices from Registration Licensing and Supervision: Proposal for Israeli regulations

T. Schlesinger, T. Biran and M. Barshad
Soreq Nuclear Research Center, Yavneh 70600

A review was conducted of the basic considerations and international guidelines for the exemption of certain radioactive sources and practices (involving potential exposure to low level ionizing radiation) from registraion licensing and supervision.
The resulting document includes such exemptions in the U.S.A., U.K. and the OECD countries.

Based on the above and taking into consideration the legal and administrative structure of the control of radioactive substances and machines and devices emitting ionizing radiation in Israel, the document proposes a system of general licences (partial exemptions) and of exemptions of certain sources and practices. The most important of these are:

- Television receivers and VDUs (with limits on the radiation level in contact with the external surface).
- Certain nuclear gauges.
- Smoke detectors and certain beta lights.
- Calibration radioactive sources with limited activities.
- Very-low-level radiopharmaceuicals for in vitro studies.
- Natural radioactive ores.

Rn Gas Level as an Indicator to the Radiological Impact of Rn Progeny

M. Margaliot and T. Schlesinger.

Soreq Nuclear Research Center, Yavneh 70600, Israel.

and

A. Kazir

Tel-Aviv University, Ramat-Aviv, Israel

Introduction:

It is widely accepted[1,2] that the radiological implications of ^{222}Rn stem from the alpha emitting Rn progeny, rather than from the Rn gas itself.
In practice it is however common to measure the Rn gas level, rather than the Rn progeny, due to the technical complexity of the Rn progeny measurements[3]. The dose equivalent due to human exposure to Rn progeny is derived from the Rn gas level, assuming a constant, partial, equilibrium between the radon and its progeny.
As the actual equilibrium state of the Rn progeny is dependent on environmental conditions, it is believed[1] that a correct radon progeny exposure assessement, should involve a direct measurement of the progeny level.
In the following, it is sugested that in spite of the irrefuteable radiological role of the radon progeny, the radon gas level serves, practically, as a better indicator to radiological respiratory health hazards, than does the measured radon progeny level itself.
This sugestion is based on an evaluation of the information produced by commercially available Rn progeny meters, and of the radiological significance of the unattached fraction of the Rn progeny.

1. The disequilibrium in the radon series.

Radon enters human dwellings mainly from the ground under the buildings. The Rn atoms undergo alpha disintegration and thus the subsequent radon progeny series ("daughters") is formed.
The progeny atoms tend[12] to get attached to surfaces in their near vicinity. These may be the surfaces of the dwellings walls, and of various airborne particles. The fate of those radon progeny atoms, and their relative radiological significance, are presented briefly below:
a. Progeny atoms attached to walls ("plateout"): As these atoms are not airborne, they do not constitute a part of the breathable air and hence, do not contribute to the respiratory tract[1,2] exposure.

b. Progeny atoms attached to large (>3 μm) particles.
These particles are trapped by the respiratory tract, mostly in the nasolaryngeal region.
The retention time of these particles in this region is rather short, and the lining tissue in this region is considered to be relatively insensitive to cancer induction by radiation. Consequently, the contribution of this group of radon progeny atoms, to respiratory cancer induction, is considered to be negligible[1].

c. Radon progeny atoms attached to medium size (0.1-3 μm) particles.
A fraction of this group of atoms is trapped and retained in the respiratory tract (mainly in the tracheobronchial region).
The average retention time of these particles in this region is about 20 minutes[4], and the basal cells of the epithelium in this region are considered to be the most sensitive to cancer induction by radiation. It is thus widely accepted that this group of radon progeny is the main radiative source of respiratory cancer.[1,2]

d. Unattached radon progeny atoms.
This fraction includes, in addition to free single atoms, (rather a rarity) also those progeny atoms which are attached to extremely small (<<0.1μm) particles.
These atoms also get trapped in the tracheobronchial region of the respiratory tract, but due to their small size, they have a relatively high diffusion coefficient, which results in very high (compared to the attached fraction) deposition and long retention of this fraction in this region. The resulting health hazard is considered to be 6-11 times[15] higher than that of the attached fraction of the radon progeny (in terms of dose to tissue per atom). In the present study, the dose equivalent enhancement factor of 9.4, cited by Jacobi & Eisfeld[5] will be used.

2. The equilibrium factor F:

In order to describe the radon progeny level, it is common to relate this level to the radon gas level by the equilibrium factor F defined by eq.1

Eq 1. $$F = \text{actual PAEC}/(100\%\ \text{PAEC})$$

where PAEC= Potential Alpha Energy Concentration in air, and (100% PAEC) is the PAEC that would prevail under conditions of full equilibrium between the radon and its progeny.
It is customary (i.e. Jacobi in [1]) to express the dose equivalent due to respiratory exposure to radon progeny, in terms of the radon gas level, utilizing F:

Eq 2a. $$D = C_r \cdot t \cdot F \cdot A$$

where D is the dose equivalent, C_r is the radon concentration, t is the exposure duration, A-a conversion contant and F-the equilibrium factor.
Another common[10] form of using F is given in eq 2b:

Eq 2b. $$EEC_r = F \cdot C_r$$

where F and C_r are as above and EEC_r is the Equilibrium Equivalent Concentration of radon. The EEC_r is linked directly to human exposure, and this is the unit used in some publications regarding radon risk estimations[7,8].
The actual value of F depends on some environmental factors, the main of which are the surface/volume ratio of the given environment (i.e. a small and furnished room has a relatively large total surface/volume ratio, which results in an enhanced attachment of radon progeny atoms to the walls and furniture, and hence, in a reduced F), and the aerosol (dust particles etc.) concentration in the air.
The effect of the last is due to the fact that a high aerosol concentration enables the radon progeny atoms to get attached to the airborne particles, rather than to the walls, and thus higher aerosol concentrations result in higher F values. The effect of aerosol concentration on F is presented in Eq. 3, which is based on a least square fit (squared correlation coefficient=0.97) to the Experimental data of Wicke et. al.[11], and Toohey et. al.[13], reffering to typical indoor conditions (including plateout on walls and furniture).

Eq 3. $$F = 0.3 + 0.1 \cdot \ln(C_a - 3.4)$$

where F is the equilibrium factor, and C_a is the aerosol concentration (in particles/mm^3). This expression is valid only for the C_a range ~5 - ~80 particles/mm^3, to which the above publications (11,13) refer.

3. The unattached fraction f_u:

Due to their small size, the unattached Rn progeny atoms have a higher diffusion coefficient than the attached progeny atoms, and this leads to their high radiological impact. Using the enhacement factor of 9.4, cited above[5], the dose equivalent due to tracheobronchial exposure to Rn progeny is given by:

Eq. 4. $$D = C_r \cdot F \cdot (1 + 9.4 \cdot f_u) \cdot A \cdot t$$
where C_r is the radon concentration, F-the equalibrium factor, f_u is the unattached fraction (in terms of alpha energy) of Rn progeny entering the respiratory tract, A-a conversion constant, t-the exposure duration and D- the dose equivalent.

The value of f_u is also dependent on the ambient aerosol concentration, as a high aerosol level reduces the probability of a Rn progeny atom to remain unattached. Experimental data regarding the

dependence of the unattached fraction on the aerosol concentration has been published by Stranden & Berteig[14].
Analysis of the data in their publication (Fig 9. thereof) yields (squared correlation coefficient=0.98) the following relation:

Eq. 5. $$f_u = 0.75\ mm^3/C_a$$

where the meaning of the f_u and C_a is as above. Eq 5 refers also (as did equation 3) to typical indoor conditions only.
It is thus apparent that while increasing the aerosol concentration increases F, it decreases the unattached fraction f_u and consequently, the net effect of varying the aerosol concentration, on the dose equivalent, tends to cancel out, and the dose equivalent is rather weakly dependent on the equilibrium factor F. This can be seen by combining equations 3,4 and 5, to give:

Eq. 6. $$D = C_r \cdot F \cdot \{1+7.05/[\exp((F-0.3)/0.1)+3.4]\} \cdot A \cdot t$$

The meaning of the variables is as above.

equation 6 is presented graphically in Fig. 1.

Fig. 1: Dependence of Rn progeny dose equivalent on F.
(for a constant Rn gas level)

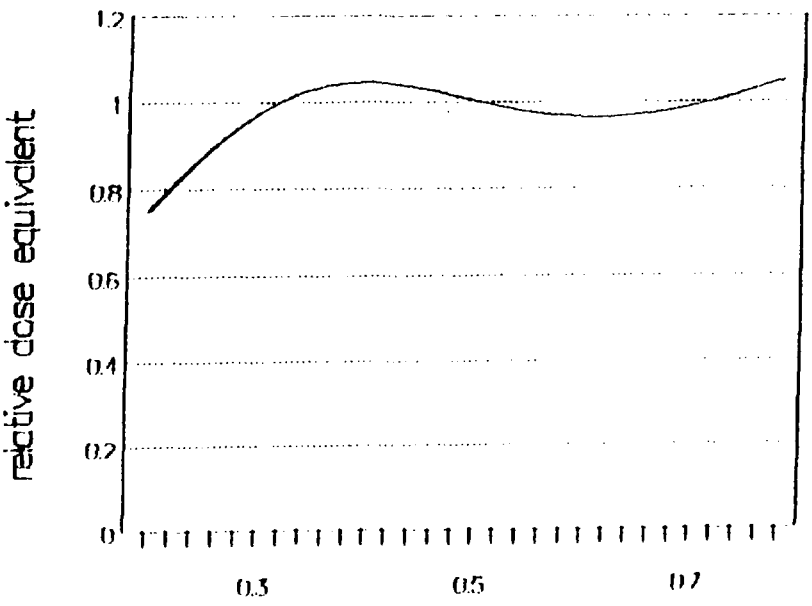

As can be seen, the dose equivalent due to the inhalation of Rn progeny varies by less than ~±20% over the F range 0.2-0.8, for a

constant Rn level. It is also apparent that for the F range 0.3-0.7 (typical to dwellings[1]), the variation of the dose equivalent is even smaller, and is <±10%.

It thus appears that the Rn gas level can serve as a direct indicator of the dose equivalent due to inhalation of Rn progeny, regardless of the equalibrium factor F, with an estimation error of less than ± 20%.

As the commercially available Rn progeny meters do not differentiate between attached and unattached progeny[3], it is evident, according to the present approach, that the readings of these meters may lead to much larger errors in the estimation of the dose equivalent.

References.

1) ICRP Pub 50; Lung Cancer Risk From Indoor Exposure to Radon Daughters, Pergamon Press. (1987).
2) NCRP Rep 94; Exposure of the population in the US and Canada from natural background radiation. NCRP, Bethesda, MD. (1987)
3) NCRP Rep 97; Measurement of radon and radon daughters in air. NCRP, Bethesda, MD. (1988).
4) R.F. Phalen, R.G. Guddy, G.L. Fisher, O.R. Moss, R.B. Schlesinger, D.L. Swift and Hsu-Chi Yeh; Main Features of the Proposed NCRP Respiratory Tract Model. Radiat. Prot. Dosim 38:179 (1991)
5) W. Jacobi and K. Eisfeld; Internal dosimetry of inhaled Rn daughter In: M. Gomez (Ed); Proc. Int. Conf. on radiation hazards in mining: control, measurements and medical aspects. Soc. Of mining engineers, p31, New York (1982)
6) ACGIH Technical Commity. Air Sampling Procedures; Particle Size-selective Sampling in the Workplace. ACGIH (1985).
7) Unscear Report to the general assembly, NY, (1988).
8) IAEA: Facts about low level radiation. IAEA/PI/A14E (1989).
9) J. Porstendorfer; Behaviour of radon daughters in indoor air. Radiat. Prot. Dosim. 7:107 (1984).
10) United Nations Scientific Commitee on the Effects of Atomic Radiation: Sources and effects of Ionizing Radiation. Report to the gerneral assembly, p. 48-80, New York (1977).
11) A. Wicke and J. Porstendorfer; Radon daughter equalibrium in dwellings. In: Radiation Environment, K.G. Vohra Ed. p481-488, Weily Eastern Ltd (1982).
12) W.H. Marlow; Electrical charge in radon daughter deposition: a critical review. Radiat. Prot. Dosim. 24:211
13) R.E. toohey, M.A. Essling, H. Wang and J.Rundo; Some measurements of the equalibrium factor of radon daughters in houses. ANL annual rep. 82-65. Aragonne National Lab. (1982)
14) E. stranden and L. Berteig; Radon daughter equalibrium and unattached fraction in mine atmospheres. Health. Phys. 42:479 (1982)
15) ICRP Pub. 32; Report of the International Commission on Radiological Protection on Limits for Inhalation of Radon Daughters by Workers Pergamon Press, Oxford. (1981).

THE CONTRIBUTION OF THE PHARYNGEAL PUMP TO ESOPHAGEAL TRANSIT.

Zelikovsky L and Keren S. Institutes of Nuclear Medicine and Gastroenterology, Hillel Yaffe Medical Center, Hadera.

The pharynx acts as a pump that injects its contents into the esophagus with a high velocity. The aim of the study was to assess the role of the pharyngeal pump to esophageal transit. 33 healthy volunteers and 17 patients with motility disorders were studied after approval by the Helsinki committee. A raisin containing 50 μCi pertechnetate and serving as a point was swallowed with water source . A functional image of the position of the point source in time was obtained, by acquiring and processing 20 frames per second, during an interval of 20 seconds. The study comprised comparisons of: 1) Multiple successive swallows, versus a single swallow. 2) different volumes of water, versus a marshmallow ingested by a single swallow. The velocity (mm/sec) and distance (mm) of transit, attributable to the pumping action of the pharynx, were calculated from the slope and height of the appropriate segment of the tracing.

Results:	velocity (mm/sec)	Distance (mm)
Successive Swallows	157.3	119.6
Single Swallow	156.5	147.2
5 ml Single Swallow	163.3	159.8
10 ml single Swallow	195.1	169.8
15 ml single swallow	246.0	181.7
Marshmallow	133.5	122.0
Achalasia (n=8)	162.3	165.0
Nutcracker (n=9)	132.4	134.2

The conclusions are: 1) The method used is appropriate for quantifying pharyngeal pump function. 2) The pharyngeal pump plays a major role in esophageal transit. 3) The volume and viscosity of the bolus, both influence pharyngeal function.

The Use of Natural Radioactivity in the Sediment Transport Study

B.Shteinman[1], A.Gutman[2] and I.Gertner[3]

[1]Kinneret Limnological Laboratory
Israel Oceanographic & Limnological Research
P.O.B. 345, Tiberias, Israel 14102

[2]Israel Electric Corporation, Ltd.
P.O.B. 10, Haifa, Israel 31000

[3]Technion - Israel Institute of Technology
Haifa, Israel

Sediment transport phenomenon is important in coastal engineering and marine ecology. The bottom relief builds up from sediments drawn under different flow regimes, waves energetics and other factors. It is desirable to follow up the sediment trajectories on a regular basis and especially after storms and during persistent winds setup. Simple and reliable way of monitoring the sediments of fixed origin will be helpful in predicting many important effects, such as the coasts erosion. The aim of this paper is to present the method of using natural radioactivity of sediments for their follow up through the river-lake system.

Sediments of different origin differ by their isotopic composition and may be classified by specific gamma spectra signature. The use of passive gamma spectra for sediment transport studies was first proposed about thirty years ago [1] and successfully applied on several rivers and seas since then [2].

Figure 1 presents the map of gamma activity over the bed of the River Kura mouth offing, obtained during underwater surveys in summer (a) and automn (b) of 1963 [1]. An example of gamma spectrum used in this study is presented in figure 2. The major peak in the curves was at 1.46 Mev line of K^{40} isotope. Four levels of gamma radiation were defined by integrating counts over chosen spectral ranges. Each level related to some characteristic type of the bed load. The highest level (1) accounted on the area of the liquid silts sized less then 0.01 mm, level (2) standed for the sandy silts of 0.01-0.05 mm, level (3) corresponded to fine fractions of the river origin, settled down the sea bed. The native marine grounds were characterized by background level (4) values.

The suggested method of passive gamma radiation is being used now, among other methods, in the study of sediment transport from River Jordan into Lake Kinneret. Figure 3 presents a bathimetric map of the lake. Different depth profile on the north and on the south from Tiberias may point to prevailing sediment trajectories from River Jordan mouth along the western coast up to Tiberias. Following up the sediment trajectories under different meteorological conditions will be helpful in clarifying this and similar problems. Also the picture of sediment behavior is extremely important in the study of the lake ecology.

Three points marked in the map of figure 3 are the places where the probes of bottom ground were taken. Granulometric and gamma spectrum analysis were performed. Gamma spectra of the probes were obtained using 3X3" NaI well type detector and measuring system, developed in the Van De-Graaff Accelerator Laboratory at Department of Physics of Technion [3]. Typical spectrum of the probes is presented in figure 4 and shows two spectral ranges suitable for tracing purposes: 1.46 Mev line of K^{40} and lower energy range of the U-Th family. The spectral resolution seems to be good enough for posed goals, but it can be improved by mathematical means of spectra unfolding [4].

The very preliminary results are presented in Table 1.

TABLE 1. COUNTS OF GAMMA RADIATION IN THE VICINITY OF K^{40} SPECTRAL LINE (1.46 MEV) OF THREE PROBES FROM THE BOTTOM OF LAKE KINNERET.

No	Distance from Jordan mouth (m)	Depth (m)	Mean Diameter (mm)	Counts
1	0	2.5	0.14	24,424
2	300	8	0.08	15,292
3	800	22	0.03	14,039

From the data presented in Table 1 it can be concluded that the sediments in the River Jordan mouth contain more K^{40} isotopes than the native Lake Kinneret bottom. Another conclusion is that the suggested method may be workable in tracing sediments and mapping the accumulation zones on River Jordan - Lake Kinneret bottom.

REFERENCES.

[1] B.S.Shteinman
Investigation methods of sediment dynamics of river estuaries.
Symposium on the hydrology of deltas, Bucuresti, Romania, May 6-14, 1969.

[2] Ju.A.Ebad-zade, Ed.
Sediment dynamics in rivers and water systems.
Moscow, 1978, 244p. (in Russian).

[3] G.Koren, I.Gertner and U.Shreter
Isotopes separation experiments in natural UF_6 by CF_4 and CO_2 lasers, analyzed by gamma-ray spectrometry.
Applied Physics Letters, v.41, p.397 (1982).

[4] A.Gutman, E.Elias and E.Levitan
Unfolding of complex gamma spectra.
13th Annual Meeting of the Nuclear Societies of Israel, Tel-Aviv, February 1986.

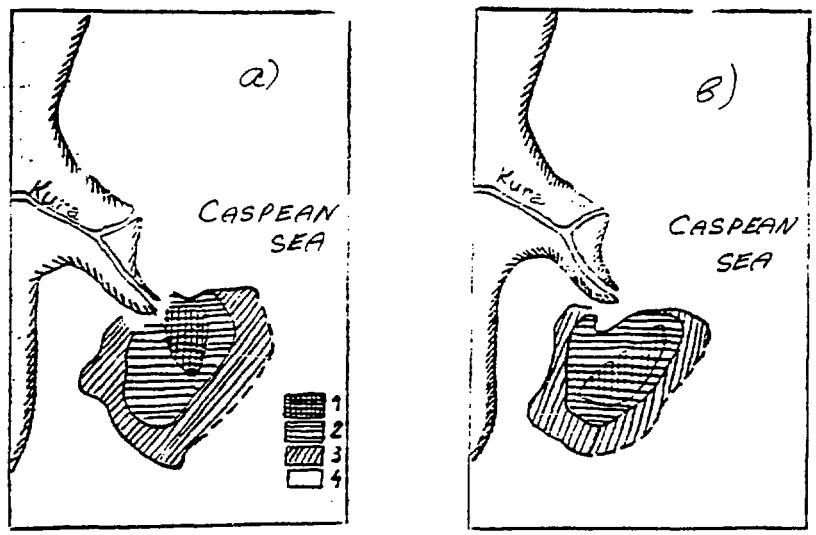

Fig.1 Intensity of passive gamma radiation from the bottom at River Kura offing: a) summer 1963, b) automn 1963.

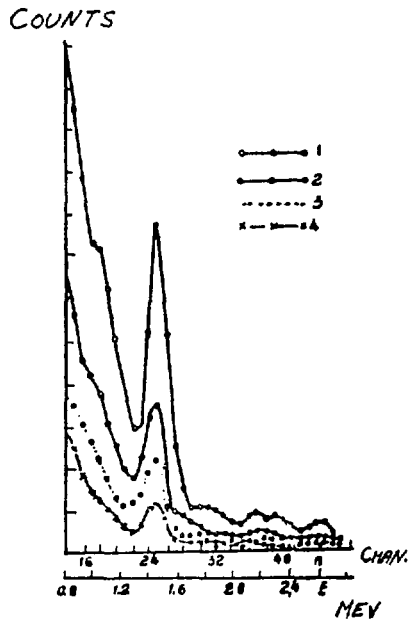

Fig.2 An example of the gamma spectrum from the bottom of River Kura offing (1963).

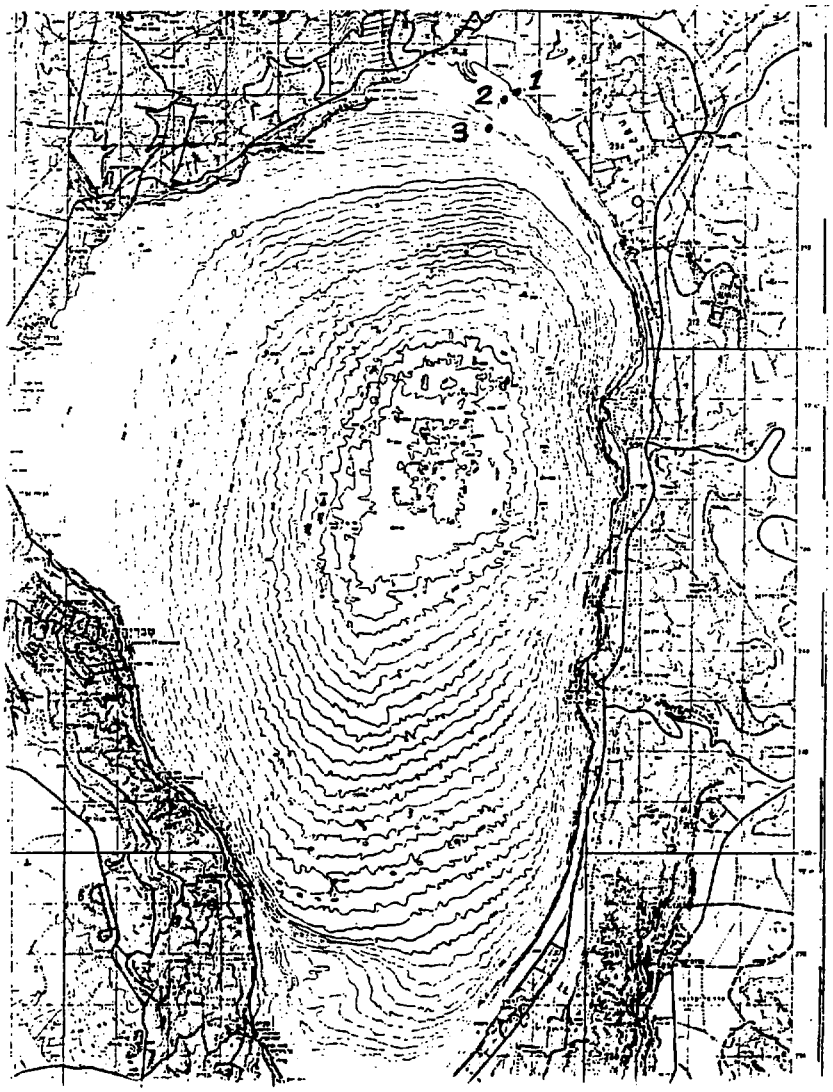

Fig.3 A bathimetric map of Lake Kinneret with marked points of bottom probes (1992).

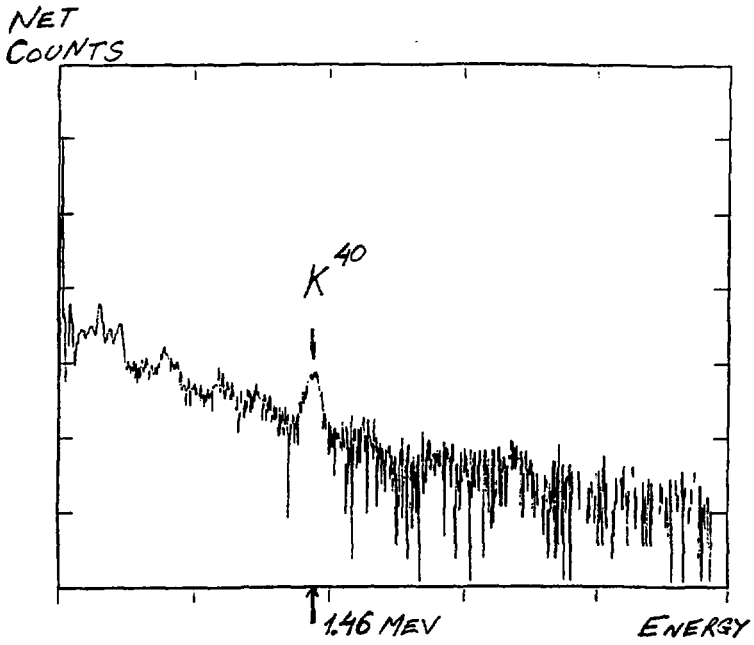

Fig.4 An example of gamma spectrum of the bottom probe from Lake Kinneret (1992).

Uptake and Distribution of 99mTc-MD32P During Tibial Repair and Around Titanium & Hydroxyapatite Implants in a Rat Model (Abstract)

J. Shani, Z. Schwartz, D. Kohavi, A.W. Soskolne, D. Amir, Touma, H. and J. Sela, Hebrew University-Hadassah Medical Center, Jerusalem, Israel, in collaboration with L.D. Swain and B.D. Boyan from the Texas University Health Science Center, San Antonio, Texas, USA.

The purpose of this study was to examine the validity of using labeled MDP in studying bone formation and calcification, in two distinct processes: during bone healing and after inserting implants into such bones.

The model we used was the bone healing after tibia ablation of 250 gm albino "Sabra" rats. In each rat the right tibial bone was exposed under anaesthesia, and a dental burr was used to penetrate the cortical bone into the marrow cavity. Bone marrow was evacuated by repeated washings with saline, introduced by a cannule. The left tibia of each rat remained intact and served as control. In some experiments - Titanium and Stainlesss steel were implanted, and bone healing around them was studied.

Removal of tibial bone marrow in rats is followed by primary bone formation, resorption and marrow restitution. This is a slow process, spread over four weeks, in which the busiest bone calcification corpuscles are the matrix vesicles. They accumulate calcium and phosphat to form amorphous calcium-phosphate complexes that convert to hydroxyapatite. Through our years of research we learned that the highest density of the matrix vesicles is on the 6th day after injury, when their number and diameter values are the highest, and when the evacuated marrow have been replaced by primary bone.

In our study we followed up the injected phosphates in the whole tibia, during its healing process. We could tell specifically whether the phosphates went into the organic or the inorganic compartment. Osteoblasts secrete collagen fibers, that form a net which directs the process of primary calcification. These are the major component of the bone's inorganic compartment.

In the first experiment we injected ^{45}Ca, ^{32}P-labeled phosphoric acid ($H_3{}^{32}PO_4$), 99mTc-PYP, 99mTc-HDP or 99mTc-MDP into injured rats, and found out that the highest incorporation of all three markers in the whole bone was on the sixth day after injury. The same general finding was noticed in the organic phase: all three markers had their peak of incorporation on the 6th day. The difference was noticed only in the inorganic phase, where only 99mTc did not show any differential uptake in the injured tibiae. Our results indicate that all 3 phosphates tested (MDP, HDP and PYP), Ca and phosphoric acid, accumulated equally in the organic

phase, but the 3 99mTc- labeled phosphates did not incorporate into the inorganic phase.

These results seemed awkard, as the three 99mTc-labeld phosphates were expected to incorporate with the inorganic matter, as they are the corner stone of hydroxyapatite. Thereforte, we designed an experiment where we injected dually-labelled 99mTc-MD32P to a group of injured-rats, and counted separately the 99mTc and the 32P, in order to examine the possibility that 99mTc04 is separated in the tissues from its phosphate moiety. Sure enough, 99mTc and the 32P labels went to different compartments: the 32P of 99mTc-MD32P was accumulated in the inorganic phase, and the 99mTc was concentrated in the organic phase. We also injected internally-labelled MD32P, and MD32P labelled externally with decayed 99Tc, which went primarily to the inorganic phase, while its 99mTc-label itself went to the organic phase. This descrepancy may result from separation of the Tc from the MDP moiety, prior to the phosphate's incorporation in the mineral. We concluded that for scanning bone healing one may use 99mTC-MDP, as long as one realizes that it does NOT represent the process of bone mineralization and calcification, but it is only a marker for bone matrix formation.

Another process which starts during primary mineralization is interaction between implant materials and their surrounding bone. We studied the effect of 2 bone-bonding implants, Stainless steel and titanium, on primary calcification, using computerized morphometry at the transmission electron microscopy level and determination of alkaline phosphatase activity of isolated matrix vesicles. After sacrifice, new bone was processed for microscopy, and areas of calcification were selected. Tracing was done by automated computerized analysis, and matrix vesicles distribution by number, density, type, diameter and distance from the calcified front was measured. At 3, 6, 14 and 21 d after operation, the rats were sacrificed, and tissues adjacent to the implant were removed. Matrix vesicles enriched membrane fractions were isolated and alkaline phosphatase measured, in parallel experiments.

Insertion of Stainless steel and Titanium implants result in increase in the matrix vesicle number when compared to controls. Vesicular diameter increased following insertion of Titanium. The matrix vesicles in the Titanium group were significantly smaller in diameter when compared to the Stainlss steel group, and were at a smaller distance from the calcified front compared to the titanium group. Titanium implants stimulated alkaline phosphatase up to day 21st of healing, with a peak on day 6. In the contralateral leg increase was observed only on day 3. The insertion of Stainless steel had no effect on alkaline phosphatase activity, in any of the experimental days.

These results indicate that bone-bonding implants have the capability of altering the process of primary mineralization by influencing the behaviour of matrix vesicles. The differences between the implants were expressed by different influences on the matrix vesicles' morphometric and biochemical parameters. The effects of bone bonding implants on primary calcification may be the key step in the events that produce the bone implant interface.

Epithermal Neutron Spectrometer

Gad Shani
The Davide and Irene Sala Chair in Nuclear Engineering
Ben Gurion University, P.O.B. 653, Beer-Sheva ISRAEL 84105

The measurement of the neutron energy spectrum in the epithermal range (1 keV to a few hundred keV) is very important for several scientific technological and medical applications. In the latter, the measurements of neutron dosimetry for simple surveillanace, or for diagnostic (body element activation analysis) or therapeutic purposes, are very important but difficult to achieve. During the last several years, there has been renewed inerest in boron neutron capture therapy (BNCT) to treat brain tumors.[1] To achieve neutron penetration greater than a few centimeters into the human head, the incident neutrons must have epithermal energies. Neutrons will then thermalize in the tumor vicinity to interact with the ^{10}B atoms in the tumor. An experimental method is needed to measure the epithermal neutron energy spectrum of the beam used for patient irradiations.

In the present work, a new neutron spectrometer is described. It measures the energy range from 1 keV to a few hundred keV, based on the reaction $^{3}He(n,p)^{3}H$. Two solid state detectors are used to measure the resultant charged particles (p and ^{3}H) energy.

The sum of the two particles is the neutron energy E_n plus the reaction Q value (764 keV). The fwhm detector resolution is = 3%. The detector efficiency , = 3% for thermal neutrons, is proportional to 1 / E (i.e., to the detection reaction cross section). Cooling improves the resolution. To avoid obscuring of the low keV energy range by thermal neutrons, the detector was covered with a 1 mm layer of Cd. Background due to neutron interaction with the Si detector, and with the detector construction materials and gamma rays, was removed by repeating

the foreground measurement with no ^{3}He in the detector. Neutron spectra were measured both with a moderated ^{252}Cf source and with an epithermal beam at the Brookhaven Medical Research Reactor (BMRR). Results were in good agreement with Monte Carlo calculations using the MCNP code.

The Si detector are contained in a copper box. Copper was chosen to obtain good electric shileding for the detectors and the leads.The silicon detectors, made in the Instrumentation Department at Brookhaven National Laboratory (BNL) were 1 cm^2 , 300 μm thick diodes made of 4 $k\Omega$-cm n - type wafers. They were thermally oxidized for edge and surface pasivation. The fabricant of the detector was generally performed by planar processing[2]. The detector is a p^+n n^+ structure with the contacts formed by ion implantation. Total depletion is obtained at 30V.

The gas pressure in the detector was kept low to reduce the probability of collisions of the charged particles (p and ^{3}H) with the gas. Such collisions cause energy loss, hence degradation of the resolution. The gas pressure also affects the detector efficiency. A pressure of less than 1/4 atm (190 mm Hg) was found to be a reasonable compromise.

The electronic system was composed of two branches, an energy branch and a timing branch for each detector. The two energy pulses were added after amplification in a summing amplifier which provided the total energy pulse. The timing system was used to assure that the two pulses which were summed, originated from the same reaction, i.e., the two pulses should be apparent within a short time interval.

Since the cross-section for the reaction $^{3}He(n,p)^{3}H$ at thermal neutron energy is much higher than it is in the keV range and since there are numerous thermal neutrons in the spectrum, thermal neutrons have to be removed so that they do not obscure the measurement of the lower keV range. This was accomplished by coverin the detector with a 1 mm thick sheet of Cd.

Several neutron spectra measurements were made with the present system. A demonstration of the detector performance with thermal neutrons is shown in

Fig. 1. Data were obtained using low ^3He pressure in the detector, summing the two energy pulses in coincidence and subtracting background by measurement with no He^3 in the detector. The fwhm resolution in this case was 5%. The peak is a double peak, which may be due to a mismatch of the gains in the two energy branches. A few higher energy neutrons can be observed in the spectrum.

Epithermal neutron spectrum measurement was done at the Brookhaven medical Reactor epithermal beam. The epithermal neutron beam was obtained by filtering the neutrons from the reactor core. The filter consisted of various layers of D_2O, Al_2O_3, Bi and Cd.

The neutron spectrometer was positioned facing the center of the epithermal beam window (25 x 25 cm^2) at a distance of 20 cm from the window. Several measurements were done, some using a detector which was Cd-covered to remove thermal neutrons.

An example of the measured neutron spectrum with the Cd covered detector is shown in fig. 2. It is compared with Monte-Carlo (MCNP) calculated results (unpublished report). There is good agreement between the measured and calculated results. Corrections were made for counts in the low energy range of the measurements because of the very high absorptions of the Cd and the detector resolution. The correction was made by fittings a gaussian to the first 20 channels, then normalizing to the rest of the measured spectra and to the calculated values.

References

1. R.G. Fairchild and V.P. Bond in Proc. of the First Int. Symp. on Neutron Capture
Therapy, Oct. 12-14, 1983. Eds. R.G. Fairchild and L. Brownell.
Brookhaven National Laboratory, Upton NY 11973. BNL 51730.
2. J. Kemmer, Nucl. Ins. Meth. 169 449, 1980.

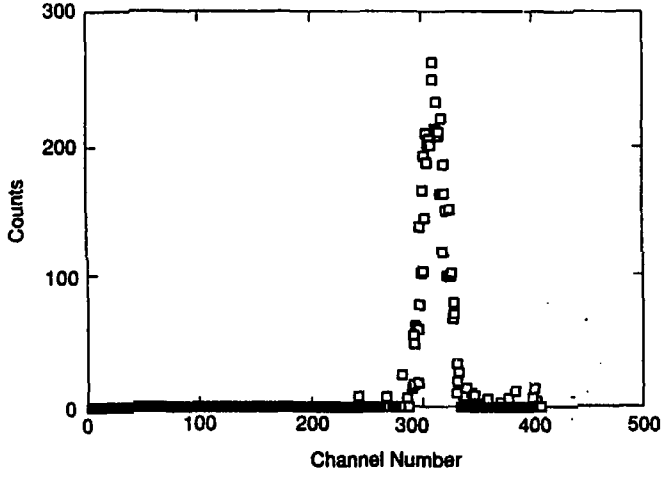

Fig. 1 Thermal Neutron Spectrum

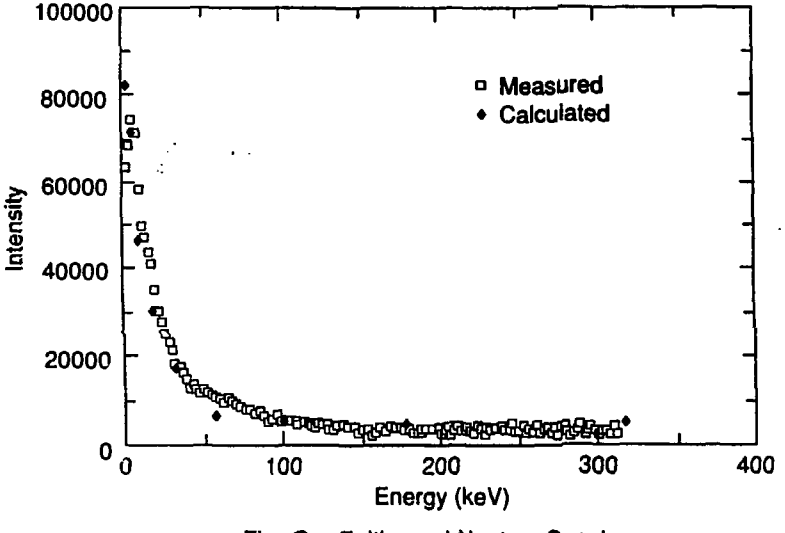

Fig. 2 a Epithermal Neutron Spectrum

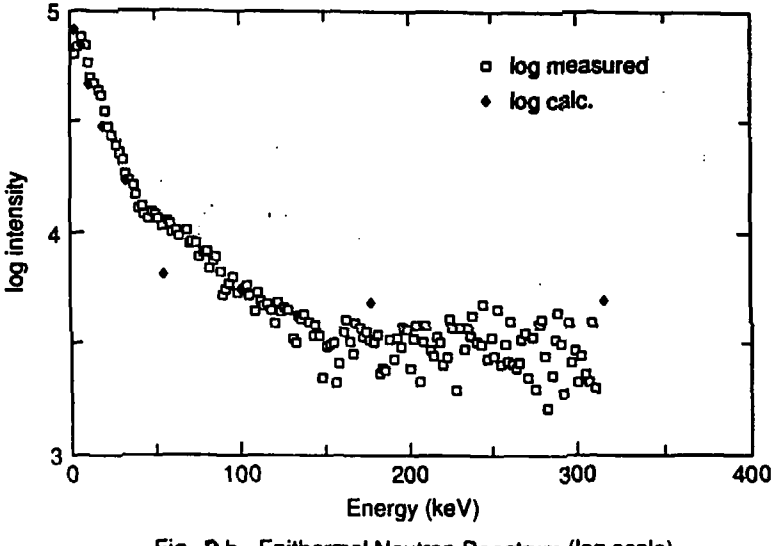

Fig. 2 b. Epithermal Neutron Spectrum (log scale)

DETERMINATION OF TRACE AMOUNTS OF CADMIUM, COBALT, IRON, MOLYBDENUM, SELENIUM AND ZINC IN THE SECOND-GENERATION BIOLOGICAL REFERENCE MATERIAL FREEZE-DRIED HUMAN SERUM BY NEUTRON ACTIVATION ANALYSIS

N. Lavi* and Z. B. Alfassi**

*Soreq Nuclear Research Center, Yavne, Israel

**Ben-Gurion University of the Negev, Beer-sheva, Israel

Abstract

The concentrations of Cd, Co, Fe, Mo, Se and Zn in the second generation biological reference material freeze-dried human serum were determined by neutron activation analysis, with enrichment by coprecipitation. The pre-concentration of these trace elements was accomplished by converting the dissolved trace metal ions into their pyrrolidine- dithiocarbamate (1-pyrrolidine carbodithioate) chelates, followed by a coprecipitation with a metal carrier of Ni. The coprecipitation was carried out after irradiation of the biological material. The validity of the method was checked using certified biological reference material NIST SRM 1577 Bovine Liver: the concentratios of trace elements found by the proposed method agreed well with the published certified data.

The concentrations (dry weight) of these trace elements were found to be as follows: Cd (1.9 ± 0.3 ng g^{-1}), Co (3.4 ± 0.7 ng g^{-1}), Fe (25.52 ± 1.61 μg g^{-1}), Mo (7.1 ± 1.2 ng g^{-1}), Se (1.035 ± 0.029 μg g^{-1}) and Zn (9.47 ± 0.12 μg g^{-1}.

The limits of detection (LOD) for Cd, Co, Fe, Mo, Se and Zn under the prevailing experimental conditions were found to be 0.2, 1, 100, 0.8, 2 and 30 ng, respectively.

DAS - Diagnosis and Advisory System for IRR-1 Reactor

Y. Bartal, A. Merhav, A. Nagler, H. Hirshfeld and S. Lagstein

Soreq Nuclear Research Center, Yavne

In the last couple of years, Expert Systems have become increasingly important as a potential solution to some previously intractable problems of human activity. The industrial sector has found Expert Systems very useful for:

- Increasing plant safety.
- Increasing industrial reliability and throughput.
- Preserving the expertise of retiring workers.
- Distributing the knowledge of experts to less qualified workers.

The nuclear industry has begun to look at Expert Systems for all of the above reasons, but particularly to increase plant safety[1].

Most effort in this respect has been done in the direction of nuclear power plant, and only a small number of works have been done for research reactors such as Soreq Nuclear Center's research reactor - IRR-1[2-13].

A research reactor's safety issue is quite different from that of a nuclear power plant. First, the potential risks are much smaller because the thermal power is smaller. Second, when a research reactor malfunctions in any respect, there is much less economic penalty in shutting it down and exploring the reason for the problem off line. Third, a nuclear power plant is operated continuously and the problem solving 'know how' personnel is supposed to be available on site. On the other hand a research reactor is shut down more often, and then the problem solving personnel is usually located off site.

It should be emphasized that reactors such as IRR-1 do have real potential risks of even core melt during the first hours after shutdown[14].

In order to help the IRR-1 operating and safety personell in their duty, the DAS Expert System has been developed. DAS is a Diagnosis and Advisory System whose purpose is twofold:

(A) To help the safety expert in the process of diagnosing an abnormal situation, and taking the right actions needed.

(B) To be used as a knowledge preserving training tool for operating or safaety personell who need to gain experience in diagnosing potential safety problems.

DAS is implemented in PROLOG and is operated in Hebrew on an IBM PC compatible. It is composed of a friendly user interface, a backward chaining inference engine and a knowledge base. The inference engine is responsible for deducing the right conclusions out of the available evidence. The knowledge base includes

all the specific 'know how' rules needed for diagnosing a potential problem in the reactor.

DAS includes the following features:

- Visual simulation of the warning board on which the user marks any warnings which are active.
- All potential problems are presented in decreasing order of certainty.
- Pull down menus which make program usage simple and easy.
- Accumulated knowledge can be presented on screen, stored on disk, restored from disk and erased for a new consultation.
- User activity is recorded and stored on disk for easy analysis of program's usage.
- On-line general and specific help which is available by a single key press.
- 'How' option enables the user to get an explanation as to how DAS arrived at its conclusions.
- 'Why' option explains why a specific question is being asked.
- A rule compiler which compiles simple Hebrew written knowledge into an internal format.
- Debugging tools enable the user to trace DAS's inferences both on-line and off-line.

Acknowledgment

We would like to acknowledge Dr. Alex Hoffman from the Licensing Division of the IAEC for his encouragement and support for this work.

References

1. Use of Expert Systems in Nuclear Safety, IAEA-TECDOC-542, 1990
2. H. Makowitz, W.K. Lehto and J.I.Sackett,
   Tightly coupled transient analysis of EBR-II - an INEL engineering simulation project,
   Proc. of the 23rd Intersociety Energy Conversion Engineering Conf.
   p. 467-472, Vol1, ASME, NY, USA 1988
3. T. Kameyama, T. Uekata, Y. Oka S. Kondo and Y. Togo,
   Development of expert system on personal Computer for diagnosis of nuclear reactor malfunctions
   J. of the Atomic Energy Society of Japan, Vol. 30 no. 1 p. 42-48, 1988
4. J.T. Robinson and P.J. Otaduy,
   An expert system for alarm diagnosis and filtering,
   Topical meeting on AI and other inovative cimputer applications in the nuclear industry, 1987

5. J.A. Mullens,
ESTATE,
Conf. on power plant simulation, p. 49-53, 1988

6. L. Ho, C. Tseng and S. Chang,
Application of artificial intelligence techniques to TRR operation,
Int. topical meeting on advances in human factors in nuclear power systems, p. 520-525, 1986

7. J.A. Bernard and F.J. Wyant,
Recent experimental results from the MIT-SNL program on the control of reactor neutronic power,
Tr. of the Am. Nucl. Soc. vol. 61, p. 124-126, 1990

8. T. Sofu, E. Eryurek, R.E. Uhrig, H.L. Dodds and D.H. Cook,
Estimation of HFIR core flow rate using back propagation network,
Tr. of the Am. Nucl. Soc. Vol. 61, p. 123-124, 1990

9. M.A.S. Guth,
Some uses and limitations of fuzzy logic in artificial intelligence reasoning for reactor control,
Nuclear Engineering and Design vol. 113, no. 1, p. 99-109, 1989

10. M. Chaix and B. Desbriere,
An expert system to assist with diagnosis and decision-making in radiation protection,
Radiation Protection in Nuclear Energy: Proc. of an Int. Conf. vol. 1, p. 383-389, IAEA 1988

11. N.E.Clapp Jr., F.H. Clark, J.A. Mullens, P.J. Otaduy and D.K. Wehe,
Application of expert systems to heat exchanger control at the 100-megawatt High-Flux Isotope Reactor,
Proc. of the Controls West Conference. Part of the Int. Industrial Controls Conf. and Exhibition/Controls West p. 208-211 1985

12. D.E. Smith, L.F. Kocher and S.E. Seeman,
A knowledge-based refueling assistant at FFTF,
Tr. of the Am. Nucl. Soc. Vol. 50, p. 292-293, 1985

13. M.P. Diwakar, N.C. Rathod, B.R. Bairi, M.D. Darbhe and S.S. Joklekar,
Developing a pc-based expert system for fault analysis of reactor instruments,
Vivek V. 2(1) p. 19-29 1989

14. A. Nagler, J. Gilat and H. Hirshfeld,
Evaluation of LOCA in a swimming-pool Type Reactor using the 3D-AIRLOCA Code,
Proc. of the International Meeting on Reduced Enrichment for Research and Test Reactors, Berlin, Fed Rep. of Germany, 1989

CALCULATION OF HELIUM LEAKAGE THROUGH GRAPHITE REFLECTOR OF HTR

I. Anteby, E. Kochavi, I. Shai

The Pearlstone Centre for Aeronautical Engineering Studies,
Dept. of Mechanical Engineering, Ben-Gurion University, Beer-Sheva, Israel.

S. Gruntman

N.R.C.N., Beer-Sheva, Israel.

Abstract

A simple procedure is presented for computation of flow through gaps in an assembly of blocks. This procedure enables estimation of bypass flows through the reflector of a gas cooled nuclear reactor. The method is based on a simplified channel network representation of the gaps configuration. Using a computer program the procedure was applied for verification on an experimental model. The results of the computation were in good agreement with the experimental data. A typical three dimensional model of a gas cooled reflector was also computed.

Introduction

In a gas cooled reactor the heat is transferred from the core to heat exchanges by means of gas flow. The flow path is designed to cool also the reflector. The reflector is usually a construction made of accurately fitted graphite blocks (Fig. 1). However, even in the best fitted assembly, the gaps between individual blocks enable gas flow in between the blocks, driven by pressure difference. These multy-bypass flows, may grow to a considerable part of the overall gas flow, thus reducing the main flow through the core. Since this may increase the temperatures in the core, it is important to be able to predict the multy-bypass flows in the early design stage. The aim of this work is to suggest a simple procedure for estimating these flows.

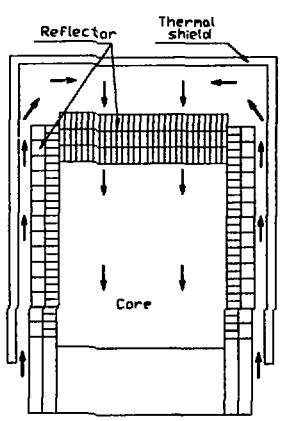

Fig. 1 - Gas flow in a typical gas-cooled reactor

The principle of the procedure is to model each gap as a duct with known length and cross section. The whole "gap maze" is simplified by modeling a finite network of channels connecting predefined nodes. A computer program was written to calculate the flows and pressures in a network.

The model

The actual flow in the gaps between blocks is geometrically complicated. Flows vary in directions and speeds. Therefore, a realistic model of the overall complex is impossible. Some individual pathes may be isolated and modelled by means of finite elements or finite difference methods. Modelling the whole construction, however, is not only an immense work, it will probably be unpractical if not impossible.

In order to simplify the problem the following assumptions were introduced:

The entire structure can be assumed as having a finite number of nodes which are interconnected by a given number of one dimensional ducts. Each duct is specified as having a uniform cross section, an hydraulic diameter and a given length. The nodes and the ducts form a network in which the sum of the flows to each node is zero, and the flow in each duct is only in the longitudinal direction. For example, fig. 2 shows a symmetric model of a two dimensional block assembly.

Further principles of the simplified model are:

a) Calculation of friction factors according to Reynolds number, using empirical equations. Laminar and turbulent flows are considered with a transition Reynolds number of 4000.

b) Not more than one duct may connect two individual nodes.

c) A node can constrain it's pressure on another node (master - slave). This enables the definition of symmetry conditions.

d) The flow-resistance of each duct is determined by its dimensions and surface roughness. It is also possible to define a local resistance to model sharp curvatures, transitions etc.

e) The flow is of constant density. Although dealing with gas flow at different pressures, it is reasonable to assume that the pressure drops are much smaller then the absolute working pressure.

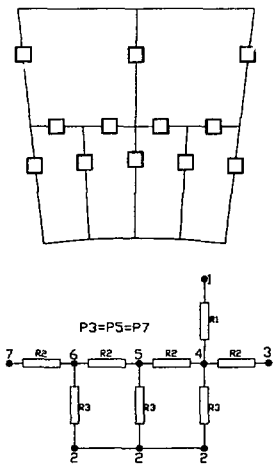

Fig. 2 - a symmetric model of a two dimensional block assembly.

One can start the calculations by computing a simple model. The results of this calculation may be used to refine the model step by step. After determining the main flow paths it is possible to isolate them and compute them by more accurate means. The parameters of the simple model can be corrected accordingly. Individually isolated assemblies may be constructed and tested for further adjustment. This procedure can be carried on until reaching convergence.

Method of Solution

The method of solution is based on the scheme presented in [1]. For incompressible flow of a fluid from point i to point j in an horizontal duct, the pressure drop is given by *Fanning* or *Darcy-Weisbach* equation:

$$p_i - p_j = \rho \frac{Q_{ij}^2}{2A^2}\left[f\frac{L}{D_H}+K\right] \quad . \tag{1}$$

Here, f is the dimensionless *Moody* friction factor, ρ is the fluid density, Q_{ij} is the volumetric flow rate from point i to point j in a duct with cross section area A, D_H is the hydraulic diameter, L is the duct length, and K is a dimensionless loss coefficient for accounting local losses in the duct such as bends. The value taken for the friction factor f depends on *Reynolds* number:

$$Re = \frac{\rho Q_{ij} D_H}{A\mu} \tag{2}$$

with μ the dynamic viscosity of the fluid. For Laminar flow ($Re < 4000$) $f = 64/Re$, and for Turbulent flow ($Re > 4000$) the *Moody* plot of the *Colebrooke-White* correlation (which is a transcendental equation for f) should be used. In the present work, an approximate explicit equation for f (for Turbulent flow) [2] is used:

$$f = \left[1.14 - 2\log_{10}\left(\frac{\varepsilon}{D_H}+\frac{21.25}{Re^{0.9}}\right)\right]^{-2} \tag{3}$$

with ε being the duct surface roughness. This equation is generally within 0.5% of the *Colebrook-White* equation.

Equation (1) may be written as:

$$|p_i - p_j| = c_{ij} Q_{ij}^2 \tag{4}$$

with

$$c_{ij} = \frac{\rho}{2A^2}\left[f\frac{L}{D_H}+K\right] \tag{5}$$

in which the sign of Q_{ij} is plus or minus for flow from i to j or vice versa, respectively. In the following version of equation (4), Q_{ij} will automatically have the correct sign:

$$Q_{ij} = (p_i - p_j)\sqrt{\frac{1}{c_{ij}|p_i - p_j|}} \quad . \tag{6}$$

At any node j, where the pressure is not specified, the sum of the flows from neighbouring nodes i that are connected, must be zero:

$$\sum_i Q_{ij} = \sum_i (p_i - p_j)\sqrt{\frac{1}{c_{ij}|p_i - p_j|}} = 0 \quad . \tag{7}$$

When applied at all nodes, equation (7) yields a system of simultaneous equations in the unknown pressures. This system is solved by the successive-substitution method [1]. Since $(p_i - p_j)$ is more sensitive than $(|p_i - p_j|)^{1/2}$ to variations in p_j, an appropriate recursive equation for calculating the pressures is:

$$p_j = \frac{\sum_i a_{ij} p_i}{\sum_i a_{ij}} \quad , \tag{8}$$

in which

$$a_{ij} = (c_{ij}|p_i - p_j|)^{-1/2} \quad . \tag{9}$$

Equation (8) is applied repeatedly at all nodes until each computed pressure p_j does not change by more than a specified value. The last estimated value of p_i is always used in the right-hand side of (8).

After pressures are converged, the volumetric flow rates for all ducts are calculated using (6), along with respective Reynolds numbers. Than a new set of c_{ij} is calculated using (3) and (5). The previous solution process for the pressures is repeated, each time with a better estimate of f for each duct. The whole computation is repeated until volumetric flow rates converge. Fig. 3 is a flow chart of the computer program which performs the computation.

Results

Some verification tests where performed by comparing numerical results to a pipe network that was constructed and tested. Results agree well with experimental test.

A typical three dimensional model of a gas cooled reflector was computed using the described procedure. Calculations were made on a symmetrical section in order to evaluate the overall flow through the gaps. The results obtained agreed qualitatively with experimental data.

References

[1] B. Carnahan, H.A. Luther, J.O. Wilkes, ***Applied Numerical Methods***, John Wiley & Sons Inc., N.Y. (1969).

[2] A. K. Jain, Accurate Explicit Equation for Friction Factor, *ASCE J. Hydraulics Div.* **102**, 674-677 (1976).

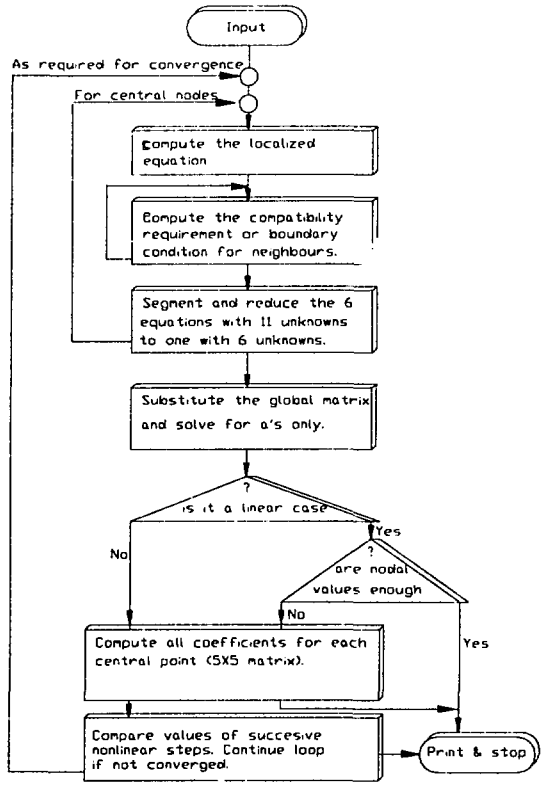

Fig. 3 - A flow chart of the computer program